Chem Soc Rev

REVIEW ARTICLE

View Article Online
View Journal | View Issue

Check for updates

Cite this: *Chem. Soc. Rev.*, 2017, **46**, 5975

# Counter electrodes in dye-sensitized solar cells

Jihuai Wu,* Zhang Lan, Jianming Lin, Miaoliang Huang, Yunfang Huang, Leqing Fan, Genggeng Luo, Yu Lin, Yimin Xie and Yuelin Wei

Dye-sensitized solar cells (DSSCs) are regarded as prospective solar cells for the next generation of photovoltaic technologies and have become research hotspots in the PV field. The counter electrode, as a crucial component of DSSCs, collects electrons from the external circuit and catalyzes the redox reduction in the electrolyte, which has a significant influence on the photovoltaic performance, long-term stability and cost of the devices. Solar cells, dye-sensitized solar cells, as well as the structure, principle, preparation and characterization of counter electrodes are mentioned in the introduction section. The next six sections discuss the counter electrodes based on transparency and flexibility, metals and alloys, carbon materials, conductive polymers, transition metal compounds, and hybrids, respectively. The special features and performance, advantages and disadvantages, preparation, characterization, mechanisms, important events and development histories of various counter electrodes are presented. In the eighth section, the development of counter electrodes is summarized with an outlook. This article panoramically reviews the counter electrodes in DSSCs, which is of great significance for enhancing the development levels of DSSCs and other photoelectrochemical devices.

Received 13th May 2017

DOI: 10.1039/c6cs00752j

rsc.li/chem-soc-rev

Open Access Article. Published on 25 August 2017. Downloaded on 4/25/2024 1:35:01 PM.
This article is licensed under a Creative Commons Attribution-NonCommercial 3.0 Unported Licence.

## 1. Introduction

### 1.1. Solar cells

Sustainable development is a major challenge for the planet (Fig. 1). On 25 September 2015, the 193 countries of the UN General Assembly unanimously adopted the 2030 Development Agenda entitled: Transforming our world: the 2030 Agenda for Sustainable Development.[1] The agenda contains 17 sustainable development goals with 169 associated targets which have to be implemented and achieved in every country from year 2016 to 2030.[1] Energy is crucial for achieving almost all of the sustainable development goals, from its role in the eradication of poverty through advancements in health, education, water supply and industrialization, to combating climate change.

*Engineering Research Center of Environment-Friendly Functional Materials, Ministry of Education; Institute of Materials Physical Chemistry, Huaqiao University, Quanzhou, Fujian 362021, China. E-mail: jhwu@hqu.edu.cn*

**Jihuai Wu**

*Jihuai Wu is Professor in Chemistry and Materials and the Vice-president at Huaqiao University, China. He obtained his master's degree in Materials in 1988 from Huaqiao University, China, and obtained his PhD degree in Chemistry in 1999 from Fuzhou University, China. His main research focuses on photo-electronic functional materials and devices, superabsorbent polymers, photo-catalytic intercalated nano-materials, especially dye-sensitized solar cells and perovskite solar cells. He has published 381 scientific articles and 23 authorized invention patents. In 2014, 2015, and 2016, he was selected as Elsevier's Most Cited Chinese Researcher.*

**Zhang Lan**

*Zhang Lan received his PhD degree in Materials Science from Huaqiao University, China, in 2009. He joined the Institute of Materials Physical Chemistry, Huaqiao University, in 2009, and became an associate professor in 2012. His main interests are the synthesis and application of nano-materials in dye/quantum dot sensitized solar cells and organic–inorganic hybrid solar cells.*

Open Access Article. Published on 25 August 2017. Downloaded on 4/25/2024 1:35:01 PM.
This article is licensed under a Creative Commons Attribution-NonCommercial 3.0 Unported Licence.

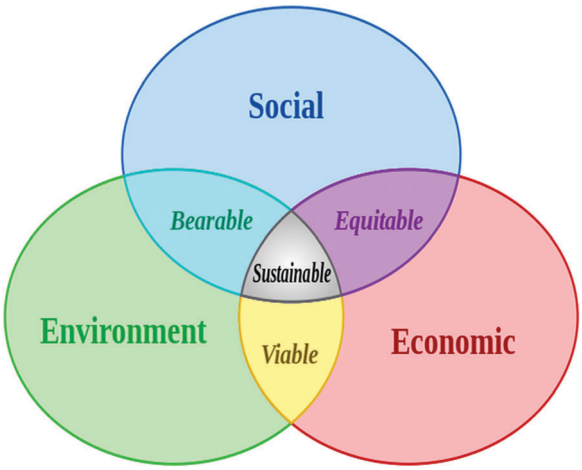


Fig. 1 Scheme of sustainable development: at the confluence of three constituent parts.[2] Reprinted with permission from ref. 3. (CC BY-SA 3.0).

Goal 7 is about energy resources, which is to ensure access to affordable, reliable, sustainable and modern energy for all.[1]

Energy is the single most important challenge that humanity is confronted with today. As Nobel Laureate Richard E. Smalley outlined in 2003, energy will be the top problem for humanity for the next 50 years.[4] United Nations' Secretary-General Ban Ki-moon remarked that renewable energy has the ability to lift the poorest nations to new levels of prosperity.[5] If energy is the lifeblood of the world economy, Ban argued that renewable energy represents an infusion of humanity.[5] The global concern over this energy problem can mainly be attributed to accelerating economic, exhaustible and ecological factors. Economic growth at a high speed requires more energy support; exhaustible fossil fuels widely used now demand renewable energy sources; ecological deterioration caused by fossil fuel combustion and greenhouse effect means that people have to use environmentally friendly energy sources.[6–10]

The research and development of renewable energy resources have received great attention worldwide. According to the REN21's 2016 report, renewables contributed 19.2% to global energy consumption in 2014 and 23.7% to global electricity production in 2015.[11] Global investments in renewable technologies amounted to more than US$286 billion in 2015, with countries like China and the United States heavily investing in wind, hydro, solar and biofuels.[11] Globally, there are an estimated 7.7 million jobs associated with renewable energy industries, with solar photovoltaics being the largest renewable employer.[12]

The Sun is a champion among all energy sources, and the Earth receives 174 petawatts (PW) of incoming solar radiation

**Jianming Lin**

*Jianming Lin is Professor in Materials and the Dean of materials department at Huaqiao University. He received PhD degree in polymers from Tianjin University, China, in 2002. His main research focuses on photo-electronic functional materials and devices, superabsorbent polymers, photocatalytic intercalated nanomaterials, especially dye-sensitized solar cells.*

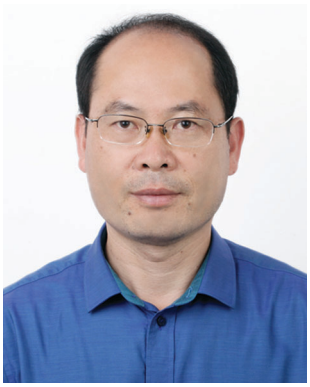

**Miaoliang Huang**

*Miaoliang Huang is Professor in Materials at Huaqiao University. He received PhD degree in physical chemistry from Fujian Institute of Research on the Structure of Matter, Chinese Academy of Sciences, in 2003. His current research interests focus on the synthesis and application of nano photocatalytic materials and photo-electronic functional materials.*

**Yunfang Huang**

*Yunfang Huang is a professor in Materials Chemistry at Huaqiao University, China. He obtained his PhD degree in Materials Science in 2007 from Huaqiao University, China. He joined the Institute of Materials Physical Chemistry, Huaqiao University, in 1998. His main research interests include photocatalysis, photo-electronic functional materials, dye-sensitized solar cells, and the related materials and device development.*

**Leqing Fan**

*Leqing Fan is an associate professor in Materials Chemistry at Huaqiao University, China. He received his master's degree in Materials Science from Huaqiao University in 2003 and then his PhD degree in Physical Chemistry from Chinese Academy of Sciences in 2006. His main research interests include supercapacitors, dye-sensitized solar cells and inorganic–organic hybrid materials.*

 This journal is © The Royal Society of Chemistry 2017

Open Access Article. Published on 25 August 2017. Downloaded on 4/25/2024 1:35:01 PM.
This article is licensed under a Creative Commons Attribution-NonCommercial 3.0 Unported Licence.

at the upper atmosphere in a year.[13] The total solar energy absorbed by the Earth's surface is approximately 3850 zettajoules (ZJ) per year,[14] which is more energy in one hour than what the world used in one year.[15,16] The amount of solar energy reaching the surface of the planet is so vast that in one year it is about twice as much as what will ever be obtained from all of the Earth's non-renewable resources of coal, oil, natural gas, and mined uranium combined.[17] A solar cell, or photovoltaic cell (PV), is a device that converts sunlight directly into electricity by taking advantage of the photoelectric effect. Among all the renewable energy technologies, photovoltaic technology is considered as the most promising one.[18–21] Solar PV has been turned into a multi-billion, fast-growing industry, and the most potential of any renewable technologies.[22] The abundant, clean, safe, and affordable photovoltaic technology has been considered to be the most promising one among all the novel energy technologies.[19,20]

The photovoltaic effect was experimentally demonstrated first by French physicist Edmond Becquerel. In 1839, at the age of 19, he created the world's first photovoltaic cell in his father's laboratory. In this experiment, silver chloride was placed in an acidic solution and illuminated while connected to a platinum electrode, generating voltage and current.[23,24] Consequently, the photovoltaic effect is termed "Becquerel effect". In 1883, American inventor Charles Fritts created the first working photovoltaic cell by coating the semiconductor selenium with a thin layer of gold to form the junctions, and the device showed an efficiency of only 1%.[25] In his miraculous year of 1905, Albert Einstein proposed the quantum theory of light and explained the photoelectric effect,[26] for which he received the Nobel Prize in Physics in 1921. The first practical silicon solar cell with an efficiency of 6% by a team of scientists was publicly demonstrated on 25 April 1954 at Bell Lab.[27] The silicon solar cells were used in the US satellite Vanguard I in 1958. This milestone greatly promoted the research and development of solar cells.[28]

The scientific research and industrial development of PV technology must focus on high-efficiency, low-cost, and stability, which are called the "Golden Triangle Issues". With increasing public awareness of sustainable development, the fourth issue of environmental-harmony should be emphasized as well.[29] In order to meet these challenges, three generations of solar cells have been evolved up to now. The first generation cells, also called conventional, traditional or wafer-based cells, are made of polycrystalline silicon or monocrystalline silicon. Si solar cells dominate the PV market and produce efficiencies between 12% and 16%, according to the manufacturing procedures and wafer quality. However, the sophisticated production steps and high environmental costs have led to the use of polycrystalline Si, instead of monocrystalline Si, which further promoted the search for environmentally friendly and low cost alternatives. Second generation solar cells are often called thin-film technologies, including cadmium telluride (CdTe), copper indium gallium selenide (CIGS), and other cells. The thin-film solar cells sandwich active materials between two glass sheets and provide potential for cost reduction in the manufacturing process due to material saving, low temperature processes, and high automation in series production, particularly in flexible cells. However, difficult module technology and limited stability have led to a small market share (<12%) of the thin film cells. After approximately 30 years, the third generation solar cells appeared. The third generation solar cells are often described as emerging PV, most of which are still in the research or development phase. This new generation of PV technologies includes dye-sensitized solar cells, perovskite solar cells, organic/polymer solar cells, quantum dot solar cells, *etc.* Though of lower efficiency than Si-based solar cells and the thin film cells, the third generation cells claim low processing costs and minor environmental impact which elicit intensive research and development.[29–37]

The current classification for generations of solar cells is a bit puzzling and illogical, especially that of the second-generation thin film technologies and the third-generation emerging PV. This is due to the fact that the current classifications are based on different coordinate systems. First generation cells, Si crystalline cells, are classified on the basis of active materials; the second generation cells, thin film technologies, are of manufacturing technology; the third generation cells, emerging PV, are of time emergence and technology maturity. In our opinion, the generations of solar cells should be based on the active materials used and the order of the invention. In this way, the first generation cells should be element (silicon) solar cells, started from 1954, when Chapin *et al.* first showed a silicon crystalline cell with an efficiency of 6% in Bell Lab.[27] The first generations shall include monocrystalline, multicrystalline, microcrystalline, nanocrystalline, and amorphous Si cells. The second generation cells should be compound solar cells, since Cusano first invented a CdTe solar cell with an efficiency of 6% at RCA Lab in 1963.[38] The second generations shall contain CdTe, CIGS, GaAs, and CZTSSe cells, in which the active materials are II–VI or III–V compounds. The third generation cells should be hybrid (composite) solar cells, beginning with the dye-sensitized solar cell prototype with an efficiency of 7.1% that Gratzel and O'Regan first proposed in 1991.[39] The third generations are comprised of dye-sensitized cells, perovskite cells, organic cells, and quantum dot cells, and their corresponding typical active materials are dye/$TiO_2$/electrolyte, $TiO_2$/perovskite/spiro-OMeTAD, PCBM/MDMO-PPV, and ZnO/PbSQD, respectively.[37] In addition, there is another category of solar cells, under which are tandem cells, multi-junction cells, and concentrator cells. Because the active materials for these cells have no significant difference, they cannot be distinguished by any of the generations.

Today, solar cells are used in all sorts of devices, from handheld calculators to rooftop solar panels. Global installed PV capacity reached at least 177 gigawatts in 2014, enough to supply one percent of the world's total electricity consumption. PV silicon cell prices have fallen from $76.67 per watt in 1977 to $0.36 per watt in 2014. Similar to Moore's Law in IT industry, in PV industry there is Swanson's law, which is an observation that solar cell prices fall 20% for every doubling of cumulative shipped volume (Fig. 2a). The Law is named after Richard Swanson, the founder of SunPower Corporation.[40] A study by Farmer *et al.* shows that price/kWh has dropped by 10% per year since 1980, and predicts that solar could contribute 20%

Open Access Article. Published on 25 August 2017. Downloaded on 4/25/2024 1:35:01 PM.
This article is licensed under a Creative Commons Attribution-NonCommercial 3.0 Unported Licence.

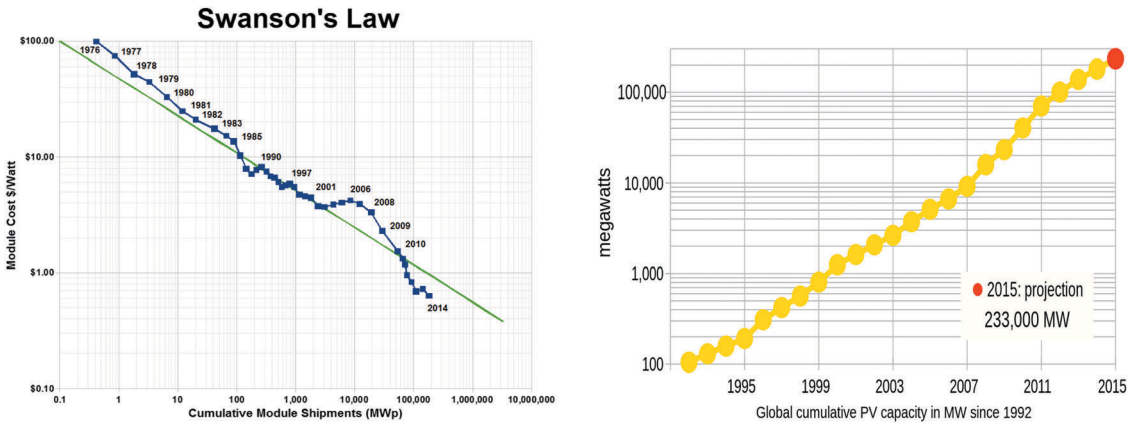


Fig. 2 (a) Swanson's law – the learning curve of solar PV. Adapted with permission from ref. 40. Copyright (2006) John Wiley & Sons Ltd. (b) Growth of photovoltaics – worldwide total installed PV capacity. Adapted with permission from ref. 41. Copyright (2016) Elsevier.

of total electricity consumption by 2030,[41] whereas the International Energy Agency predicts 16% by 2050.

Solar PV is growing the fastest in Asia, with China and Japan currently accounting for half of worldwide deployment.[42] Within the last few decades, the solar PV featured an annual growth rate of more than 20%,[29,37,43–45] and the growth rate even reached 28% in 2015.[11] However, the present solar PVs contribute only 1.2% (2015) to the total world energy consumption,[11] leaving a large room for industrial development and scientific research. Fig. 3 shows the development history of the best research-cell efficiencies from 1976 up to now.

### 1.2. Dye-sensitized solar cells

Early in 1839, Becquerel's pioneering photoelectric experiments were done with liquid not solid-state devices. In his experiment, illumination of solutions containing silver halide produced a current between two platinum electrodes immersed in electrolytes.[23] This effect is now recognized as being due to the semiconductor nature of silver halide grains with an energy band gap of 2.7–3.2 eV, and is therefore insensitive to the visible light.[47]

In general, the photoelectric conversion relies on the energy band gap of the semiconductor. Unfortunately, the semiconductors with narrow band gaps to absorb visible light are susceptible to photocorrosion. Also, the semiconductors, stable under illumination, such as $TiO_2$ and $Nb_2O_5$, exhibit a too wide bandgap to collect effectively visible light. The dilemma was resolved by surface modification of the semiconductors by visible-light sensitive dye molecules.[47–49] Sensitization of wide-bandgap semiconductors using dyes has a long (century-old) history, dating back to the early days of photography.[50–56]

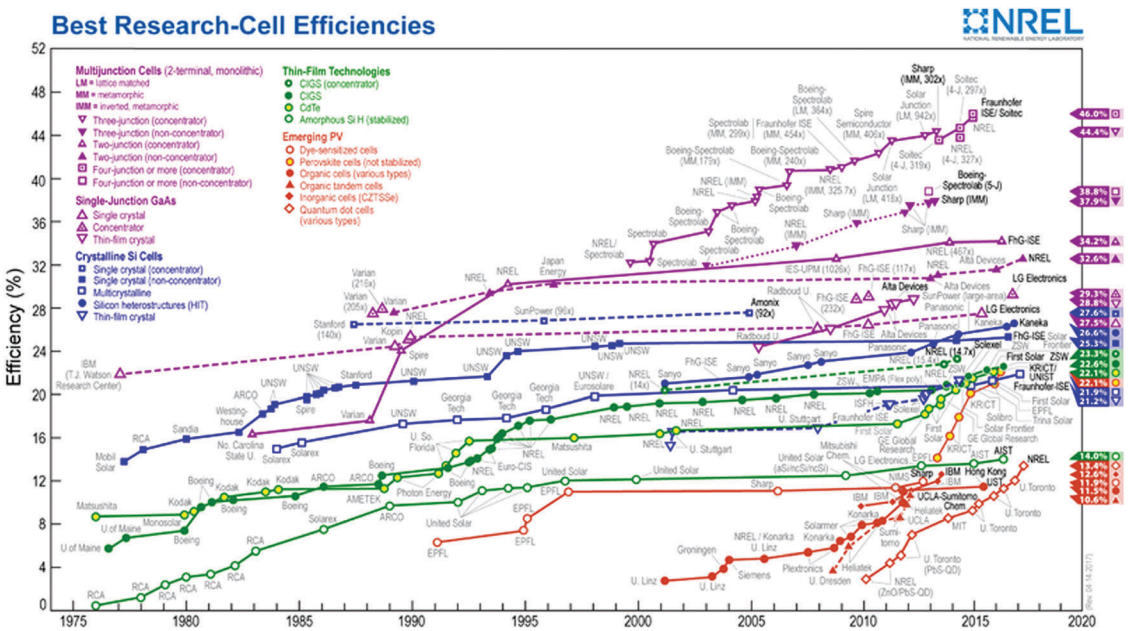


Fig. 3 Conversion efficiencies of best research solar cells worldwide for various photovoltaic technologies since 1976 by National Renewable Energy Laboratory (NREL). Reprinted with permission from ref. 46. (CC BY-SA 3.0).

Open Access Article. Published on 25 August 2017. Downloaded on 4/25/2024 1:35:01 PM.
This article is licensed under a Creative Commons Attribution-NonCommercial 3.0 Unported Licence.

Its recent development was promoted by the application in solar energy conversion, especially bipyridyl Ru complexes with anchoring groups to attach them to the oxide semiconductor surface.

At the beginning, the smooth semiconductors were used as electrodes in dye-sensitized photoelectrochemical cells to absorb dye. Only the first monolayer of adsorbed dye results in efficient electron injection into the semiconductor, and the light harvesting efficiency of the flat electrode was very small and the efficiency of the solar cell was extremely low below 1%.[57] Attempts to harvest more light by using multilayers of dyes were in general unsuccessful. The mesoporous semiconductor electrode, typically 10 mm thick with a porosity of 50%, has a surface area over a thousand times that of a flat electrode of the same size. It can provide enough area for dye chemisorption in the monomolecular layer and harvest all the incident light.[58–60] The Gratzel group replaced the planar semiconductor electrode with a mesoporous film of $TiO_2$ nanocrystalline particles, and the energy conversion efficiency of the solar cell increased by an order of magnitude.[61–63] Consequently, O'Regan and Gratzel published the landmark paper in *Nature* "A low-cost, high-efficiency solar cell based on dye-sensitized colloidal $TiO_2$ films" (later was known as dye-sensitized solar cell, DSSC, or Gratzel cell), boasting an efficiency of 7.1–7.9%.[39]

The development of dye-sensitized solar cells (DSSCs) in the 1990s opened up a new horizon and rapidly propelled photovoltaics technology into the era of the third generation solar cells. DSSCs have attracted wide attention and have been believed as one of the most promising solar cells in the third generation PV technology. This field is growing fast; it can be seen from Fig. 4 that the publications on "solar cells" increased from 1195 papers in 2000 to 16 909 papers in 2015 (increased 14 times), among them, the number of publications on "dye-sensitized solar cells" increased from 60 in 2000 to 2060 in 2015 (increased 34 times), while the number of articles on counter electrodes increased from 4 in 2000 to 447 in 2015. Although still of lower efficiency than silicon cells, the DSSCs offer several advantages over their competitors, such as easy preparation, low productive and environmental cost, as well as short energy payback time (<1 year), enhanced performance under real outdoor conditions, bifacial cells capture light from all angles, outperform Si competitors for indoor applications, and lower standards for material purity, meaning that processing under vacuum and high temperatures is not required. All these advantages accelerate the research and development of DSSCs.[10,39,47,52,63–68]

The working principle of DSSCs differs substantially from that of the first generation and second generation solar cells and is closely related to natural photosynthesis where light absorption and charge carrier transportation are carried out by different substances. Concretely, the constituent components and fundamental processes of DSSCs are schematically illustrated in Fig. 5.

The fundamental processes include:[10,39,47,52,68,69]

(1) sensitizer photoexcitation to produce excited dye;

(2) electron injection into the conduction band of metal oxide resulting in the production of oxidized dye;

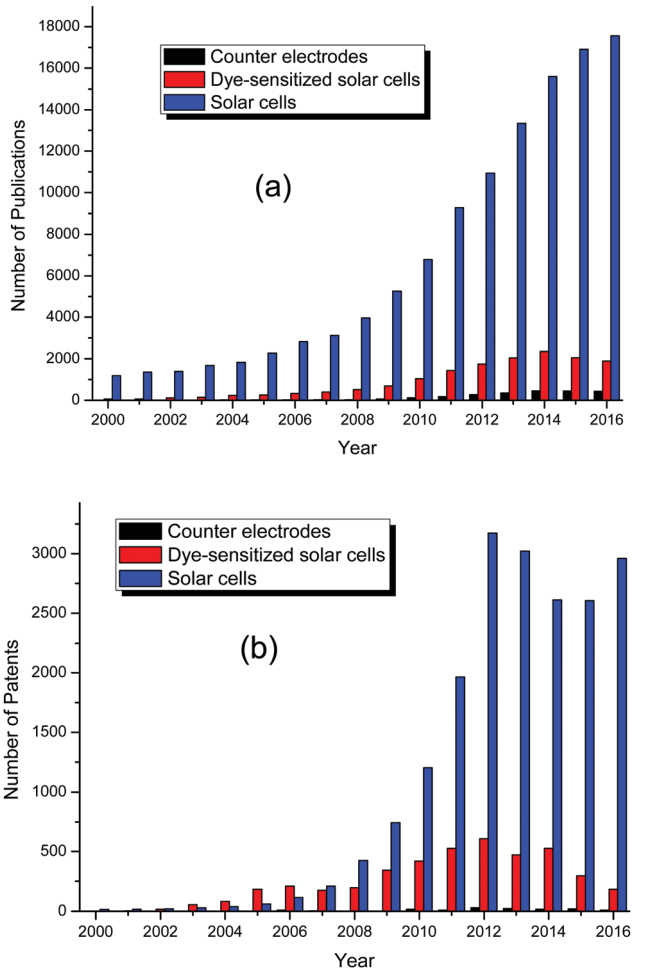


Fig. 4 Number of (a) published articles and (b) patents per year. Obtained from ISI Web of Science and WIOP (World Intellectual Property Organization) Patentscope (2017-05-08) by keyword searching: "solar cell", + "dye-sensitized", and + "counter electrode".

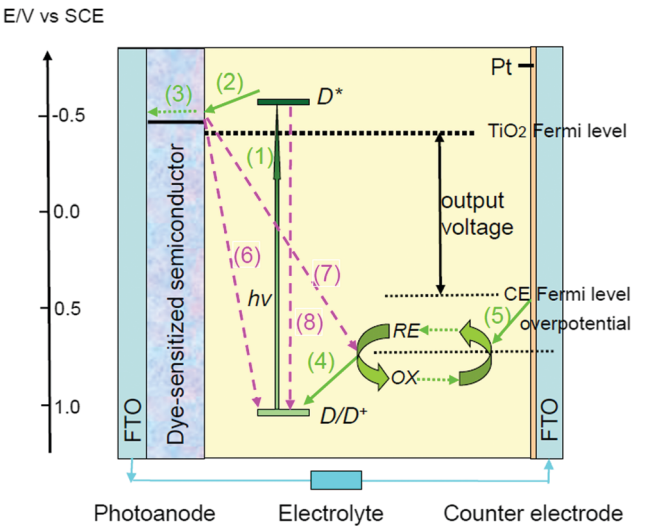


Fig. 5 Fundamental processes and constituent components of dye-sensitized solar cells.

Open Access Article. Published on 25 August 2017. Downloaded on 4/25/2024 1:35:01 PM.
This article is licensed under a Creative Commons Attribution-NonCommercial 3.0 Unported Licence.

(3) electron transportation to the anode and flow to the counter electrode *via* an external circuit;

(4) oxidized dye regeneration by accepting electrons from the reduced redox couple;

(5) oxidized redox couple regeneration at the cathode by accepting electrons from the anode;

(6) electron recombination by donating electrons to oxidized dye;

(7) electron recombination by donating electrons to the oxidized redox couple;

(8) relaxation of the excited dye to its ground state by a non-radiative decay process.

For "Gratzel cells", processes (1)–(5) are required reactions for completing the light-to-electric conversion.[10,49,67,68] Processes (6) and (7) are dark reactions which result in charge carrier recombination and this is disadvantageous for enhancing the efficiency of DSSCs. However, these dark reactions do not have a significant negative effect owing to their slower reaction speed compared with that of the required processes.[43,63,65,67,70] The typical time constants for the required reactions (green) and the dark reactions (red) are shown in Fig. 6.[68,71] Besides the aforementioned, the orientated migrations of electrons, ions and molecules in the $TiO_2$ mesoporous layer and the electrolyte layer also affect the performance of DSSCs.

Research for optimizing the photovoltaic performance of dye-sensitized solar cells focuses on modulating the physicochemical properties of the four main components (Fig. 5) of the device: (i) the sensitized dye, (ii) the metal oxide semiconductor, (iii) the redox couple electrolyte and (iv) the counter electrode. For a high-effective solar cell, all components require fine-tailoring.

At the heart of the system is a mesoporous oxide layer composed of nanometer-sized particles sintered on a transparent conductive glass substrate, such as indium-doped tin oxide (ITO) or fluorine-doped tin oxide (FTO) glass. This mesoporous metal oxide film acts as a high surface area support for the sensitizer, a pathway for electron transportation and a porous membrane for diffusion of the redox couple. The oxide semiconductor most frequently used in DSSCs is titanium dioxide (anatase); it is an inert, low cost, widely available, non-toxic and biocompatible material, and has a larger bandgap (3.2 eV) and a higher conduction band edge energy, leading to a higher Fermi level and $V_{OC}$ in DSSCs.[72,73]

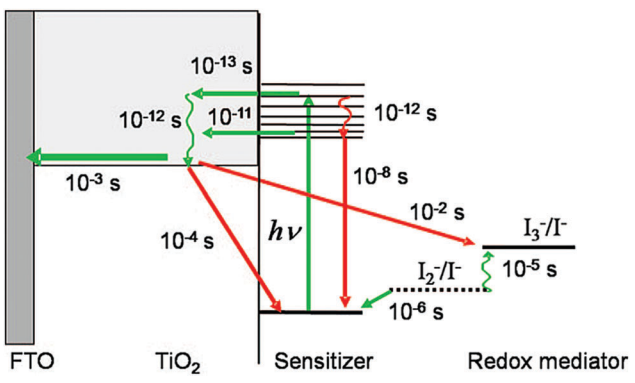


Fig. 6 Typical time constants for the forward reactions (green) and the dark reactions (red) in a Ru-dye-sensitized solar cell with iodide/triiodide electrolyte under working conditions (1 Sun). Reproduced with permission from ref. 71. Copyright (2009) American Chemical Society.

Attached to the surface of the oxide semiconductor film is a monolayer of dye sensitizer. The role of the dye in DSSCs consists in acting as a molecular electron pump. It harvests incident sunlight, pumps an electron into the semiconductor, accepts an electron from the charge mediator, and then repeats the cycle.[52] As an efficient dye sensitizer, it should have wide and strong absorption in the visible range, even in the NIR range, strongly anchoring groups (–COOH, $-H_2PO_3$, $-SO_3H$, *etc.*) to bind the dye on the semiconductor surface, high stability and reversibility in the oxidized, ground and excited states, a suitable redox potential in relation to the semiconductor and the charge mediator, and photo, thermal and electrochemical stability.[49,68,74,75] The updating of the highest efficiency of DSSCs is often accompanied by the discovery of new dyes.

The electrolyte sandwiched between the photoanode and the counter electrode (CE) is of crucial importance for stable operation of a DSSC because it must carry the charge between the photoelectrode and the counter-electrode for regeneration of dye and itself.[10,48,49,75] Photo-excitation of the dye results in the injection of an electron into the oxide semiconductor and the electron donor (triiodide) in the electrolyte must reduce the oxidized dye to the ground state as rapidly as possible. The electron acceptor (iodide) migrates to the CE to compensate its missing electrons and the electron donor (triiodide) is regenerated, the circuit being completed *via* electron migration through the external load. For regeneration of dyes and electrolytes, the redox potential of the redox couple should be considered full. Also, the redox couple must be fully reversible, chemically stable, and have no significant absorption in the visible light range. The solvent should be of low viscosity to permit the rapid diffusion of charge carriers and to provide good dispersion of the redox couple, compatible with suitable sealing materials, and not cause desorption of the dye or even the dissolution of semiconductors on the electrode.

Among the various electrolytes, the polymer electrolytes are the most extensively investigated systems.[10,76,77–79] In recent years, the scientific community has turned its efforts in the direction of aqueous electrolytes; by means of DSSCs fabricated with water-based electrolytes, reduced costs, non-flammability, reduced volatility and improved environmental compatibility could be easily achieved.[80–84]

Solid hole conductors capable of transporting charge and regenerating the dye, such as spiro-MeOTAD, can be used as charge mediators in DSSCs.[85–87] The charge carrier transportation and dye recombination for this solid-state DSSC is different from that in liquid-state DSSCs using liquid electrolytes; the charge carriers are transported *via* hole hopping in hole conductors rather than ionic migration in electrolytes.

### 1.3. Counter electrodes in dye-sensitized solar cells

An electrode is a solid electric conductor through which an electric current enters or leaves an electrolytic cell or other

 This journal is © The Royal Society of Chemistry 2017

Open Access Article. Published on 25 August 2017. Downloaded on 4/25/2024 1:35:01 PM.
This article is licensed under a Creative Commons Attribution-NonCommercial 3.0 Unported Licence.

medium. An electrode in an electrochemical cell is referred to as either an anode or a cathode (words that were coined by William Whewell at Faraday's request).[88,89] The anode is now defined as the electrode at which electrons leave the cell and oxidation occurs (indicated by a minus symbol, "−"), and the cathode is defined as the electrode at which electrons enter the cell and reduction occurs (indicated by a plus symbol, "+"). For dye-sensitized solar cells, the anode is the electrode on which the metal oxide semiconductor is deposited, and is also called photoanode, owing to the fact that incident sunlight often comes from here. The cathode is the electrode on which platinum and other conducting materials are deposited, and is more often called counter electrode, because it exists relative to the anode; a more important reason is that Gratzel first used "counter electrode" in his pioneering paper in *Nature* in 1991.[39]

In DSSCs, the CE undertakes three functions:[49,90–93] (i) as a catalyst, it promotes the completion of process (5), *i.e.*, the oxidized redox couple is reduced by accepting electrons at the surface of the CE, and process (4), *i.e.*, the oxidized dye is reduced by collecting electrons *via* ionic transport materials in solid state DSSCs (Fig. 5). (ii) As a positive electrode of primary cells, it collects electrons from the external circuit and transmits them into the cell. Thus the ultimate function of the CE is to return the electrons from the external load back into the "circulation" within the cell. (iii) As a mirror, it reflects the unabsorbed light from the cell back to the cell to enhance utilization of sunlight.[94] According to these basic functions, an optimal CE should possess the following qualities as required: high catalytic activity, high conductivity, high reflectivity, low-cost, high surface area, porous nature, optimum thickness, chemical, electrochemical and mechanical stability, chemical corrosion resistance, energy level that matches the potential of the redox couple electrolyte, good adhesivity with TCO, *etc.* Benchmark parameters for an ideal CE include 80% optical transparency at a wavelength of 550 nm, $<20\ \Omega\ sq^{-1}$ sheet resistance ($R_S$), and 2–3 $\Omega\ cm^2$ charge transfer resistance ($R_{CT}$).[8,95] The overvoltage should be as low as possible at photocurrent densities up to 20 mA $cm^{-2}$. However, it is not easy for one material to achieve all these parameters simultaneously in most of the cases. For example, the required $R_{CT}$ and $R_S$ can be achieved in carbon-based CEs, but optical transparency is not ideal.

The CE has important effects on the photovoltaic parameter of DSSCs. The theoretical maximum photovoltage of the DSSC is determined by the energy difference between the redox potential of the mediator and the Fermi level of the metal oxide semiconductor on the photoanode and can only be obtained at zero current. Under load, however, the output voltage is usually less than the open circuit voltage. This voltage loss comes from the overall overpotential of the CE (Fig. 5), which comes from the delivery of current through the electrolyte (the mass-transfer overpotential) and through the electrolyte/counter electrode interface (the kinetic overpotential or charge-transfer overpotential). The former is mainly influenced by the ionic conductivity of electrolytes and the transportation of mediator species from the CE to the photoanode, whereas the electrocatalytic properties of the CE surface towards mediator reduction will determine the magnitude of the latter.[96,97] An effective CE should have good conductivity and exhibit high electrocatalytic activity for reduction of the redox couple. The reduction reaction ($I_3^- + 2e \rightarrow 3I^-$) on naked ITO (indium tin oxide) or FTO (fluorine-doped tin oxide) glass is extremely slow.[93,98] Thus, in order to minimize the charge transfer overpotential, catalytic materials should be coated on conducting substrates to speed up the reaction.

In DSSCs, the transportation of charge carriers from the photoanode to the CE must meet various resistances, including:[98–101] the series resistance ($R_S$) comprising the sheet resistance of TCO glass and the contact resistance of the cell; the resistance at TCO/$TiO_2$ contact ($R_{TCO-TiO_2}$); the transport resistance of electrons in the $TiO_2$ film ($R_{TiO_2}$); the charge-transfer resistance of the charge recombination between the electrons in the $TiO_2$ film and $I_3^-$ in the electrolyte ($R_{CT}$); the Warburg parameter describing the Nernst diffusion of $I_3^-$ in the electrolyte ($Z_d$); the charge-transfer resistance at the CE/electrolyte interface ($R_{CE-electrolyte}$); and the charge-transfer resistance at the exposed TCO/electrolyte interface ($R_{TCO-electrolyte}$). In DSSCs, the charge-transfer resistance at the CE/electrolyte interface ($R_{CE-electrolyte}$) is often dominant among multiple charge-transfer resistances, and thus the $R_{CT}$ often refers to $R_{CE-electrolyte}$, if there is no special note. Among these charge-transfer resistances, the series resistance ($R_S$) and the charge-transfer resistance at the CE/electrolyte interface ($R_{CT}$) are enslaved to the CEs.

The series resistance of a solar cell dominates fill factor (FF) losses,[102] especially in large area commercial solar cells. A smaller series resistance ($R_S$) will give a higher FF, which results in a high conversion efficiency.[101,103–105] The catalytic activity of the CE can be explained in terms of current density ($J$), which is calculated from the charge transfer resistance ($R_{CT}$):

$$R_{CT} = RT/nFJ \quad (1)$$

where $R$, $T$, $n$, and $F$ are the gas constant, temperature, the number of electrons transferred in the elementary electrode reaction ($n = 2$) and the Faradays constant, respectively.[106]

In order to improve the performance of DSSCs, many scientists have been devoting their research to the CEs. Based on the above selection criteria, many materials have been chosen as the CE of dye-sensitized solar cells, and good progress has been achieved. Novel CE materials present excellent properties even better than those of platinum which are significant to promote the industrialization of dye-sensitized solar cells. According to the material composition, the CEs can be made of platinum, other metal materials, carbon materials, transition metal compounds, conductive polymers, and composites. According to the literature search based on ISI Web of Science and WIOP (Fig. 7), the carbon materials are the most commonly used CE materials in DSSCs, and published papers' share of the total articles on CEs amounts to 23% and the patents account for 47% of the total.

### 1.4. Preparation of counter electrodes

There are many kinds of preparation methods for CEs in DSSCs, including thermal decomposition, electrochemical deposition, chemical reduction, chemical vapor deposition, hydrothermal

Open Access Article. Published on 25 August 2017. Downloaded on 4/25/2024 1:35:01 PM.
This article is licensed under a Creative Commons Attribution-NonCommercial 3.0 Unported Licence.

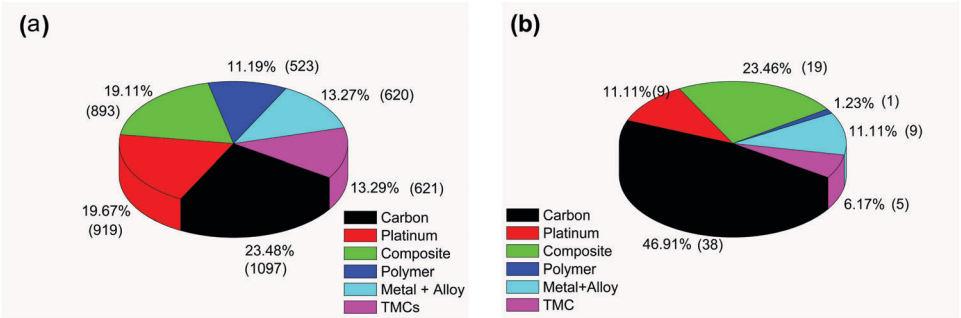


Fig. 7 Percentage (number) of (a) published articles and (b) patents on counter electrodes in dye-sensitized solar cells. Obtained from ISI Web of Science and WIOP (World Intellectual Property Organization) Patentscope (2017-05-08) by keyword searching: "dye-sensitized solar cell" + "counter electrode" + "carbon ■"; + "platinum ■"; + "composite ■"; + "polymer ■"; + "metal and alloy ■" + "transition metal compound including carbide; nitride; oxide; and sulfide ■".

reaction, sputter deposition, *in situ* polymerization, *etc.* The preparation methods have a great influence on particle size, surface area, morphology as well as the catalytic and electrochemical property of the electrodes. The smaller particles and larger surface areas of the electrodes will produce more catalytic active sites and promote the improvement of electrocatalytic activity of the electrodes. With the rapid development of electrode materials in recent years, the preparation methods are diversified. All of the preparation techniques aspire for highly catalytic and conductive electrode materials.

**1.4.1. Thermal decomposition.** Thermal decomposition or pyrolysis is often used for preparing CEs, and is relatively easy and simple. It can help in obtaining CE materials with a porous structure by thermally decomposing the precursor. Tang *et al.* prepared a microporous Pt film with a pore diameter of 100–150 nm by a facile rapid thermal decomposition method.[107] The microporous Pt electrode had higher catalytic activity and smaller resistance than the conventional Pt electrode. The DSSC based on the microporous Pt CE achieved an efficiency of 8.15%; this efficiency is increased by 21.28% compared to the DSSC with conventional Pt CE. Wu *et al.* synthesized bimodal mesoporous carbon (BMC) with embedded Ni nanoparticles (BMCNi) by thermal pyrolysis of the nickel–organic framework (NiOF) in a nitrogen environment followed by acid treatment.[108] The NiOF enabled the formation of small mesopores (3.6 nm). The thermal decomposition and acid treatment generated large mesopores (23.6 nm). The small mesopores contributed to high surface area and the large mesopores contributed to speed up the transport of electrolyte species. Consequently, the DSSC based on the BMCNi CE achieved an efficiency of 8.6%, which was higher than that of the DSSC with Pt (8.4%). Zheng *et al.* prepared podlike nitrogen-doped carbon nanotubes encapsulating FeNi alloy nanoparticles (Pod(N)-FeNi) by the direct pyrolysis of organometallic precursors.[109] DSSCs with Pod(N)-FeNi CE achieved an efficiency of 8.82%, which was superior to that of the DSSC with sputtered Pt CE.

**1.4.2. Electrochemical deposition.** Electrochemical deposition is widely used in the preparation of CEs of DSSCs. Owing to deposition at lower temperatures, the electrodes prepared by electrodeposition have a strong adhesive force and do not have residual thermal stress between the deposition layer and the substrate layer; uniform films can be made on the surface with various complicated shapes; the coating thickness and chemical compositions of the films can be controlled easily. In one word, electrochemical deposition is a very effective technology for preparing CEs. Electrochemical deposition includes galvanostatic electrodeposition, potentiostatic electrodeposition, pulsed electrodeposition, electrophoretic deposition, *etc.* The performances of as-prepared CEs rely on deposition conditions, such as the deposition method, the concentration of ions in solution, pH value, reaction time and temperature, deposition potential, current density, *etc.*[110] Among these factors, the deposition method and electrochemical parameters have more effect on the compositions, morphology and properties of the resultant electrodes.

Zhong *et al.* prepared a Pt CE by the galvanostatic electrodeposition method.[111] The electrodeposited Pt has a much higher electrocatalytic activity than the pure Pt electrode. The electrocatalytic activity of Pt increases with depositing current density. A large current density leads to small Pt grains (~nanometer) and a small current density generates large Pt grains (~100 nanometers). Yoon *et al.* prepared a Pt CE in the presence of a structure-directing surfactant (C16EO8) by the potentiostatic electrodeposition method.[112] The DSSC fabricated with the electrochemically deposited Pt CE exhibited a higher efficiency of 7.6% while the devices with the sputter-deposited or commonly used thermally deposited Pt CEs showed efficiencies of only approximately 6.4%. Hsieh *et al.* investigated the Pt film with a nanoflowers (PtNFs) structure on ITO glass prepared by the pulse reversal electrodeposition (PRE) technique.[113] The DSSC based on the as-prepared PtNF CE showed a conversion efficiency of 7.74% while the cell with an additional thin (2 nm) sputtered layer of Pt on the PtNF film showed a much higher efficiency of 8.13%. Sun *et al.* prepared a NiS CE by a facile periodic potential reversal (PR) technique to supersede Pt CEs of DSSCs.[114] The CEs prepared by PR have a large surface area and higher catalytic activity than those prepared by the traditional potentiostatic (PS) technique. The DSSC with the NiS deposited by the PR technique performed much better (6.82%) than that obtained by the PS method (3.22%).

 This journal is © The Royal Society of Chemistry 2017

Open Access Article. Published on 25 August 2017. Downloaded on 4/25/2024 1:35:01 PM.
This article is licensed under a Creative Commons Attribution-NonCommercial 3.0 Unported Licence.

**1.4.3. Chemical reduction.** Compared with other methods, the chemical reduction technique has some advantages, such as simple procedure, easy operation, reaction at low temperature, and low cost, which make this technique suitable for large-scale production applications. Huo *et al.* prepared CoS films by repetitive electrophoretic deposition and ion exchange deposition, and then treated them with $NaBH_4$ + $H_2SO_4$.[115] The resultant honeycomb-like CoS CE had a large specific surface area, good catalytic activity and lower charge-transfer and series resistances. The DSSC based on the CoS CE achieved a power conversion efficiency of 7.72%. Dao *et al.* synthesized Pt nanourchins (PtNUs) on FTO glass by facile one-pot room temperature chemical reduction of $H_2PtCl_6$ using formic acid.[116] The PtNUs have very low charge-transfer resistance and a large surface area with a 3D nanostructure. The DSSC based on PtNUs achieved an efficiency of 9.39% while the efficiency of the DSSC with Pt-sputtered CE was only 8.51%. In order to achieve better dispersion and particle size control, Song *et al.* explored direct deposition of Pt nanoparticles by using a simple and urea-assisted homogeneous deposition and ethylene glycol (EG) reduction method.[117] The hydrolysis of urea at lower temperature produced platinum hydroxide, which was distributed on the FTO substrate due to the electrostatic repulsion, and then reduced to Pt by EG. Owing to the high electrocatalytic activity and small charge transfer resistance at the electrolyte/electrode interface, the DSSC based on the as-prepared Pt CE achieved a high efficiency of 9.34%.

**1.4.4. Chemical vapor deposition.** Chemical vapor deposition (CVD) is a chemical process used to produce high-quality solid materials. In a typical CVD, the substrate is exposed to one or more volatile precursors; the precursors react and/or decompose on the surface of the substrate to produce the desired deposit. Physical vapor deposition uses a liquid or solid source and chemical vapor deposition uses a chemical vapor. Nowadays, CVD technology is widely applied in the preparation of various materials, including semiconductors, synthetic diamonds, oxides, sulfides, nitrides, carbides, and two or multi-element compounds. Polymerization by CVD is perhaps the most versatile among all applications. The physical and chemical properties of the as-prepared material can be precisely controlled by gas doping during the deposition process.

Nam *et al.* prepared aligned carbon nanotube (CNT) arrays by chemical vapor deposition.[118] A highly ordered array structure (Fig. 8) is beneficial for the fast electron transfer and is helpful for the rapid diffusion of the electrolyte inside the electrode. The DSSC based on the as-prepared CNT CE achieved a high conversion efficiency of 10.04%. Xue *et al.* developed a strategy for creating 3D graphene–CNT hollow fibers with radially aligned CNTs (RACNTs) seamlessly sheathed by a cylindrical graphene layer *via* a one-step chemical vapor deposition method using an anodized Al wire template.[119] By controlling the anodization time and Al wire diameter, the diameter of the graphene hollow fiber and the length of the RACNTs can be tuned. These fibers, with a controllable surface area, meso-/micropores, and superior electrical properties, are excellent electrode materials for all-solid-state wire-shaped supercapacitors and DSSCs.[120] The DSSCs using the fiber as a CE achieved a power conversion efficiency of 6.8% and outperformed their counterparts that used Pt wire as CE by a factor of 2.5.

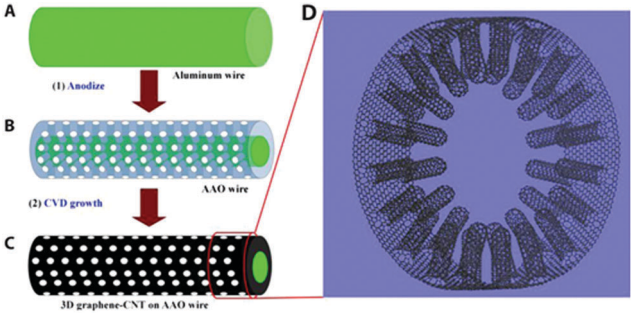


Fig. 8 Schematic diagrams showing the synthesis and microstructures of a 3D graphene–RACNT fiber. (A) Aluminum wire. (B) Surface anodized aluminum wire (AAO wire). (C) 3D graphene–RACNT structure on the AAO wire. (D) Schematic representation of the pure 3D graphene–RACNT structure. Reprinted with permission from ref. 119. Copyright (2015) American Association for the Advancement of Science (AAAS).

**1.4.5. Hydrothermal reaction.** Hydrothermal reaction is a reaction occurring in an aqueous medium at high temperature and pressure. Compared with other methods, the hydrothermal reaction method is easier for researchers to operate and to realize large-scale preparation. This method helps to produce various materials and structures by controlling the reaction temperature, time, pressure, packing ratio and reactant ratio. The hydrothermal reaction is often used in the preparation of CEs, particularly in transition metal compound and composite CEs.

Xiao *et al.* prepared a PtNi alloy with slender tentacles by a hydrothermal method and used the PtNi alloy as the CEs for DSSCs.[121] Owing to its 3D surfaces, the 2 h hydrothermal-processed PtNi CE had the highest catalytic activity and the lowest charge transfer resistance. The DSSC based on this PtNi bimetallic CE achieved a conversion efficiency of 8.95%, which was close to that of the device with pure Pt CE (9.24%) under the same conditions. Huo *et al.* synthesized $CoMoO_4/Co_9S_8$ hybrid nanotubes by a simple two-step hydrothermal method.[122] The $CoMoO_4/Co_9S_8$ CE had a rough surface and smaller $R_S$ and $R_{CT}$ than a Pt CE. The DSSCs assembled with a $CoMoO_4/Co_9S_8$ CE achieved a power conversion efficiency of 8.60%, which is higher than that of DSSCs with a $Co_9S_8$ CE (7.69%) or a Pt CE (8.13%).

**1.4.6. Sputter deposition.** Sputter deposition is a physical vapor deposition (PVD) method of thin film deposition by sputtering. This involves ejecting a material from a "target" that is a source on a "substrate" such as a conductive glass. Sputtering is one of the main processes for making efficient photovoltaic solar cells. An important advantage of sputter deposition is that even materials with very high melting points are easily sputtered. The films prepared by sputtering have high purity, uniformity, repeatability, better adhesion on the substrate, and accurately controlled loaded amount. Sputtering can be performed top-down while evaporation must be performed bottom-up. Based on the materials used and controlling modes, there are radio frequency (RF) sputtering, vacuum sputtering, magnetron sputtering, ion-beam sputtering, reactive sputtering, ion-assisted sputtering, *etc.* The standard counter electrode,

Open Access Article. Published on 25 August 2017. Downloaded on 4/25/2024 1:35:01 PM.
This article is licensed under a Creative Commons Attribution-NonCommercial 3.0 Unported Licence.

frequently used for comparison, sputtered Pt electrode, is made by this sputter deposition method.[123]

Cheng *et al.* reported the preparation of high quality copper indium gallium diselenide (CIGS) thin films by magnetron sputtering from a single ternary alloy target and annealing under Se vapor at 550 °C for 30 min.[124] The CIGS films as CE exhibited good electrocatalytic activity and high conductivity. The DSSC with the CIGS CE achieved an efficiency of 7.13%, comparable to the efficiency of the DSSC using a Pt CE (6.89%). Soo *et al.* prepared nickel nitride ($Ni_2N$) films with a cauliflower-like nanostructure and tetrahedral crystal lattice by reactive sputtering of nickel under a $N_2$ atmosphere at room temperature.[125] The $Ni_2N$ electrodes displayed superior electrocatalytic activity for the polysulfide redox electrolyte. Compared to the CdSe-based quantum dot-sensitized solar cell (QDSSC) using Pt CEs with an efficiency of 2.01%, the CdSe-based QDSSC using the $Ni_2N$ CEs achieved an efficiency of 2.80%.

**1.4.7. *In situ* polymerization.** The *in situ* polymerization reaction is often used in the preparation of conductive polymer CEs, such as those based on polyaniline (PANI), polypyrrole (PPy), and polythiophene (PT) derivatives, poly(3,4-ethylenedioxythiophene):polystyrenesulfonate (PEDOT), *etc.* The appropriate initiator is added in the organic monomer solution, which triggers the polymerization of these organic monomers. If a conductive glass substrate is placed in the reaction solution, the polymer will *in situ* grow on the surface of the substrate, and a conductive polymer CE thus is *in situ* obtained. The conventional polymerization method is simple, but it often produces some disadvantages, including the aggregation of polymers and large interfacial charge transfer resistance between polymers and substrates, which is not conducive to the improvement of photovoltaic performance of DSSCs. Using *in situ* polymerization, the disadvantages will be avoided, and the photovoltaic parameters of DSSCs will be improved.[126]

Anothumakkool *et al.* prepared a flexible, free-standing, Pt- and TCO-free counter electrode from polyethylenedioxythiophene (PEDOT)-impregnated cellulose paper by simple and scalable *in situ* polymerization all through a roll coating technique.[127] The PEDOT paper (40 μm thick) had high conductivity (357 S $cm^{-1}$) and low sheet resistance (4 Ω $sq^{-1}$), which are superior to that of the conventional FTO substrate. A DSSC based on the PEDOT CE displayed an efficiency of 6.1%, and the efficiency of the DSSC based on the Pt/FTO CE was 6.9%.

The preparation technology of counter electrodes is more sophisticated than the above mentioned methods. However, there is no method that is omnipotent and the choice of preparation methods should be based on the actual situation.

### 1.5. Characterization of counter electrodes

In order to understand the relative reaction process mechanism, such as charge generation, charge transfer and charge recombination,[68,128–130] to design novel materials and enhance the photovoltaic performance of the DSSCs, a variety of characterization methods have been developed.[131–133] Electrochemical and photoelectrochemical methods have been considered as the most powerful tools in investigating the process mechanism, analyzing component interactions and evaluating the performances of the DSSCs.[129,134,135] They include current–voltage (*I–V*) characterization, cyclic voltammetry (CV), electrochemical impedance spectroscopy (EIS), intensity-modulated photocurrent spectroscopy (IMPS) and intensity-modulated photovoltage spectroscopy (IMVS).

**1.5.1. Photovoltaic measurements.** The current–voltage (*I–V*) characteristic curve is the relationship between the output current and voltage of the solar cell under standard full spectrum irradiation, and is used to determine the photovoltaic parameters of the device.[10,68,136] In the *I–V* curve (Fig. 9), the open circuit voltage ($V_{OC}$) and short circuit current ($I_{SC}$) or short circuit current density ($J_{SC}$) are the intercepts of the *J–V* curve in the lateral and vertical axes, respectively. $J_{SC}$ is the current density of the cell in short circuit connection ($V = 0$), which indicates the maximum photocurrent output capability of the cell; $V_{OC}$ is the voltage of the cell in open circuit connection ($I = 0$), which indicates the maximum photovoltage output capability of the cell. At the inflection point of the curve corresponding to the photocurrent ($I_{mp}$) and photovoltage ($V_{mp}$) of the maximum output power ($P_{max}$), the projected rectangular area of this inflection point is the actual maximum output power of the device. The ratio of $P_{max}$ to the product of $V_{OC}$ and $J_{SC}$ is defined as the fill factor (FF), which takes a value from 0 to 1. Various power losses in the solar cells are electrically equivalent to resistances in series and in parallel (shunt) and reduce the FF. A high FF value means a more preferable rectangular shape for *I–V* curves and high efficiency for the device.

The overall sunlight-to-electric power conversion efficiency ($\eta$ or PCE) of the DSSC can be calculated as follows:

$$\eta = \frac{I_{mp} V_{mp}}{P_{in} A} = \frac{J_{SC} V_{OC} FF}{P_{in}} \quad (2)$$

where $P_{in}$ is the power density of the incident light and $A$ is the active surface area of the cell.

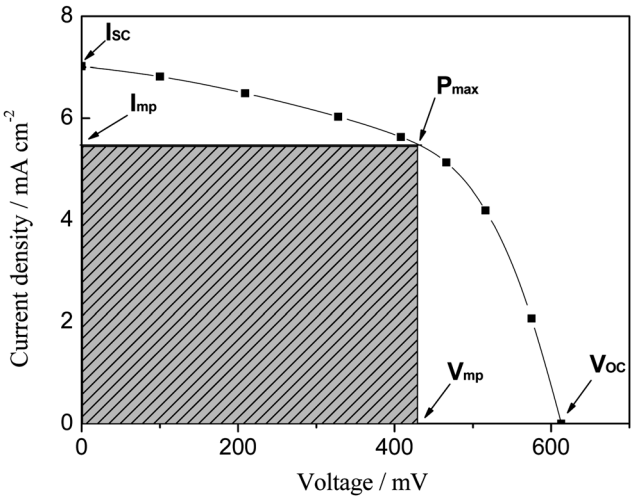


Fig. 9 *J–V* characteristic curves for the DSSCs.

Open Access Article. Published on 25 August 2017. Downloaded on 4/25/2024 1:35:01 PM.
This article is licensed under a Creative Commons Attribution-NonCommercial 3.0 Unported Licence.

The incident photon to current conversion efficiency (IPCE), sometimes referred to as "external quantum efficiency" (EQE), corresponds to the number of electrons ($N_e$) measured as photocurrent in the external circuit divided by the number of monochromatic photons ($N_p$) that strike the solar cell in unit time, which is an important parameter for determining the photovoltaic performance of solar cells. It can be written as

$$\mathrm{IPCE}\,(\lambda) = \frac{N_e}{N_p} = \frac{1240 \times J_{SC}(\lambda)}{\lambda \times P_{in}} \quad (3)$$

Here, $J_{SC}$ ($\lambda$) is the short-circuit photocurrent density (mA cm$^{-2}$) under monochromatic light illumination with wavelength ($\lambda$, nm) and $P_{in}$ is the power (mW cm$^{-2}$) of incident light. According to the IPCE generation, the IPCE is related to the sunlight harvesting efficiency (LHE), quantum efficiency ($\varphi_{inj}$) for electron injection into the $TiO_2$ conduction band from the excited state of the dye, and charge collection efficiency ($\varphi_{cc}$) at the interface between the surface of TCO glass and $TiO_2$ film. Thus, IPCE can be expressed as[63,68,137]

$$\mathrm{IPCE}\,(\lambda) = \mathrm{LHE}(\lambda)\varphi_{inj}\varphi_{cc} \quad (4)$$

Traditionally, the IPCE is measured under short-circuit conditions. There are two essential methods: the DC and the AC method. After a systematic study, the Han group recommended the AC mode with a frequency lower than 5 Hz and the DC mode with a large photon flux ($10^{16}$ cm$^{-2}$ s$^{-1}$) of the monochromatic light in the measurement of IPCE.[138]

DSSC is a photochemical solar cell. It has a high interfacial capacity and thus slow electrical response, which means a longer response time to achieve the same photoelectric conversion as a Si solar cell. Han *et al.* found the dependence of photovoltaic data of the DSSCs on the voltage sweep direction and sampling delay time.[138,139] They defined voltage sweep from short circuit to open circuit as normal scan and that from open circuit to short circuit as reverse scan. Their results showed that greater $V_{OC}$ and FF were obtained from the reverse scan, while the $J_{SC}$ remained the same. With an increase of sampling delay time, the differences between the reverse and the forward were reduced, and the power conversion efficiency was almost unchanged when the sampling delay time was more than 40 ms. Aoki *et al.*[140] and Takagi *et al.*[141] also obtained similar results. Additionally, determining the cell area using a shading mask with an area smaller than that of $TiO_2$ electrodes will improve measurement accuracy.[138,139]

The standard irradiance spectrum for solar cell measurements is AM 1.5 G; however, the actual light source often used is a white light from a solar simulator, and most of the solar simulators do not provide a standard AM 1.5G spectrum. A careful correction is needed.[142,143]

**1.5.2. Cyclic voltammetry.** Electrochemical methods are used to characterize all the components of the DSSCs. They give important information on the energy levels of the components, the reversibility of electrochemical reactions and the kinetics of electrochemical processes. Cyclic voltammetry (CV) is an important tool for investigating counter electrodes.[144–146] A three-electrode system is widely used to carry out cyclic voltammetry which consists of a working electrode, a reference electrode, and a counter (auxiliary) electrode. The potential is swept at a constant rate and reversed at a certain point, while the current is monitored continuously. The potential is measured between the working electrode and the reference electrode, while the current is measured between the working electrode and the counter electrode. These data are plotted as current ($I$) *versus* applied potential ($E$, often referred to as "potential").

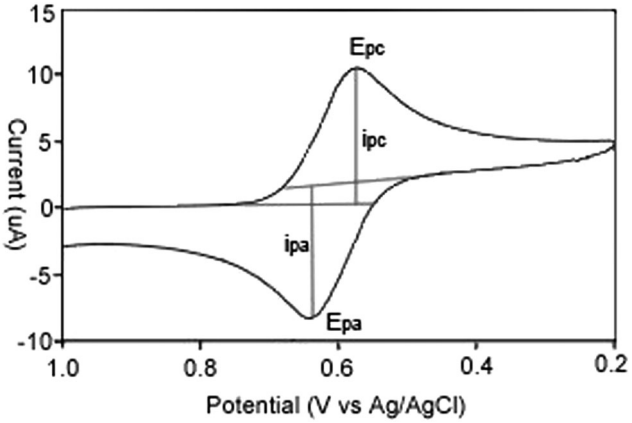


Fig. 10 Typical cyclic voltammogram where $i_{pc}$ and $i_{pa}$ show the peak cathodic and anodic current respectively for a reversible reaction.

A typical cyclic curve is shown in Fig. 10. The waveform of even reversible redox couples is complex owing to the combined effects of polarization, diffusion and rate of electron transfer. The potential difference between the two peaks ($\Delta E_p = |E_{pc} - E_{pa}|$) is an important parameter. The $\Delta E_p$ value is negatively correlated with the redox reaction rate, and the electron transfer rate can be calculated from $\Delta E_p$ by the theory suggested by Nicholson in 1965.[145] The theory shows that smaller $\Delta E_p$ results in a faster redox reaction, indicating a higher electrocatalytic activity.[145] In the ideal reversible couple for an $n$ electron process, $\Delta E_p = E_{pa} - E_{pc} = 56.5$ mV/$n$.[144] The experimentally observed values are often greater. For instance, for the one electron process, $\Delta E_p$ approached 70 or 80 mV. The difference between theory and practical measurements is deemed as the activation barrier or overpotential for electron transfer. Larger overpotential is disadvantageous for the redox reaction.

As for current, reversible couples are characterized by $i_{pa}/i_{pc} = 1$. In other words, the more reversible the redox couple is, the more similar the oxidation peak will be in shape to the reduction peak. When a reversible peak is observed, thermodynamic potential (a half cell potential) $E^0_{1/2}$ can be determined. Many redox processes observed by CV are quasi-reversible or non-reversible. In such cases the thermodynamic potential $E^0_{1/2}$ is often deduced by simulation. The irreversibility is indicated by $i_{pa}/i_{pc} \neq 1$. The irreversible deviations are attributable to a subsequent chemical reaction that is triggered by the electron transfer. Such electrochemical processes can be complex, involving isomerization, dissociation, deposition, *etc.* Additionally, the scan rate determines the peak current. If the electron transfer at the electrode surface is fast and the current is limited by the diffusion of measured species to the electrode

Open Access Article. Published on 25 August 2017. Downloaded on 4/25/2024 1:35:01 PM.
This article is licensed under a Creative Commons Attribution-NonCommercial 3.0 Unported Licence.

surface, then the peak current will be proportional to the square root of scan rate. The correlation among peak current density ($J_{red}$), diffusion coefficient ($D_n$), and scan rate ($\nu$) can be expressed by the Randles–Sevcik equation:[147,148]

$$J_{red} = KACn^{1.5}D_n{}^{0.5}\nu^{0.5} \quad (5)$$

where $K$ is a constant (=2.69 × $10^5$), $n$ is the number of electrodes contributing to the charge transfer, $A$ is the electrode area, and $C$ represents the bulk concentration of redox species.

In DSSCs, the iodide/triiodide couple is often used as a redox mediator in liquid electrolytes. The CV curves in iodide/triiodide electrolytes often contain two pairs of redox peaks. The left pair refers to reaction (6) and the right pair corresponds to reaction (7). Reaction (6) has a significant influence on the performance of the DSSCs, and this should be majorly concerned, especially in the anode reaction.[149,150]

$$I_3^- + 2e^- \rightarrow 3I^- \quad (6)$$

$$3I_2 + 2e^- \rightarrow 2I_3^- \quad (7)$$

**1.5.3. Electrochemical impedance spectroscopy.** Electrochemical impedance spectroscopy (EIS) is a powerful tool for studying the kinetics of charge transport and electron–hole recombination and for evaluating the electrocatalytic activity of counter electrodes in DSSCs.[151–154] In principle, the potential applied to a system is perturbed by a small sine wave modulation and the resulting sinusoidal current response (amplitude and phase shift) is measured as a function of modulation frequency. From the applied perturbation and the measured response, the magnitude of the impedance is determined. The impedance is defined as the frequency domain ratio of the voltage to the current and is a complex number. According to the appropriate equivalent circuit, the measured data are fitted by some software and the electrochemical parameters such as series resistance ($R_S$), charge transfer resistance ($R_{CT}$), diffusion resistance ($Z_W$) and constant phase element (CPE) can be obtained, and thus the electrochemical properties of the system can be analyzed.[155] There are various dielectric mechanisms in an electrochemical system, and each dielectric mechanism has its characteristic frequency, and each electrochemical impedance and process in this system thus can be investigated by this method.[68,137,148] EIS data are often expressed in a Nyquist plot or a Bode plot. In a complete Nyquist plot for DSSCs, there are usually three semicircles. The starting point is series resistance ($R_S$), mainly caused by the conductive substrate, connecting wires, *etc.*; the first semicircle (high frequency) refers to the charge transfer resistance ($R_{CT}$) at the CE/electrolyte interface; the second semicircle (middle frequency) corresponds to the charge transfer resistance ($R_{CT}$) at the anode/dye/electrolyte interface; the third semicircle (low frequency) is attributed to the redox species diffusion resistance ($Z_W$).[148,154] Owing to the small distance between two electrodes and the low viscosity of the electrolyte, the third semicircle is often not observed.

Huang *et al.* studied the p-type dye-sensitized NiO solar cells by EIS.[154] To determine the Pt amount on counter electrodes, three counter electrodes with the same area and different

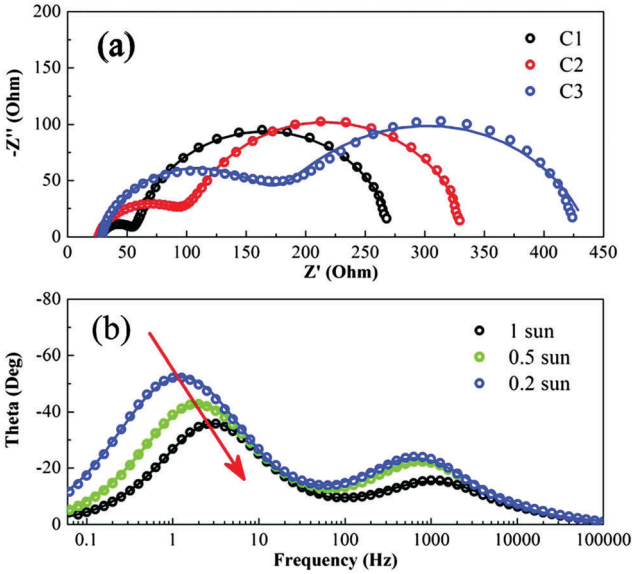


Fig. 11 (a) Nyquist plots of NiO p-DSSCs (C1–C3) using different counter electrodes under 1 Sun at open circuit voltage. Solid lines show the fitting curves. (b) Bode plots of the cell C3 under different illumination intensities (1 Sun, 0.5 Sun, and 0.2 Sun). Solid lines show the fitting curves. Reprinted with permission from ref. 154. Copyright (2011) American Chemical Society.

Pt amounts (C1, 10 μg $cm^{-2}$; C2, 2 μg $cm^{-2}$; and C3, 1 μg $cm^{-2}$) were prepared. It is clear that the C1 electrode has a smaller charge transfer resistance ($R_{CT}$) at the electrolyte/electrode interface than the other two electrodes from the first semicircle at the high frequency region in the Nyquist plots shown in Fig. 11(a). The low resistance of the C1 electrode is due to its high platinum loading, which facilitates electrocatalytic activity towards the iodide/triiodide redox couple.

To understand the kinetic process related to the second semicircle in the Nyquist plot, the illumination intensity was changed from 0.2 to 1.0 Sun. Fig. 11(b) shows the Bode plots using C1 as CE under different light intensities at open circuit. With the decrease of light intensity, the low frequency peak obviously shifts to the lower frequency region, implying a trend of longer time constant. As we know, the recombination process is expected to be slow under low light intensities due to the less photogenerated hole in the NiO film. Therefore, the results in Fig. 11(b) provide strong evidence to assign the second semicircle in the Nyquist plots to the recombination charge transfer process at the NiO/dye/electrolyte interface.[154]

**1.5.4. Intensity-modulated photocurrent and photovoltage spectroscopy.** Intensity-modulated photocurrent spectroscopy (IMPS) and intensity-modulated photovoltage spectroscopy (IMVS) are photoelectrochemical techniques, which are fairly similar to the EIS method. They are based on a controllable modulation of incident light intensity. The input signal is generally composed of a bunch of stable background light signals and a beam of light signal which is perturbed by a small sine wave modulation, and the two parts are superimposed on the target. The output signal is the corresponding steady state photocurrent and modulated photocurrent (short circuit state)

Open Access Article. Published on 25 August 2017. Downloaded on 4/25/2024 1:35:01 PM.
This article is licensed under a Creative Commons Attribution-NonCommercial 3.0 Unported Licence.

or steady state photovoltage and modulated photovoltage (open circuit state). By comparing the frequency response of the input signal and the output signal amplitude and phase, and fitting relative data from IMPS and IMVS, the electron diffusion coefficient ($D_n$), electron life time ($\tau_n$), absorption coefficient ($\alpha$) and important information can be obtained, which provide useful tools to study the electron transport mechanism and charge transfer kinetics in DSSCs.[136,156–162]

Under short circuit conditions, the photocurrent response is measured at different frequencies in IMPS and the electron transport time ($\tau_d$) can be expressed as

$$\tau_d = \frac{1}{2\pi \times f_{\min,\mathrm{IMPS}}} \quad (8)$$

Here, $f_{\min,\mathrm{IMPS}}$ is the frequency corresponding to the lowest point of the imaginary part of the IMPS spectrum. Under open circuit conditions, the photovoltage response is measured at different frequencies in IMVS and the electron life time ($\tau_n$) can be expressed as

$$\tau_n = \frac{1}{2\pi \times f_{\min,\mathrm{IMVS}}} \quad (9)$$

Here, $f_{\min,\mathrm{IMVS}}$ is the frequency corresponding to the lowest point of the imaginary part of the IMVS spectrum. The charge collection efficiency ($\eta_{cc}$) can be obtained by as follows:

$$\eta_{cc} = \frac{1}{1 + \tau_d/\tau_n} \quad (10)$$

The shorter the $\tau_d$ and the longer the $\tau_n$ are, the higher is the $\eta_{cc}$, which is conducive to enhance the photovoltaic performance of DSSCs.

IMPS/IMVS and EIS are frequency-domain techniques. IMPS/IMVS measures the current/voltage response to a modulated light intensity superimposed on a steady light intensity, whereas EIS measures the current response to a modulated applied bias superimposed on a constant applied voltage. The analysis of IMPS/IMVS is based on the models and equations, whereas EIS is evaluated using resistance and capacitance elements as an equivalent circuit.[101,160,162–164] IMPS/IMVS and EIS have their own strengths and weaknesses in the study of transportation and recombination. For instance, EIS is not suitable for the research on the electron transport process in $TiO_2$ films owing to the Warburg feature associated with electron transport, which may overlap with other processes.[165–167] However, the IMPS technique is suitable to examine the electron transportation in $TiO_2$ films over a range of light intensities.[168,169] The electron transfer process across both the $TiO_2$/dye/electrolyte interface and the electrolyte/Pt–TCO interface can be detected by EIS at any bias under illumination or in the dark. The IMVS mainly involves the electron transfer process across the $TiO_2$/dye/electrolyte interface at open circuit under illumination. But the IMVS can obtain the characteristic time for electron recombination, and the technique is not affected by TCO glass or the counter electrode.[154]

By combining EIS, IMPS and IMVS, the Dai group studied the relationship between the series resistance ($R_S$) and the dynamic process of DSSCs.[170] The results showed that under short circuit conditions, electron transport was dominated by the series resistance in TCO ($R_h$) and at the electrolyte/Pt–TCO interface ($R_1$). These resistances had no significant influence on charge recombination under open circuit conditions. As $R_h$ or $R_1$ increased (without silver grid lines or without Pt), the electron transit time (delay time, $\tau_d$) became longer and the electron lifetime ($\tau_n$) remained invariant. To investigate the influence of the Nernst diffusion resistance ($R_3$), they varied the thicknesses of the bulk electrolyte layer, and found that $R_3$ affected the electron transfer and charge transport.[170] $R_3$ limited the electron extraction from the $TiO_2$ film to the external circuit, and influenced the electron transfer from the $TiO_2$ film to triiodide in the electrolyte.

# 2. Transparent and flexible counter electrodes

## 2.1. Conductive substrates

In DSSCs, the counter electrode is constructed by coating different kinds of conductive materials on a conductive substrate. According to the working principle of the DSSCs, the main function of the conductive substrate is collecting and transmitting electrons, transmitting light, and supporting the solar cell. Therefore, the substrates must meet the following three requirements: high conductivity, good light transmittance on at least one side, proper mechanical strength to support the cell body to form a sealed stable device. According to these requirements, three kinds of materials can be candidates for electrode substrates in DSSCs: conductive glass, conductive plastic and metal substrate.

**2.1.1. Conductive glass substrates.** Transparent conducting films (TCFs) are widely applied in various photoelectronic devices, such as liquid-crystal displays, OLEDs, touchscreens, and photovoltaics.[171] For photovoltaic applications, TCFs are fabricated from both inorganic and organic materials. Inorganic films typically are made up of a layer of transparent conducting oxide (TCO) on transparent glass to form a conductive glass substrate. In general, TCO used as electrode materials in solar cells should have a bandgap greater than 3.2 eV to avoid absorption of light over most of the solar spectra and have incident light transmittance greater than 80%; meanwhile, it should have a minimum carrier concentration on the order of $10^{20}$ $cm^{-3}$ for low resistivity and electrical conductivity higher than $10^3$ S $cm^{-1}$ for efficient carrier transport. Mobility in these films is limited by ionized impurity scattering due to the large amount of ionized donors, and mobility is on the order of 40 $cm^2$ $V^{-1}$ $s^{-1}$ for the best performing TCOs. In addition, the current TCOs used in industry are primarily n-type conductors, meaning their primary conduction is as donors of electrons. This is because electron mobility is typically higher than hole mobility.[172,173]

In a DSSC, the conductive glass substrate plays an important role in transmitting the incident light and collecting the electrons. In this sense, transmittance and conductivity may be equally important.[174] The TCO includes indium-doped tin

Open Access Article. Published on 25 August 2017. Downloaded on 4/25/2024 1:35:01 PM.
This article is licensed under a Creative Commons Attribution-NonCommercial 3.0 Unported Licence.

oxide (ITO), fluorine-doped tin oxide (FTO), aluminum-doped zinc-oxide (AZO), antimony-doped tin oxide (ATO), *etc.* Among them, ITO and FTO are the most widely used in DSSCs. The ITO glass shows high transparency and high electrical conductivity at room temperature, which make it an important candidate for electrode substrates in DSSCs. However, indium is a rare element, and the application of ITO is limited. More importantly, the conductivity of the ITO layer is severely destroyed at high temperature. When it is heated at 300 °C or higher, its electrical resistance increases more than three times which is ascribed to the fact that the oxygen from atmosphere bonds to a portion of the oxygen-vacancies in the heated ITO, and thus reduces electron supply and conductivity of the substrates. As the anode substrate of DSSCs, the TCO glass must be calcinated at 400–600 °C to solidify an oxide semiconductor on it. Thus, ITO glass cannot qualify for this task.[175,176]

The transparent conducting oxide of FTO has good light transmittance, good electrical conductivity, good adhesion with the glass substrate, high Moh's hardness, good chemical stability, corrosion resistance and other merits. More importantly, FTO has been known to be resistant to heat up to 600 °C, which makes FTO the most widely used electrode substrate in DSSCs among the several kinds of TCOs.[177]

Due to the different configurations, materials and fabricated conditions used, the choice of an appropriate TCO for the photoanode of DSSCs is not always easy, and the reports are often ambiguous.[178] For example, Zumeta and Sima *et al.* highly recommended FTO as the TCO, owing to its low and temperature-stable resistivity.[176,178] On the other hand, Yoo *et al.* reported a better photovoltaic performance of the DSSC with ITO/ATO/$TiO_2$ than with the conventional FTO.[179] However, owing to no requirement for high temperature calcination, ITO is often used as a rigid conductive substrate for CEs.

**2.1.2. Conductive polymer substrates.** Nowadays, polyethylene terephthalate (PET) and polyethylene naphthalate (PEN) are the most common plastic substrates.[180] The ITO coated on PET film (ITO/PET) and PEN film (ITO/PEN) are the most often used conductive polymer substrates in DSSCs.[181,182] For a rigid substrate used in DSSCs, the heat treatment at 450 °C for 30 min is an indispensable step to solidify the anode and cathode films on the surface of the conductive layer and to remove residues, binders and solvent presented in the precursor. However, for polymer PET and PEN substrates, thermal stability primarily depends on the maximum processing temperatures. When practical processing temperatures exceed 150 °C, the ITO/PET and ITO/PEN substrates start to deform, and even melt at 235 °C.[183] The temperature of thermal treatment for polymer substrates cannot exceed 150 °C.[184,185] Such a low annealing temperature cannot effectively decompose the residues from the precursor and also results in poor adhesion between the electrode films and the plastic substrates. In order to overcome these problems in conductive polymer substrates, a lot of new methods have been explored, such as screen printing, ink-jet printing, gravure printing, electrospray, electrophoretic deposition, spin coating, calendering press, static press, UV irradiation, electrospinning, photoplatinization, electrodeposition, and atomic layer deposition.

The commercial ITO/PET and ITO/PEN conductive polymer substrates are prepared by magnetron sputtering ITO on the PET and PEN substrates and then are annealed at high temperature. The high impedance ITO/polymer substrate is mainly used in the touch screen in mobile communication. The low impedance ITO/polymer substrate is mainly used in the field with high conductivity requirements, such as transparent electrodes for solar cells, electrode materials in electrochromic devices, membrane switches, *etc.* Both kinds of conductive polymer substrates have high transparency (>80%) in the visible spectrum, a low sheet resistance of 10–15 Ω $sq^{-1}$, which is close to the typical value of the FTO-coated glass (7–15 Ω $sq^{-1}$), high thermo-stability, low moisture permeability, and high chemical stability. Compared with the PET substrate, the PEN substrate has better heat resistance, water resistance, radiation resistance and higher Young's modulus.

Pringle *et al.* deposited PEDOT on the ITO-PEN substrate by a cheap and facile electrodeposition technique.[186] The DSSC with PEDOT/ITO-PEN cathode achieved a PCE of 8%, while the device based on Pt/FTO achieved a PCE of 7.9% under the same conditions. Pt spray-coated on ITO/PEN as the CE coupled with a Ti foil anode yielded a DSSC with a PCE of 8.5%.[187] Interestingly, a quasi-solid-state DSSC assembled with an optimized PET membrane exhibited a PCE of 10.25% under an irradiation of 100 mW $cm^{-2}$.[188]

In addition to PET and PEN, polyimide (PI) can also be used as a polymer substrate owing to its excellent thermal/chemical stability and superior mechanical strength.[189,190] Lin *et al.* deposited a bilayer $Ni_3S_2$/Ni–P film on a PI substrate through a series of chemical/electrochemical processes.[191] The bottom layer Ni–P replaced conventional TCO as a conductive layer, and the top layer $Ni_3S_2$ was used as the catalyst for $I_3^-$ reduction. The resultant flexible and TCO-free CE DSSC yielded an impressive PCE of 6.28%, which is higher than that of the DSSC based on the Pt/ITO/PEN flexible CE.

Interestingly, a cellulose fibre-based photoanode and a nanoscale microfibrillated cellulose-based biopolymer electrolyte were successfully prepared and used in DSSCs, and the devices produced a PCE of 3.55% under 1 Sun irradiation.[192]

Owing to features such as high flexibility, transparency[193] and easy-to-process polymer thermoplasticity[194] poly(dimethylsiloxane) (PDMS) membranes were used as top- and bottom-sealing substrates to replace glass/metals. A light-cured polymer-based flexible DSSC with a patterned ''Fakir''-shaped super-hydrophobic architecture on the external side (shown in Fig. 12) achieved a conversion efficiency exceeding 5%.[195]

**2.1.3. Metal substrates.** Metal materials have excellent electrical conductivity, good flexibility and ductility, thermal stability withstanding high temperature treatment, lower sheet resistance compared to ITO, as well as low cost. The use of metal materials as electrode substrates of DSSCs can not only reduce the cost of the devices, but also help to improve the performance of the solar cell by reducing the internal resistance. Nowadays, numerous metals are tried as substrates in DSSCs including StSt, W, Ti, Co, Ni, Pt, Al, Cu, Zn, *etc.*

The metal foil or sheet are not light transmissible, so they cannot be used as substrates of the photoanode (or photoelectrode). The metal mesh and wire allow sunlight to go through, and they

Open Access Article. Published on 25 August 2017. Downloaded on 4/25/2024 1:35:01 PM.
This article is licensed under a Creative Commons Attribution-NonCommercial 3.0 Unported Licence.

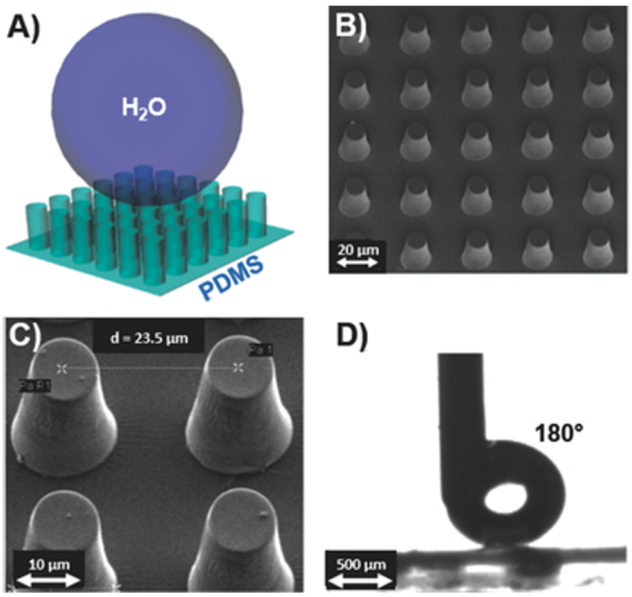


Fig. 12 (A) "Fakir"-shaped external side of the PDMS membrane; (B and C) FESEM images of the pillared array uniformly distributed on the PDMS surface; (D) super-hydrophobic nature of the fabricated substrate as verified by water-contact-angle measurements. Reprinted with permission from ref. 195. Copyright (2016) John Wiley & Sons Ltd.

can be used as substrate materials of electrodes by ingenious design. Besides the lack of transparency, another disadvantage of the metal substrate is it is more prone to corrosion in the aggressive redox electrolyte medium.[196–198] Among these metals, high purity (>99%) titanium foil is the most stable and resistant to corrosion due to the formation of a natural passivating oxide on its surface. The drawback of this material is the higher cost (12–40 \$ per $m^2$) compared to stainless steel (StSt) sheets (4 \$ per $m^2$).[199] The Ma group[196] and the Toivola group[197] researched the corrosion behaviors of titanium, nickel, aluminum, and copper, as well as stainless steel (StSt), zinc-coated steel and plain carbon steel in a liquid electrolyte containing the triiodide/iodide redox couple, and found that titanium and stainless steel have better chemical stability than others. Other cheaper metals such as nickel or aluminum may also work well if proper protection is provided, for instance, the TiN/polyimide composite coating on the photoelectrode[200] or thick catalyst coating on the CE.[201]

Man *et al.*[198,202] investigated the influence of metal substrates and found that W, Ti, StSt, and Zn could be n-type semiconductor oxides after annealing. On the other hand, Al, Co, and Ni could be insulating oxides, which were effective supporting substrates when thin layers of both ITO and $SiO_x$ were sputtered on the metal surfaces.

### 2.2. Transparent counter electrodes

Different from the routine CEs with a smooth surface to reflect the unabsorbed light back to the cell and enhance utilization of sunlight, some special CEs are transparent and allow sunlight to pass, such as photocathodes, bifacial electrodes, mesh electrodes, *etc.* The photocathode was first assembled by Paulose *et al.* in 2006.[203] In their device, a 6 μm long highly ordered nanotube-array film made by potentiostatic anodization of titanium foil was used as anode (not photoanode). Owing to the light-proof anode, sunlight only entered from the cathode, which bored a photocathode and backside illuminated DSSC. Chen *et al.* reported a back-illuminated DSSC with an efficiency of 7.1% by using a high transparency Pt photocathode and a $TiO_2$ anode fabricated using electrophoretic deposition (EPD) on Ti-foil.[204]

The bifacial DSSC is fabricated with a transparent anode and a transparent CE, and incident light enters the device from its front or rear surfaces. In 2008,[205,206] Ito *et al.* first reported a bifacial DSSC assembled with a conventional anode and a transparent platinum CE (Fig. 13a), and obtained a conversion efficiency of 6% for incident light striking its front or rear surfaces. After that, many transparent CEs were used in bifacial DSSCs, such as those made from polyaniline,[85,207] PEDOT:PSS,[208] $FeS_2$,[209] NiSe,[210] graphene,[211] and even metal wires.[212] The Wu group[85,213–215] made a novel design for bifacial cells in that an ordinary mirror was appended closely on the back of the CE (Fig. 13b), which reflected the unabsorbed light back to the cell, so that the irradiation light was fully utilized and the

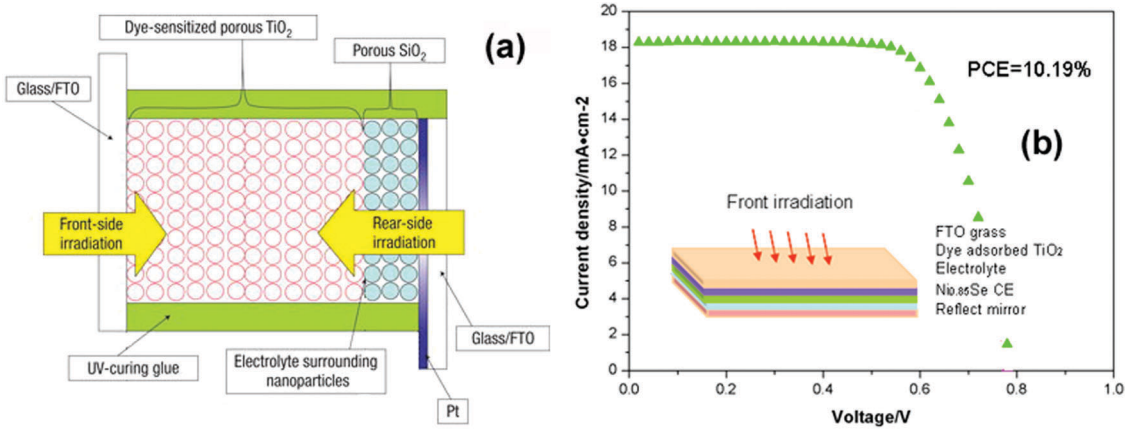


Fig. 13 (a) Bifacial DSSC assembled with a transparent anode and transparent Pt CEs. Reprinted with permission from ref. 205. Copyright (2008) Macmillan Publishers Ltd. (b) Bifacial cells appended with a mirror on the back of CE. Reprinted with permission from ref. 214. Copyright (2017) Elsevier.

Open Access Article. Published on 25 August 2017. Downloaded on 4/25/2024 1:35:01 PM.
This article is licensed under a Creative Commons Attribution-NonCommercial 3.0 Unported Licence.

conversion efficiency was effectively enhanced. The DSSC using the $Ni_{0.85}Se$ CE exhibited an efficiency of 8.96%. When adding a mirror under the $Ni_{0.85}Se$ CE, the resultant DSSC achieved an efficiency of 10.76%.[216]

Another kind of electrodes with light transmission are based on metal meshes, also developed for organic light emitting diodes and organic photovoltaics,[216] composed of very thin metal wires (StSt or Ti). The electrodes based on metal meshes have become an important component in new types of TCO-free DSSC architectures where strong flexing is desirable. Metal meshes can be cheaper than metal foil (Ti meshes 15–20 \$ per $m^2$, StSt meshes 0.1–0.25 \$ per $m^2$),[199,217] and are also transparent thus overcoming the drawback of metal foil that light cannot go through. The model of meshes, the distance and diameter of wires directly affect the transmission of the meshes. For the anode, the aperture size/distance was around 15–20 μm, similar to the diffusion length for electrons in the $TiO_2$ layer, so as to ensure efficient charge collection.[218,219] For CEs, the aperture size could be increased up to millimeters, according to Xiao *et al.*[220]

In 2007, Fan *et al.*[221] first replaced conductive stainless steel meshes by transparent conducting oxides (TCOs), and the conductive metal mesh was coated with $TiO_2$ and used as working electrodes in flexible DSSCs. Also in 2007,[222] Murayama and his colleagues reported a new tandem cell structure for improving the photocurrent of DSSCs. Two dye-sensitized $TiO_2$ films were placed face-to-face as electrodes. As a CE, a transparent Pt mesh sheet was inserted between the electrodes. Owing to the current density of the two $TiO_2$ anodes, the conversion efficiency was improved from 1.8% to 3.9%. Xiao *et al.* fabricated an all titanium substrate solar cell using Ti foil as the anode substrate and Ti meshes as the photocathode substrate.[220] By optimizing the model and aperture of Ti meshes, the Pt/Ti CE showed a relatively high light transmittance of 92.31%, and the back-illuminated DSSC achieved a PCE of 6.69% under an outdoor natural sunlight irradiation of 55 mW $cm^{-2}$.[220]

### 2.3. Flexible counter electrodes

For photovoltaic technology, flexible solar panels offer some merits over classic rigid solar panels. As outdoor products, flexible substrate-based PVs can be easily and quickly installed on buildings with flat or curved surfaces because of the lightweight and flexible nature of them. Although the DSSCs fabricated on transparent conductive oxide (TCO) coated glass have achieved efficiencies over 14%,[223] researchers show great interest in the devices using cheaper and flexible substrates in place of the glass. Flexible solar cells have two important advantages, flexibility and lightweight, of which the former would enable them to adapt to different shapes of surfaces and the latter would enable them as a mobile power source for portable electronic devices. On the other hand, flexible DSSCs are conducive to the roll-to-roll continuous and fast manufacturing process, which will significantly reduce the production cost. Conductive glass accounts for a significant percentage of the cost of the device, and replacement of glass with a flexible substrate is expected to reduce the cost of materials.[224–226]

Flexible solar cells require flexible anodes and flexible CEs, and thus demand flexible electrode substrates. Since the conductive glass substrate is rigid, the preparation of flexible counter electrodes only uses conductive polymers and metals with flexibility as substrate materials.[225,227] Flexible CEs should possess high conductivity, good catalytic activity towards the redox couple and firm adhesion between the catalyst and the substrate,[10,68] even if processed at low temperatures. In addition, high light transmittance is mandatory for a CE when using an opaque anode.[228]

Similar to glass,[90] platinum is the most commonly utilized catalyst material due to its impressive catalytic properties. So far, sputtered Pt has often been the preferred choice for plastic CEs. In fact, Yamaguchi *et al.* demonstrated the most efficient all-plastic DSSC using sputtered Pt on ITO/PEN as CE (PCE of 8.1%).[229] Pt was deposited on the $TiO_2$ modified ITO/PEN substrate by UV photoplatinization. The flexible DSSC based on the $TiO_2$/Ti photoanode and the obtained CE (transparency of 76% and $R_{CT}$ of 0.66 Ω $cm^2$) achieved a PCE up to 8.12% which is amongst the highest values reported.[230]

Early in 1988, Gratzel *et al.* used metal titanium as the substrate and fabricated dye-sensitized solar cells without the intention of flexible devices.[62] The Wu group deeply and systematically studied the flexible DSSCs based on the Ti foil

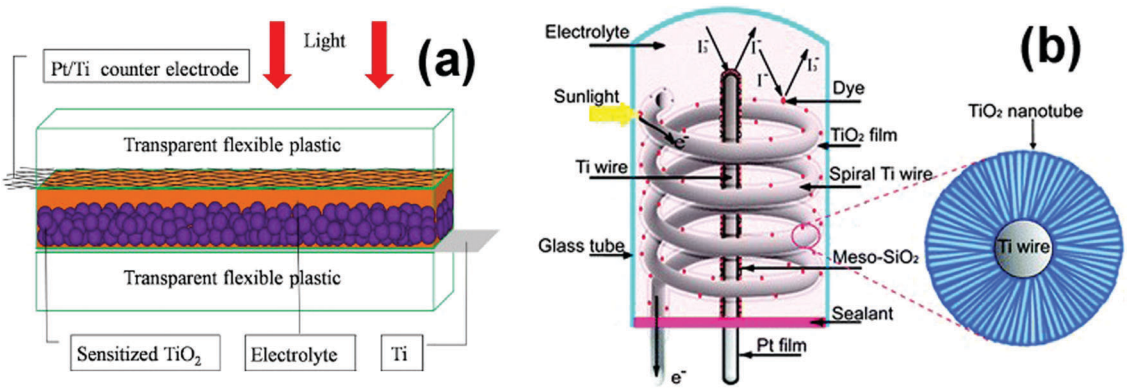


Fig. 14 (a) Flexible back-illuminated DSSC based on the Ti foil anode and the Ti mesh photocathode. Reprinted with permission from ref. 220. Copyright (2011) Elsevier. (b) Schematic diagram of a 3-D DSSC. Titania nanotubes formed on the Ti-wire served as the working electrode and the platinum film placed in between the spiral served as a counter electrode. Reprinted with permission from ref. 235 Copyright (2010) IOP Publishing.

Open Access Article. Published on 25 August 2017. Downloaded on 4/25/2024 1:35:01 PM.
This article is licensed under a Creative Commons Attribution-NonCommercial 3.0 Unported Licence.

anode and the Ti mesh photocathode.[220,231–234] The schematic design of the DSSC is shown in Fig. 14(a). Owing to the photocathode's high transparency, good electrocatalytic activity, and low charge transfer resistance and the anode's large specific area and high conductivity, under optimal preparation conditions and after various surface treatments and modifications, the flexible DSSC achieved a conversion efficiency of 6.69% and a maximum power output of 0.368 W under an outdoor natural sunlight irradiation of 55 mW $cm^{-2}$.[234]

Liu *et al.* designed a three dimensional dye-sensitized solar cell (3-D DSSC) consisting of a spiral shaped Ti-wire/TNT working electrode and platinized titanium metal wire counter electrodes, separated with a porous $SiO_2$ layer as shown in Fig. 14(b).[235] The fabricated 3D-DSSC yielded a conversion efficiency of 4.1%.

# 3. Metal and alloy counter electrodes

## 3.1. Platinum counter electrodes

Platinum is a chemical element with the symbol Pt and atomic number 78. It is a dense, malleable, ductile, precious, inert, gray-white transition metal, and was discovered by Julius Scaliger in 1735, who derived its name from the Spanish word platina, which means little silver.[90] Pt is one of the least reactive metals. It has remarkable resistance to corrosion, even at high temperatures, and is therefore considered a noble metal. Although Pt is generally unreactive, it dissolves in hot aqua regia to give aqueous chloroplatinic acid ($H_2PtCl_6$).[236] Pt possesses excellent physical and chemical properties, such as good electrical conductivity and thermal conductivity and catalytic activity, which make the material useful in a wide range of applications. Of the 218 tonnes of platinum sold in 2014, 98 tonnes were used for vehicle emission control devices (45%), 74.7 tonnes for jewelry (34%), 20.0 tonnes for chemical production and petroleum refining (9.2%), and 5.85 tonnes for electrical applications such as hard disk drives (2.7%). The remaining 28.9 tonnes went to a variety of other minor applications, such as medicine and biomedicine, glassmaking equipment, electrodes, anticancer drugs, electrical resistance wires, *etc.*[237]

The first requirement for a material to be used as CE in a DSSC is a low charge-transfer resistance and high exchange current density for the reduction of the oxidized form of the charge mediator (Fig. 5, process 5). Also, such materials must possess chemical and electrochemical stability in the electrolyte used in the device.[49,93] The best charge mediator for most of the DSSCs is the iodide/triiodide redox couple. Unfortunately however, the iodine (and triiodide) reduction reaction is not reversible in several materials and its kinetics is solvent dependent. For instance, FTO glass is a very poor counter electrode and has a very high charge transfer resistance of more than $10^6$ Ω $cm^2$ in a standard iodide/triiodide electrolyte,[98] and the electron-transfer kinetics for reduction of triiodide to iodide is very slow at the surface of ITO or FTO glass. Owing to high electrical conductivity, catalytic activity towards triiodide reduction, and high reflecting properties, platinum was first selected as the counter electrode material of DSSCs, and has been used since 1991.[39] Up to now, platinum has been the most preferred counter electrode active material for DSSCs.[48,90,97,238,239]

In 1993, Nazeerudin *et al.* reported that a 10% light-to-electric conversion efficiency was obtained by using a CE consisting of a TCO glass onto which a 2 μm-thick Pt was deposited by sputtering.[240] The thick Pt film on the conducting glass also works as a mirror to reflect the light that has not been absorbed by the dye molecules resulting in improved light harvesting efficiency. Therefore, the counter electrode performed an added function, that of a reflecting mirror. Papageorgiou *et al.* prepared a nanosized Pt catalyst by spreading a small quantity of *ca.* 5 mmol $L^{-1}$ $H_2PtCl_6$ solution in isopropanol on the conductive surface of a TCO-coated glass substrate and heating at 385 °C for 10 min.[93] This thermal decomposition technology could produce electrochemically/chemically stable electrodes and provided superior mechanical endurance or robustness and good adherence to substrates. The very low platinum loadings (<3 μg $cm^{-2}$) endowed the electrode low charge transfer resistances (<1 Ω $cm^2$) and rendered the electrode optically transparent and economical. Since then, the thermal decomposition of $H_2PtCl_6$ has been widely applied as an effective method to prepare Pt CEs.[48]

The frequently used counter electrode for DSSCs is Pt sputtered on FTO, which has a thickness of around 0.2–2 mm. Fang *et al.* investigated the influence of Pt film thickness on the performance of DSSCs.[241] It was found that the electric conductivity of the CE was enhanced with the thickness of the Pt film within a certain range. The charge transfer resistance at the electrolyte/CE interface did not change remarkably with the increase of Pt film thickness. The Pt film thickness had no significant influence on the performance of the DSSC. A thickness of 2 nm for the Pt film was enough to obtain good catalytic activity towards triiodide reduction.

Apart from sputter-coating, there are a lot of techniques to prepare nanoparticle Pt CEs, such as electrochemical deposition, thermal vapor deposition, spray pyrolysis, cyclic voltammetric deposition, electrochemical reduction, thermal decomposition, *etc.*[242–246] Dao *et al.* prepared Pt nanoparticles on a FTO glass substrate by controlling the heating rate of thermo-decomposition of Pt precursor molecules.[247] The heating rate was proved to be a sensitive parameter for morphology of Pt-NPs, the catalytic activity of Pt-NPs and subsequently the photovoltaic performance of DSSCs. The DSSCs based on the best Pt-NP CE (heating rate of 1.2 °C $min^{-1}$, charge-transfer resistance of 0.86 Ω $cm^2$) gave a PCE of 9.30%. Hauch *et al.* also obtained similar results.[98] Song *et al.* explored a urea-assisted homogeneous deposition ethylene glycol (HD-EG) method by combining *in situ* hydrolysis (HD) of urea and homogeneous reduction of ethylene glycol (EG), which resulted in good control over particle sizes and distribution of Pt NPs at the counter electrode along with better adhesion and negligible agglomeration.[248] The DSSC assembled with the CE by urea-assisted HD-EG achieved an impressive PCE of 9.34%, while the devices with the CEs prepared by EG reduction and thermal reduction produced PCEs of 8.66% and 7.99%, respectively.

Compared to the bulk Pt, Pt nanoparticles have excellent characteristic properties like high surface area, high transmittance, low charge transfer resistance, high electrical

Open Access Article. Published on 25 August 2017. Downloaded on 4/25/2024 1:35:01 PM.
This article is licensed under a Creative Commons Attribution-NonCommercial 3.0 Unported Licence.

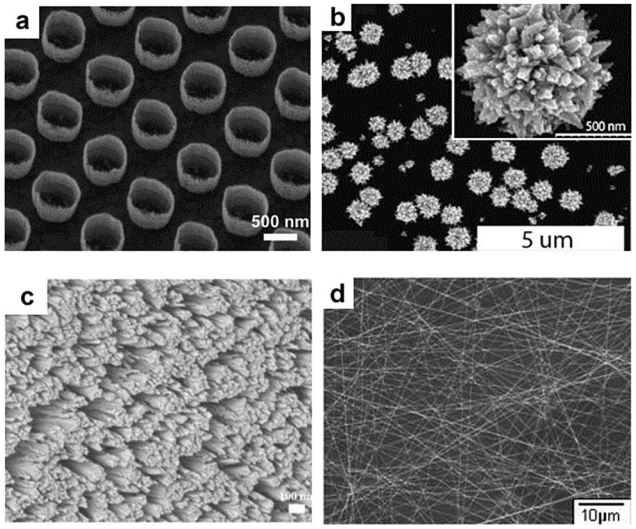


Fig. 15 SEM images of (a) Pt nanocups. Reproduced with permission from ref. 240. Copyright (2012) John Wiley & Sons Ltd. (b) Pt nanoflowers. Reproduced with permission from ref. 241. Copyright (2010) Elsevier. (c) Pt nanowires. Reproduced with permission from ref. 242. Copyright (2013) Elsevier. (d) Pt nanofiber networks. Reproduced with permission from ref. 243. Copyright (2013) American Chemical Society.

conductivity and corrosion resistance, better than any other noble metals. These key features made Pt an attractive CE material in DSSCs.[90,249] 3-D nanostructures with high surface areas add new functions to Pt CEs. These structures include multipods, nanowires, nanoflowers, nanotubes, *etc.* (some of them are shown in Fig. 15).[107,113,250–261] For instance, Jeong *et al.* demonstrated a periodically arranged Pt nanocup (NC) array with a controllable diameter and pitch size by UV-based nanoimprint lithography (NIL).[250] A larger catalytic surface area by the nanocup structure induced more active electrochemical reduction due to a lower charge-transfer resistance ($R_{CT}$) at the CE/electrolyte interface. The DSSC based on the CE having the Pt NC array with a diameter of 300 nm at a 400 nm pitch size showed a PCE of 9.75%, while the DSSC with the planar Pt CE showed a PCE of 7.87%. The Wu group grew platinum nanotubes (PNTs) on FTO substrates by a facile polycarbonate template method. With PNTs as CE and MgO as the block layer on $TiO_2$ films, the fabricated DSSC achieved an efficiency of 9.05%, and the efficiency was increased by 25.5% compared to that of the DSSC with conventional Pt CE.[254]

In a word, Pt is a preferred CE active material for DSSCs by virtue of its excellent conductivity and catalytic activities. The DSSCs with PCEs over 12% mostly use Pt as CEs.[223,262–264] Even so, it also possesses some disadvantages to be overcome. (i) Although the amount of Pt for CEs to obtain the desired catalytic effect is very small, *i.e.*, about 50 mg $m^{-2}$, and does not significantly contribute to the overall price per peakwatt, future large solar conversion systems producing electric power in the terawatt scale will prefer materials that are abundantly available.[265] After all, platinum is expensive ($\sim$ \$ 950 per Troy ounce at present) and scarce in nature.[90] (ii) There is some concern that Pt might not be stable over prolonged periods of time in the electrolyte containing $I^-/I_3^-$ redox couples as may undergo oxidation and dissolution forming $PtI_4$ or $H_2PtI_6$.[98,246,266] If only a tiny amount of Pt dissolves in the electrolyte, it would slowly redeposit on the $TiO_2$ layer and short-circuit the cell by catalyzing $I_3^-$ reduction on the photoanode.[97,266] (iii) Pt is not an effective CE active material for redox couples such as cobalt-complexes, $T_2/T^-$, and polysulfide electrolytes used in DSSCs[91,150,223,261,262] owing to the energy match between counter electrodes and electrolytes (Fig. 5). Especially, Pt electrodes used in Co-mediated electrolytes sparked off a large dispute for the $Co^{3+}/Co^{2+}$ redox couple containing various ligands such as bipyridine, terpyridine and phenanthroline.[267–269]

The future studies on Pt CEs should focus on the development of new methods and Pt-based hybrid CEs to reduce Pt dosage. Fortunately, there are many other candidates that can be used as CE active materials in DSSCs.

### 3.2. Other metal counter electrodes

Ruthenium (Ru) is a noble metal in the platinum group that is less expensive than Pt, and has low resistivity as well as a high work function. Moreover, it has excellent heat conductivity and chemically stable properties.[270] In addition, Ru can be fabricated by atomic layer deposition (ALD), which is a relatively simple and low temperature process.[271] Noh *et al.* deposited a Ru film on FTO glass by atomic layer deposition (ALD).[272] It was found that the catalytic activity and charge transfer resistance values of Ru CEs hinge on their thickness and have different change trends from the Pt CEs. Han *et al.* optimized the thickness of the Ru layer and obtained a PCE of 3.40%.[273] Palladium (Pd) has similar properties as the metal Ru. Noh *et al.* also used similar methods to investigate the palladium (Pd) CEs and similar results were obtained.[274] The DSSC based on the Pd CE achieved a PCE of 4.32%, although the Pd film was not deposited firmly compared to Ru films.

Ru is an attractive material for the counter electrode of DSSCs due to its high electrical conductivity, high electrocatalytic activity, and excellent electrochemical stability over a wide potential range.[275,276] An *et al.* synthesized Ru nanofibers by a sequential process of electrospinning, post-calcination, and hydrogen reduction.[277] The Ru nanofibers exhibited rough surfaces consisting of nano-sized grains and a unique network nanoarchitecture as shown in Fig. 16. DSSCs fabricated with Ru nanofibers as CEs showed improved photovoltaic performance, including a low $R_{CT}$ value (12.5 $\Omega$ $cm^{-2}$), a high $J_{SC}$ value (14.77 mA $cm^{-2}$), and a high PCE (6.23%), while the DSSC with commercial Pt CE showed a PCE of 6.04%. An *et al.*[277] asserted the improvement of photovoltaic performance by the Ru nanofibers as due to the following reasons: (i) the rough surfaces consisting of nano-sized grains result in a great deal of active sites, (ii) the metallic Ru phase shows high electrical conductivity and electrocatalytic activity and (iii) the unique network structure allows rapid electron transfer and electrolyte diffusion.[278–281]

Iridium (Ir) has attracted much attention because of its lower resistivity ($4.7 \times 10^{-8}$ $\Omega$ m) and lower cost (\$ 540 per oz t, in 2015) than Pt ($10.6 \times 10^{-8}$ $\Omega$ m and \$ 1200 per oz t, in 2015) yet similar electrocatalytic activity.[282] Noh *et al.* prepared Ir CEs

Open Access Article. Published on 25 August 2017. Downloaded on 4/25/2024 1:35:01 PM.
This article is licensed under a Creative Commons Attribution-NonCommercial 3.0 Unported Licence.

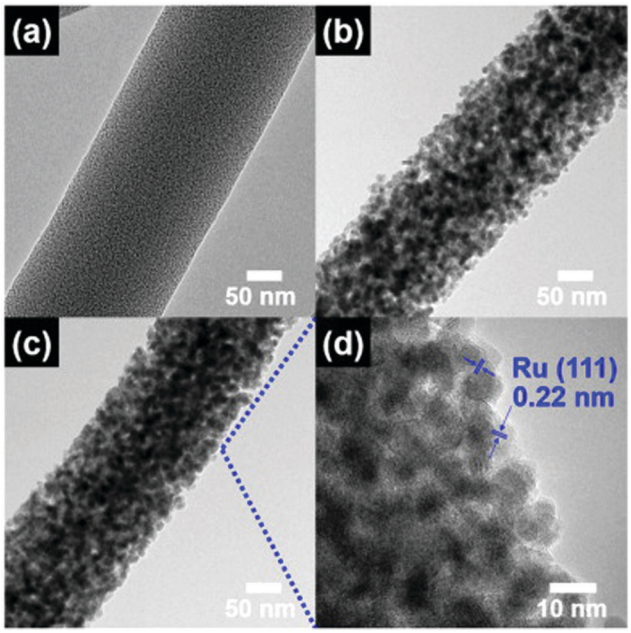


Fig. 16 Low-resolution TEM images of (a) carbon nanofibers embedded with Ru nanoparticles, (b) $RuO_2$-and-Ru nanofiber composites, and (c) Ru nanofibers. (d) High-resolution TEM images of Ru nanofibers. Reprinted with permission from ref. 277. Copyright (2016) Elsevier.

by the thermal evaporation technique and obtained a PCE of 5.19% for the DSSC.[282] Mokurala *et al.* deposited Ir films on a FTO substrate by radio-frequency (RF) sputtering at room temperature.[283] The PCE of the device fabricated with Ir-based CE was 7.2%, which was comparable to the Pt-based CE.

Gold (Au) has higher conductivity ($4.3 \times 10^5$ S cm$^{-1}$) than Pt ($0.9 \times 10^5$ S cm$^{-1}$). Au is catalytic and has an excellent corrosion resistance.[284] A transparent conductive Au/a-IZO (amorphous indium zinc oxide) bilayer with a very high conductivity of $1.2 \times 10^5$ S cm$^{-1}$ and a mobility of 65.6 cm$^2$ V$^{-1}$ s$^{-1}$ was prepared at room temperature by Sun *et al.*[285] The DSSC with the Au/a-IZO CE exhibited good photovoltaic parameters: $V_{OC}$ = 0.64 V, $J_{SC}$ = 9.83 mA cm$^{-2}$, FF = 0.59, PCE = 3.73%.

Titanium (Ti) is a silvery-white metal and possesses superior strength and durability. Ti is the most stable and resistant to corrosion due to the formation of a natural passivating oxide on its surface. Although the resistivity of Ti ($42 \times 10^{-8}$ Ω m) is higher than that of Al or Pt ($2.65 \times 10^{-8}$ Ω m and $10.6 \times 10^{-8}$ Ω m, respectively), the catalytic properties of the Ti bilayer with Pt-group metals have attracted attention. Rahman *et al.* fabricated a porous Ti/dense Ti/Al/glass composite CE for DSSCs by a DC magnetron sputtering process.[286] The dense Ti layer was used as a protective layer against corrosion of the Al layer. The solution treatment roughened the surface of the porous Ti layer, which resulted in the improvement of the photovoltaic performance of the DSSC.

Noh and Song prepared a Ti/Ru bilayer on FTO glass by RF sputtering techniques as CE in DSSCs.[287] The bilayer electrode with 50 nm-Ti/50 nm-Ru was an intermetallic phase of TiRu, which reduced interface resistance and enhanced the catalytic activity of the CEs. The PCE of the DSSC with the Ti/Ru bilayer CE was 2.40%, and the increase in efficiency was 1.48 times that of the device with a 100 nm Ru only CE. Using similar methods, Noh and Song prepared many bilayer CEs by RF sputtering techniques, including Al/Ru,[288] Au/Pt,[284] Cu/Pt,[289] *etc.* The PCE of the device with Al/Ru bilayer CE was 2.36%. The increase in efficiency was 1.46 times that of the device with a 100 nm Ru CE.[288] The PCEs of the DSSCs with Pt only and Au/Pt bilayer counter electrodes were 4.60% and 5.28%, respectively.[284] And the PCEs of the DSSCs with only Pt and Cu/Pt bilayer CEs were 4.60% and 5.72%, respectively.[289]

Silver (Ag) is a soft, white, lustrous transition metal and it exhibits the highest electrical conductivity, thermal conductivity and reflectivity of any metal. Ag shows high corrosion resistance and stability in pure air and water and is therefore used as a CE material in DSSCs. In solid-state DSSCs, noble metal electrodes such as Au and Ag are as important as Pt catalysts in liquid DSSCs.[290–292] Henry *et al.* investigated Ag and Au as CEs in solid-state DSSCs.[290] By replacing dissipative Au electrodes with reflective Ag electrodes, the light absorption of the device was enhanced, and a PCE of 5.1% was achieved under irradiation of high-intensity simulated sunlight. Silver nanowire (Ag NW) mesh electrodes are often used in various electrochemical devices and DSSCs.[293–303] Al-Mamun *et al.*[293] compared four types of CEs (Pt, AgNW, GNP (graphene nanoplatelets) and AgNW–GNP) for $Co^{3+}/Co^{2+}$ redox mediator based DSSCs. Both AgNW and GNP showed inferior catalytic activity for the $Co^{3+}/Co^{2+}$ redox couple. However, AgNW–GNP exhibited a synergistic enhancement of electrocatalytic activity for the cobalt redox couple. Owing to the lower $R_{CT}$, the AgNW–GNP based DSSC showed a comparable PCE to that of the Pt based device in spite of the higher resistance of electrolyte diffusion. Margulis *et al.*[294] developed a solution-processed, highly transparent, conductive electrode based on PEDOT:PSS and spray-deposited Ag NWs as an effective top contact for DSSCs. The role of PEDOT:PSS is twofold: it ensures ohmic contact between the hole transport overlayer and the Ag NWs and it decreases the series resistance of the device. The ssDSSC with D35 dye and Ag NW/PEDOT:PSS electrode showed a PCE of 3.6%, nearly as high as that of a reference device using an evaporated silver electrode (3.7%).

### 3.3. Alloy counter electrodes

An alloy is a mixture of metals or a mixture of a metal and another element. Alloys are defined by the metallic bonding character. An alloy may be a solid solution of metal elements (a single phase) or a mixture of metallic phases (two or more solutions). Alloys are used in a wide variety of applications. In some cases, a combination of metals may reduce the overall cost of the material while preserving important properties. In other cases, the combination of metals endows synergistic effects for the alloy materials. These two objectives should be focused on for the alloy counter electrodes used in DSSCs. Aiming at reducing the cost of CEs and enhancing the performance of the DSSC devices, many alloy CEs have been researched, including Pt alloy CEs: $Pt_{0.02}Co$, $PtCo_2$, PtCo, $PtCo_{0.50}$, $PtNi_{0.50}$, $PtNi_{0.75}$, $Pt_3Ni$, PtNi, PtFe, $Pt_{0.96}Ni_{0.04}$, PtMo, $PtMn_{0.05}$, $PtCr_{0.05}$, $PtPd_{1.25}$,

Open Access Article. Published on 25 August 2017. Downloaded on 4/25/2024 1:35:01 PM.
This article is licensed under a Creative Commons Attribution-NonCommercial 3.0 Unported Licence.

Table 1 Photovoltaic parameters of the liquid-junction DSSCs based on alloy CEs

| CE materials | $J_{SC}$ (mA cm$^{-2}$) | $V_{OC}$ (V) | FF | PEC (%) | Ref. |
|---|---|---|---|---|---|
| $Pt_{0.02}Co$ | 18.53 | 0.735 | 0.75 | 10.23 | 304 and 305 |
| $Pt_3Ni$ | 17.05 | 0.72 | 0.715 | 8.78 | 306 |
| $Pt_{0.06}Ni_{0.94}$ | 16.79 | 0.736 | 0.664 | 8.21 | 307 |
| PtCo | 16.96 | 0.717 | 0.668 | 7.64 | 308 |
| PtPd | 16.88 | 0.731 | 0.642 | 7.45 | 308 |
| PtFe | 16.71 | 0.716 | 0.649 | 7.30 | 308 |
| PtMo | 15.48 | 0.697 | 0.626 | 6.75 | 309 |
| $PtMn_{0.05}$ | 14.12 | 0.712 | 0.703 | 7.07 | 310 |
| $PtCr_{0.05}$ | 13.07 | 0.739 | 0.712 | 6.88 | 311 |
| $PtPd_{1.25}$ | 14.58 | 0.728 | 0.68 | 7.22 | 312 |
| $PtRu_3$ | 14.70 | 0.718 | 0.644 | 6.80 | 313 |
| PtAu | 16.5 | 0.654 | 0.31 | 3.4 | 314 |
| $Co_{0.85}Se$ | 16.80 | 0.742 | 0.67 | 8.30 | 314 |
| $Ni_{0.85}Se$ | 16.59 | 0.741 | 0.639 | 7.85 | 315 |
| $Cu_{0.50}Se$ | 14.55 | 0.713 | 0.62 | 6.43 | 315 |
| $Ru_{0.33}Se$ | 17.86 | 0.722 | 0.679 | 8.76 | 315 |
| $FeCo_2$ | 12.09 | 0.710 | 0.59 | 5.06 | 209 |
| FeSe | 17.72 | 0.717 | 0.721 | 9.16 | 316 |
| $CoNi_{0.25}$ | 18.02 | 0.706 | 0.66 | 8.39 | 317 |
| $Pd_{17}Se_{15}$ | 16.32 | 0.700 | 0.65 | 7.45 | 318 |
| PdNi | 15.96 | 0.67 | 0.626 | 6.70 | 319 |
| PtCoNi | 17.01 | 0.744 | 0.688 | 8.71 | 308 |
| PtPdNi | 16.34 | 0.741 | 0.684 | 8.28 | 308 |
| PtFeNi | 16.02 | 0.726 | 0.678 | 7.89 | 308 |
| PtCuNi | 18.3 | 0.758 | 0.696 | 9.66 | 320 |

$PtRu_3$, PtRu, PtAu; free-Pt alloy CEs: $CoNi_{0.25}$, CoNi, $FeCo_2$, FeSe, FeNi, $Co_{0.85}Se$, CoSe, $Ni_{0.85}Se$, NiSe, MoSe, $Cu_{0.50}Se$, $Ru_{0.33}Se$, RuSe, $Pd_7Se_4$, NiPd; and ternary alloy CEs: PtCuNi, PtCoNi, PtPdNi, PtFeNi, *etc.*[239] Some photovoltaic parameters of the liquid-junction DSSCs based on alloy CEs are listed in Table 1.

Possibly inspired by Pt bilayer film CEs,[244,245,321] Peng *et al.*[307] deposited a $Ni_{0.94}Pt_{0.06}$ film on a FTO substrate by a chemical plating method (shown in Fig. 17) and used it as the photocathode for DSSCs in 2009. The $Ni_{0.94}Pt_{0.06}$ film consisted of nanoparticles with a size of 4–6 nm and a Pt loading of 5.13 μg cm$^{-2}$. The $Ni_{0.94}Pt_{0.06}$ photocathode exhibited high catalytic activity for triiodide reduction, high light reflectance, and low charge-transfer resistance. The DSSC based on the $Ni_{0.94}Pt_{0.06}$ photocathode gave a PCE of 8.21%, which is higher than that of the DSSC with a pure Pt photocathode obtained by thermal decomposition, indicating that the $Ni_{0.94}Pt_{0.06}$ alloy electrode is a low-cost and high-performance photocathode for use in DSSCs. The basic idea is quite simple: alloying with inexpensive Ni might not only reduce the required amount of Pt metals but also facilitate the electron transfer between the CEs and the redox pairs.[98,322] Wan *et al.* obtained a PCE of 9.15% with $Pt_3Ni$ CE, displaying an evident improvement compared with the conventional pure Pt (8.33%).[306] The cell stability is also obviously increased with the $Pt_3Ni$ counter electrode.

The Tang group systematically investigated the alloy CEs used in DSSCs and has published a lot of papers in this field.[210,239,304,305,309,310,315,316,323] By using an electrochemical codeposition technique, He *et al.* synthesized $CoPt_{0.02}$ alloys and used them as CEs for DSSCs.[304] Owing to the rapid charge transfer, electrical conduction, and electrocatalysis, the DSSC with $CoPt_{0.02}$ alloy CE achieved an impressive PCE of 10.23% in comparison to 6.52% from pure Pt CE. The high conversion efficiency, low cost, simple preparation, and scalability demonstrate the potential application of CoPt alloy CEs in DSSCs. To reduce the cost of DSSC devices, one way as mentioned above is to reduce the dosage of Pt in CEs. Another way is to use Pt-free alloy CEs. Using a mild hydrothermal treatment and without any surfactant or template, Chen *et al.* prepared a binary Co–Ni alloy and used it as CE material in DSSCs.[324] The $CoNi_{0.25}$ alloy CE has an optimal charge-transfer ability and electrocatalytic activity towards triiodide reduction. The DSSC with a $CoNi_{0.25}$ alloy CE exhibited a PCE of 8.39% in comparison to 6.96% for a device based on a pure Pt CE. The profound advantages along with low cost, mild synthesis, and scalable materials promise the Pt-free binary alloy CEs to be strong candidates in robust DSSCs.

Yang *et al.* electrodeposited Ni on ZnO microrod templates and subsequently grew branched Cu, followed by galvanic displacement of outward Ni and Cu by $H_2PtCl_6$, which produced a ternary alloy CE, NiCuPt. The resultant NiCuPt alloy CE displayed superior electrocatalytic activity and charge-transfer ability, arising from good matching of work function to redox potential of the liquid electrolyte. An impressive PCE of 9.66% was obtained for the liquid-junction DSSC device.[320]

## 4. Carbon counter electrodes

Carbon is found almost everywhere and it is one of the most abundant materials on earth. It is a versatile atom capable of joining with other atoms in sp, sp$^2$, and sp$^3$ hybridized structures giving rise to millions of stable molecules. In its single element form, carbon has basically 8 allotropes (shown in Fig. 18),[325,326] namely, (i) diamond, (ii) graphite, (iii) lonsdaleite, (iv) $C_{60}$ (buckminister fullerene or bucky ball), (v) $C_{540}$, (vi) $C_{70}$, (vii) amorphous carbon, and (viii) carbon nanotubes (CNTs; buckytube). Carbon has been the subject of intense interest of researchers for decades.

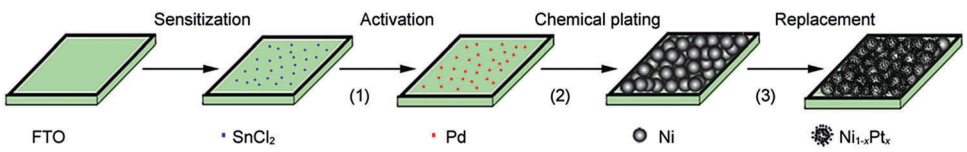


Fig. 17 Schematic flow diagram of the preparation of $Ni_{1-x}Pt_x$ films. Reprinted with permission from ref. 307. Copyright (2009) Tsinghua University Press and Springer-Verlag Berlin Heidelberg.

Open Access Article. Published on 25 August 2017. Downloaded on 4/25/2024 1:35:01 PM.
This article is licensed under a Creative Commons Attribution-NonCommercial 3.0 Unported Licence.

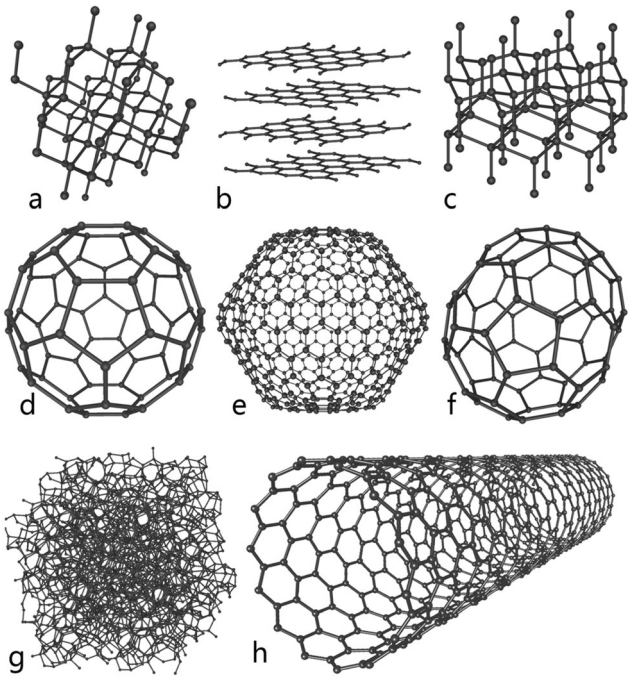


Fig. 18 Some allotropes of carbon: (a) diamond; (b) graphite; (c) lonsdaleite; (d–f) fullerenes ($C_{60}$, $C_{540}$, $C_{70}$); (g) amorphous carbon; (h) carbon nanotube. Reprinted with permission from ref. 326. (CC BY-SA 3.0).

Ever since the discovery of fullerene in 1985 by Kroto *et al.*,[327] many new allotropes of carbon have been discovered. Among them, CNTs were first discovered in the year 1991 by Iijima;[328] graphene is a single layer of carbon atoms arranged in a honey comb lattice, discovered in the year 2004 by Novoselov *et al.*[329] They were rewarded with Nobel Prize in physics in the year 2010,[329] which showed the importance of carbon nanomaterials. All these discoveries led to growing interest of many scientists in almost all the major fields of science, including chemistry, physics, biology, electronics, and medical sciences.

Carbon materials are quite attractive candidates as CE materials in DSSCs for the replacement of conventional and expensive Pt materials on account of their advantages such as low cost, high surface area, high catalytic activity, high electrical conductivity, high thermal stability, good corrosion resistance towards iodine, high reactivity for triiodide reduction, *etc.* Several carbonaceous materials such as graphene, carbon nanotubes, carbon nanofibers, activated carbon, graphite, and carbon black have been successfully employed as counter electrodes.[91,330–335]

### 4.1. Carbon black nanoparticles

In 1996, the Gratzel group first explored a graphitic-carbon black mixture as CE material and obtained a PCE of 6.67% on a series of connected photovoltaic module.[266] The functionalized graphite served to enhance electronic conductivity while the high-surface area carbon black increased the catalytic activity towards triiodide reduction. They also showed that the efficiency remained fairly constant over 100 days of light fluctuation of xenon lamp, which was equivalent to 2 years outdoor equivalent in middle Europe.[266,332] Although this type of CE resulted in 30% lowering of PCE compared to the Pt CE, it opened up a new research direction for developing low-cost Pt-free CEs. Thereafter, intensive research efforts have been focused on carbon materials.

Carbon black is a material produced by the incomplete combustion of heavy petroleum products. Carbon black nanoparticles are nanometer-sized spherical structures of carbon with an amorphous quasi-graphitic molecular structure. Most types of carbon black have parallel graphitic layers, ordered groups on the surface and a high surface-area-to-volume ratio, albeit lower than that of activated carbon. Carbon black is mainly used as reinforcing filler in tires and other rubber products. In plastics, paints, and inks, carbon black is used as a color pigment. All carbon blacks have chemisorbed oxygen complexes (carboxylic, quinonic, lactonic, phenolic groups and others) on their surfaces, varying on the basis of the production conditions. Carbon black has high electrocatalytic activity and electrical conductivity and has been known as a good candidate for CEs.[266,336] When carbon black is used as CE, its particle morphology and surface state (including size, surface area, porosity, crystallinity, thickness, shape, purity) as well as preparation conditions play a key role.

In general, the CE thickness should be below tens of microns. Murakami *et al.* investigated the influence of the thickness of carbon black as the CE on the electrochemical properties of DSSCs.[265] It was found that the large surface area of the carbon black resulted in a low $R_{CT}$ of about 2.96 Ω cm$^2$. With the increase of the thickness of carbon black, charge-transfer resistance of the CE decreases, and above tens of microns, the PCE became one-third of conventional Pt. A thickness of 14.47 μm of carbon black as the CE achieved a high PCE of 9.1% for the DSSC. This is a higher PCE for the DSSCs using conventional carbon CEs.

Wu *et al.* investigated the effect of preparation conditions of CB.[337] In their study, poly(vinylidene fluoride) (PVDF) was used as a binder to regulate the viscosity of the CB paste to facilitate the doctor blade process and the PVDF was then removed *via* thermal treatment. It was found that, after the heat treatment, all CB films had a mesoporous structure and the film thickness increased with increasing CB concentration. The CB films heated at 350 °C had low electrochemical activity, high charge transfer resistance, and poor performance when utilized in DSSCs, owing to the presence of residual PVDF. However, when heated at 450 °C, PVDF was completely removed and the resultant CB films had electrochemical properties similar to those of a Pt film. The DSSCs with the CB CE achieved a PCE of 8.35%, comparable to the device with Pt (8.29%).

Kim *et al.* investigated the influence of particle size and thickness of the CB porous layer as a CE on the electrochemical properties of DSSCs.[338] The CB layer was coated on FTO glass by a spray coating method at 120 °C. The CB particle size varied from 20 nm to 90 nm (Fig. 19a) and the CB electrode thickness was controlled from 1 to 9 μm by controlling the spraying time. As the CB particle size was decreased, the catalytic activity was improved because of the increase in the surface area and the conductivity of the CB layer. Increased CB electrode thickness

Open Access Article. Published on 25 August 2017. Downloaded on 4/25/2024 1:35:01 PM.
This article is licensed under a Creative Commons Attribution-NonCommercial 3.0 Unported Licence.

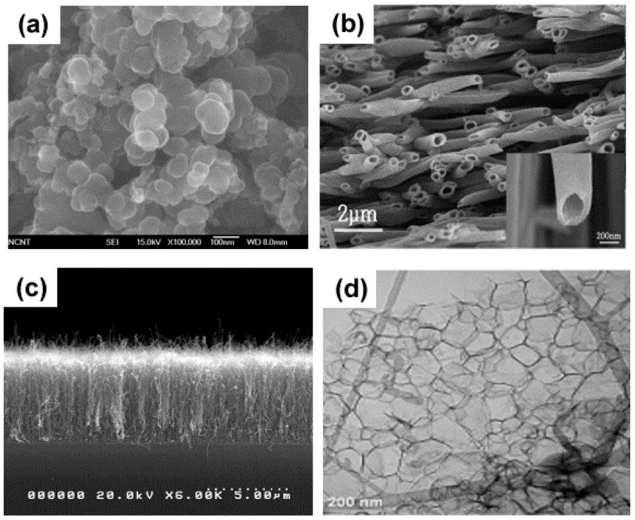


Fig. 19 SEM images: (a) carbon blacks. Reprinted with permission from ref. 338. Copyright (2012) Elsevier. (b) Hollow carbon nanofibers. Reprinted with permission from ref. 349. Copyright (2013) Elsevier. (c) Multi-wall carbon nanotubes. Reprinted with permission from ref. 118. Copyright (2010) Elsevier. (d) Honeycomb-like graphenes. Reprinted with permission from ref. 377. Copyright (2013) John Wiley & Sons Ltd.

also improved the catalytic activity and led to the low charge transfer resistance at the electrolyte/CB electrode interface. The CB counter electrode with a particle size of 20 nm and a thickness of 9 μm for DSSCs showed a PCE of 7.2% with a FF of 0.656, which was similar to the Pt CE with an efficiency of 7.6% and a FF of 0.658.

Liu *et al.* researched the CB CE used in the DSSCs employing $Co(bpy)_3^{3+/2+}$ as the redox couple.[339] The results indicated that the electrochemical behavior of CB CE was dominated by the heat treatment and the amount of CB loaded. The electrocatalytic activity of a well-prepared CB film was superior to that of conventional sputtered Pt. A Z907-sensitized solar cell with this CB CE showed a PCE of 7.21%, while the device with conventional Pt CE showed a PCE of 7.10%. An Y123-sensitized solar cell using $Co(bpy)_3^{3+/2+}$ as the redox couple and equipped with this CB CE achieved an exceptional efficiency of 8.81% without any significant mass transport limitations. Zhang *et al.* used CB as a supporter to make composite CEs of CB/polypyrrole (PPy), CB/polyaniline (PANI), and CB/PEDOT for the $T_2/T^-$ redox couple.[340] The corresponding DSSCs achieved PCE values of 5.2% (CB/PPy), 5.2% (CB/PANI), and 7.6% (CB/PEDOT), much higher than those of the DSSCs with PPy, PANI, PEDOT, and CB CEs.

From the foregoing, the thickness, particle size, preparation condition, and electrolyte compositions can affect the electrochemical properties of CB and the photovoltaic performance of the corresponding DSSCs through various mechanisms. CB nanoparticles are comparatively less expensive than other nanostructures and exhibit excellent catalytic ability. However, they are reported to be carcinogenic and cause health issues.[341]

### 4.2. Carbon nanofibers

As another carbon nanostructure, carbon nanofibers (CNFs) have been employed in DSSCs. Carbon nanofibers (CNFs) are one-dimensional fibrous structures with diameters ranging from a few nanometers to a few micrometers and lengths up to several centimeters.[342,343] Carbon fibers can be described as $sp^2$ hybridization-based linear filaments.[325] They come under the category of multiwalled nanotubes, but they are discontinuous and highly graphitic. Carbon nanofibers are cylindrical nanostructures with graphene layers stacked as cones, cups or plates.[344,345] Carbon nanofibers with graphene layers wrapped into perfect cylinders are called carbon nanotubes (CNTs). The diameter of carbon nanofibers is comparatively larger than that of CNTs, and the walls of carbon nanofibers are thicker than those of CNTs. Carbon nanofibers are generally produced by chemical vapor deposition or pyrolysis of electrospun fibers from organic precursors, like polyacrylonitrile (PAN).[342] Carbon fibers are applied in various sports accessories, because they are one of the strongest but lightest and most flexible materials.[346] Carbon fiber is also used as a composite reinforcing material and as micro-electrodes.

Joshi *et al.* studied electrospun carbon nanofibers (ECNs) as CEs for DSSCs.[347] Carbon nanofibers were made by electrospinning PAN nanofibers, which were carbonized at 1200 °C in argon. ECNs were converted into paste by adding polyoxyethylene tridecylether (POETE), as a binder, then ground and sonicated. The resulting paste was then doctor bladed onto a FTO substrate followed by sintering at 200 °C for 15 min and 475 °C for 10 min. The ECNs were relatively uniform with an average diameter of ~250 nm and tens of microns long. The ECN CEs exhibited low charge-transfer resistance and fast reaction rates for triiodide reduction. The ECN-based DSSC achieved a PCE of 5.5%.

Carbon nanofibers (CNFs) with antler and herringbone structures were studied as CEs used in DSSCs by Veerappan *et al.*[348] The doctor bladed CNFs-CE has a faster triiodide reduction rate and a lower charge transfer resistance ($R_{CT}$) of ~0.5 Ω $cm^2$ than Pt (~2.3 Ω $cm^2$) due to the nanofiber stacking morphology. Its herringbone and antler structures with graphitic layers lead to defect-rich edge planes and the larger diameter of CNFs facilitates the electron transfer kinetics. The DSSCs with the CNF CE showed a promising PCE of 7.0% for the glass based devices and 5.0% for the flexible cells with the quasi-solid state electrolyte, which is similar to the performance of the device with Pt CE.

By using concentric electrospinning and thermal techniques, the Lee group synthesized activated carbon nanofibers with a hollow core/highly mesoporous shell structure (Fig. 19b) (Meso-HACNF).[349] The core and shell diameters were approximately 200–360 nm with a total surface area of 1191 $m^2$ $g^{-1}$. The DSSC with HACNF CE achieved a PCE of 7.21%, which was comparable to that of the device based on Pt CE (7.69%). The authors attributed the high catalytic activity to the high surface area and the 1-D conducting pathway of HACNF.

A Pt/CF film with 1.0 wt% Pt loading was synthesized and used as the CE in DSSCs by Guo *et al.*[350] The Pt/CF CE had $R_{CT}$ and $R_S$ of 1.60 Ω $cm^2$ and 11.65 Ω $cm^2$, similar to the Pt CE of 1.32 Ω $cm^2$ and 11.52 Ω $cm^2$ in the $Co^{3+/2+}$ electrolyte system, indicating that Pt/CF and Pt CEs have similar

Open Access Article. Published on 25 August 2017. Downloaded on 4/25/2024 1:35:01 PM. This article is licensed under a Creative Commons Attribution-NonCommercial 3.0 Unported Licence.

electrocatalytic activities. The DSSC based on this Pt/CF CE (containing 1.0 wt% Pt) in the liquid $Co^{3+/2+}$ electrolyte system achieved a PCE of 8.97%, which was comparable to the device based on Pt CE (9.41%). This research provides a feasible route to reduce the dosage of Pt in DSSCs without sacrificing the catalytic activity.

Carbon nanofibers have larger dimensions compared to carbon nanotubes, carbon nanoparticles, *etc.*[265,332,347] This limits the effective surface area, and as a result, a higher thickness is required. A thicker layer of carbon nanofibers contributes to bulk resistance and Nernst diffusion impedance which limits the performance of the devices.[347,348] This is a shortcoming of these cost-effective carbon nanofibers.

### 4.3. Carbon nanotubes

Carbon nanotubes (CNTs) are allotropes of carbon with a cylindrical nanostructure. Nanotubes are members of the fullerene structural family. Their name is derived from their long, hollow structure with the walls formed by one-atom-thick sheets of carbon, *i.e.*, graphene. Nanotubes may contain one or more concentric shells of graphene sheets, called single-walled (SWCNT) or multi-walled carbon nanotubes (MWCNT), and may have open or closed ends. Typical diameters of SWCNTs and MWCNTs are 0.8–2 nm and 5–20 nm, respectively. The length of nanotubes can vary from less than 100 nm to a few centimeters. Owing to the material's exceptional strength and stiffness, nanotubes have been constructed with a length-to-diameter ratio of up to 132 000 000 : 1,[351] significantly larger than any other material. CNTs have extraordinary electrical conductivity, thermal conductivity and mechanical strength,[352,353] which are valuable for nanotechnology, electronics, optics and other fields of materials science and technology.

In 2003, Suzuki *et al.* firstly used SWCNTs as CE in DSSCs, and achieved a PCE of 4.5%, which was comparable to the cell based on Pt-sputtered CE under the same condition.[354] Lee *et al.* prepared MWCNTs as CEs in DSSCs.[355] Defect-rich edge planes of bamboolike-structure MWCNTs facilitate the electron-transfer at the CE/electrolyte interface, resulting in low charge-transfer resistance and an improved FF. The stability test confirmed the robustness of MWCNT-based DSSCs; the DSSC with the MWCNT CE achieved a PCE of 7.7%.[355]

The Ouyang group compared the SWCNTs or MWCNTs as CE materials in DSSCs.[332,356] In their experiments, SWCNTs or MWCNTs were mixed with poly(ethylene glycol) (PEG), and then ground in a mortar, sonicated and centrifuged. The resultant paste was doctor bladed into FTO substrates. Then the binder PEG was removed by heating. These binder-free CNT films were rough and exhibited good adhesion to substrates. For comparison, they prepared CNT-based CEs with a thickness of 10 mm by using (carboxymethyl)-cellulose (CMC) sodium salt as binder. The binder based devices showed lower efficiencies than the binder-free devices due to the high series resistance of the insulating binder and the reduced surface area by binder covering. The SWCNT based DSSC showed lower charge transfer resistance ($R_{CT}$ = 0.6 Ω $cm^2$) and slightly higher efficiency (PCE = 7.81%) than the MWCNT-based device ($R_{CT}$ = 0.75 Ω $cm^2$, PCE = 7.63%). The lower $R_{CT}$ and higher efficiency were caused by a larger surface area in SWCNT. Also the SWCNT devices showed better stability than MWCNT cells. After four weeks, the efficiency of DSSCs increased from 7.81% to 8.17% for SWCNT devices, but decreased from 7.63% to 6.63% for MWCNT-based cells.

Ma *et al.* synthesized 3-dimensional SWCNT/graphene aerogel by the spin-coating method and used it as the CE material in DSSCs.[357] The DSSC based on the 3-D CE achieved an excellent PCE of 8.31%, while the device based on conventional Pt CE achieved a PCE of 7.56%. Interestingly, PCE increased to 9.64% under the assistance of a mirror. The excellent performance of DSSCs can be attributed to the high electrical conductivity and good electrocatalytic activity induced by the SWCNTs and the excellent catalytic properties of graphene, coupled with the 3D structure with a larger surface area and good surface hydrophilicity for increased electrolyte–electrode interactions and electrolyte/reactant diffusion.

Nam *et al.* successfully prepared CNTs on FTO glass for use as CEs in DSSCs by two different methods.[118] In one method, randomly dispersed MWCNT paste was screen-printed. In the other method, relatively well-aligned CNTs were directly grown by catalytic chemical vapor deposition (Fig. 19c). The DSSC with the deposited CNT CE achieved a PCE of 10.04%, which was higher than that of the DSSCs with printed CNT CE (PCE = 8.03%) and Pt-coated CE (PCE = 8.80%) under the same experimental conditions. It was thought that the large surface area and high electron conductivity of CNTs contributed to the high DSSC efficiency.

Though carbon nanotubes show excellent conductivity and catalytic property, their current production cost compared to other carbon nanostructures is very high.[332,352] This may stimulate researchers to use low cost carbon black nanoparticles.

### 4.4. Graphene

Graphene is formed out of a flat monolayer of carbon atoms which are densely packed in a honeycomb lattice in 2-dimensions.[358] Graphene is an allotrope of carbon in the form of an atomic-scale, hexagonal lattice in which one atom forms each vertex. The carbon atoms are $sp^2$ hybridized with a C–C bond length of 1.42 Å.[359] Graphene is the basic structural element of other allotropes, including graphite, charcoal, carbon nanotubes and fullerenes. Graphene is best known for its outstanding electrical, thermal, optical, and mechanical properties.[335,360–364] As the thinnest material, graphene possesses many unusual properties, like high carrier mobility ($\sim$10 000 $cm^2$ $V^{-1}$ $s^{-1}$),[329,365–367] high specific area (2630 $m^2$ $g^{-1}$),[368,369] excellent thermal conductivity ($\sim$3000 W $m^{-1}$ $K^{-1}$),[370] high Young's modulus ($\sim$1 TPa),[360] and high optical transparency (97.7%).[371] In addition, it has been proved that the catalytic activity is enhanced by introducing oxygen species; also structural defects have the same effect on the catalytic activity.[372] Owing to such characteristics, it is no surprise that graphene materials were quickly applied in DSSCs. Among the carbon materials, CNTs and graphene are always hotter research topics than the other carbon materials.

In 2008, Xu *et al.* first studied graphene materials as CEs in DSSCs.[373] Although the CRGO (chemically reduced graphene

Open Access Article. Published on 25 August 2017. Downloaded on 4/25/2024 1:35:01 PM.
This article is licensed under a Creative Commons Attribution-NonCommercial 3.0 Unported Licence.

oxide) film as CE worked better in the DSSC (PCE = 2.2%) than did the bare FTO (PCE = 0.05%), it was obvious that many improvements should be done to reach the efficiency of the conventional Pt electrode (PCE = 4.0%). Roy-Mayhew *et al.* prepared a porous network of TRGO (thermally reduced graphene oxide) film by spin-coating a polymer-TRGO composite and thermalizing the polymer binder.[374] The functionalized graphene sheets with oxygen-containing sites performed comparably to Pt (TRGO, $R_{CT}$ = 9.4 Ω cm$^2$, PCE = 5.0%; Pt, $R_{CT}$ = 1.3 Ω cm$^2$, PCE = 5.5%). The results showed that the functional groups and defects could be tuned by increasing the amount of oxygen-containing groups, which led to the improvement of the catalytic activity of electrodes.

In order to increase the surface area and porosity, Zheng *et al.* ground CRGO in poly(ethylene glycol) and then heat treated, which led to the films with larger pores (~1 nm) and DSSCs with higher efficiencies (PCE = 7.2%) compared to those created from ultrasonicated CRGO in the polymer (PCE = 5.2%).[375] However, the PCE was still lower than that of the DSSC with Pt CEs (PCE = 7.8%). In order to increase the intrinsic activity of the electrodes, Yu *et al.* prepared N- and P-dual-doped graphene (NPG) *via* a ball-milling process, followed by thermal annealing utilizing $C_3H_6N_6$ and $(C_6H_5)_3P$ as the N and P source.[376] The metal-free material exhibits excellent electrocatalytic activity towards $I_3^-/I^-$ redox reaction. Dual-doping of N and P heteroatoms can markedly enhance the photovoltaic performance of DSSCs by a synergistic effect and a PCE of 8.57% was achieved, which was superior to that of Pt CE (7.58%), and much higher than that of the single N- or P-doped graphene electrodes. Interestingly, Wang *et al.* developed a three-dimension honeycomb-like structured graphene (Fig. 19d) by a simple reaction between $Li_2O$ and CO.[377] The graphene sheets showed superior catalytic performance, and the DSSC based on this honeycomb-like structured graphene CE achieved a PCE of 7.8%.

As shown in Fig. 20, Jeon *et al.* prepared edge-selectively halogenated graphene nanoplatelets (XGnPs, X = Cl, Br, and I) by the mechanochemically driven reaction between graphite and diatomic halogen molecules ($Cl_2$, $Br_2$ or $I_2$).[378] The contents of halogens (Cl, Br, and I) in XGnPs were 3.18, 1.77, and 0.66 at%, respectively. The XGnPs CEs showed excellent electrochemical stability and electrocatalytic activities toward $Co(bpy)_3^{3+}$ reduction. Amongst XGnPs, IGnP-CE showed the lowest $R_{CT}$ of 0.46 Ω cm$^2$. This value is much lower than that of the Pt-CE (0.81 Ω cm$^2$). Furthermore, the DSSC with IGnP-CE had the highest fill factor of 0.713 and a PCE of 10.31%, while those of DSSCs with Pt-CE were only 0.706 and 9.92%, respectively.

Wang and Gratzel prepared a graphene CE using layer-by-layer assembly of negatively charged graphene oxide and positively charged poly(diallyldimethylammonium chloride), and a following electrochemical reduction procedure.[238,379] The DSSCs using the graphene CE combined with the heteroleptic Ru complex C106TBA as sensitizer produced a high PCE of 9.54%, surpassing the DSSCs using Pt CE (9.14%).

Pt is known as the best catalyst for the regeneration of the $I_3^-/I^-$ electrolyte. However, a number of recent studies show that a carbonaceous type catalyst outperforms Pt with the cobalt redox electrolyte, due to low CT resistance at the counter electrode.[380,381] Yang *et al.* used YA422 as photosensitizer and

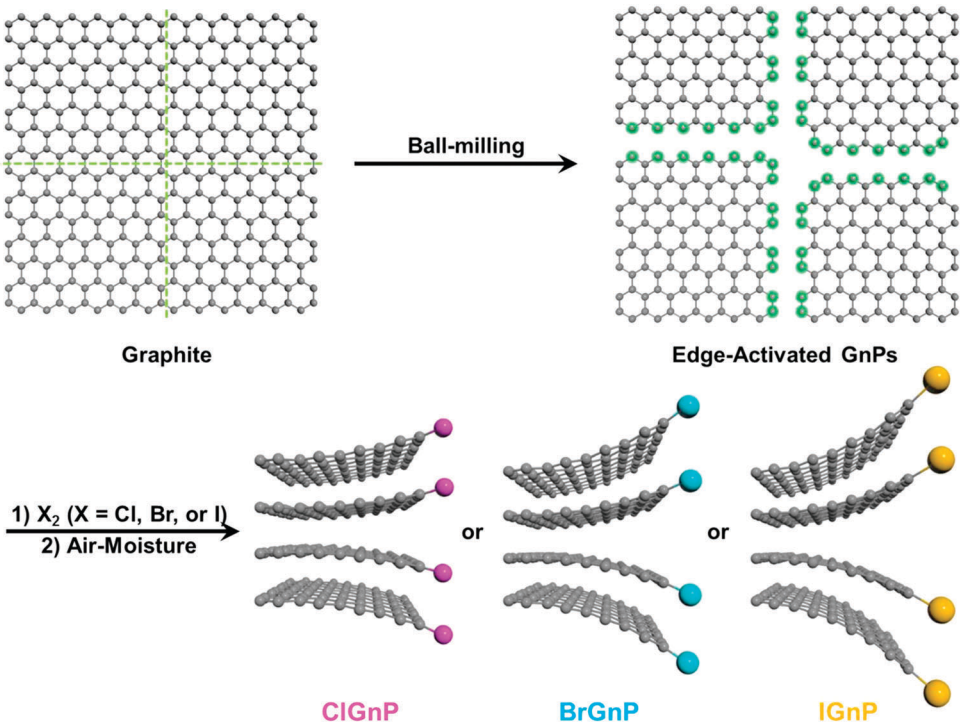


Fig. 20 Schematic representation of the mechanochemically driven reaction between graphite and halogen to produce edge-halogenated graphene nanoplatelets (XGnPs, X = Cl, Br, or I). Reprinted with permission from ref. 378. Copyright (2015) Elsevier.

Open Access Article. Published on 25 August 2017. Downloaded on 4/25/2024 1:35:01 PM. This article is licensed under a Creative Commons Attribution-NonCommercial 3.0 Unported Licence.

graphene nanoplatelets (GNP) as CE.[382] A PCE of 9.60% was obtained, and the photovoltage of the DSSC with Co-based electrolyte was higher than that with $I_3^-/I^-$ electrolyte. Applying Au + GNP as a CE, a PCE of 10.65% was achieved and the $R_{CT}$ value was lower than that of the Pt electrode. Mathew *et al.* used graphene as CE, SM315 as photosensitizer and cobalt(II/III) as redox shuttle, which resulted in a DSSC with a high $V_{OC}$ of 0.91 V, a $J_{SC}$ of 18.1 mA $cm^{-2}$, a FF of 0.78 and a PCE of 13%.[383]

The Hanaya group used the $I_3^-/I^-$ electrolyte, the conventional Pt CE, and the co-photosensitizer alkoxysilylanchor dye ADEKA-1 and carboxy-anchor organic dye LEG4, and this DSSC achieved a PCE of 11.2%.[223] In order to enhance photovoltage, an optimal $[Co(phen)_3]^{3+/2+}$ electrolyte was used, which resulted in a high $V_{OC}$ of over 1 V and a PCE of 13.8%. But a decrease of $J_{SC}$ was also observed compared to the $I_3^-/I^-$ electrolyte system. In order to recover the $J_{SC}$, according to some research studies,[380–383] an Au + GNP CE was used,[223] which succeeded in obtaining a high IPCE of up to 91%, a $V_{OC}$ of greater than 1 V and the highest record PCE of 14.3%.

Graphene exhibits a promising capability of replacing platinum in the counter electrode of DSSCs; however, its commercial production at low cost is currently not possible. Further, conventional methods of graphene synthesis involve highly toxic chemicals.[332]

### 4.5. Other carbon materials

Mesoporous carbon materials have received wide attention, due to their large internal surface area, pore volume, and tunable and narrow pore diameter. Using large porous silica LPS as templates, Srinivasu *et al.* synthesized large porous carbon (LPC) with hexagonal rod-like morphology and ordered pore structure and utilized it as the CE of DSSCs.[90,384] The nitrogen adsorption data indicated that an LPC possesses a BET specific surface area of 1300 $m^2$ $g^{-1}$ and a pore diameter of 4.4 nm. Owing to the high surface area, the DSSC with the LPC CE achieved a high PCE of 7.1%.

Graphite is often used as conductive films, for its excellent intrinsic conductivity. Li *et al.* prepared graphite nanofiber (GNF), graphite nanosheet (GNS), and graphite nanoball (GNB) and used them as the CEs of DSSCs.[385] Compared to GNF and GNS, GNB not only provided more defects in the $sp^2$ plane but also possessed abundant hydroxyl functional groups as the electrocatalytic active sites for triiodide reduction; thereby, the intrinsic heterogeneous rate and effective catalytic surface area of GNB-based CE are both higher than those of GNF-based and GNS-based CEs. The DSSC with GNB CE showed a PCE of 7.88%, which was close to that of the device with Pt CE (PCE = 8.38%), while GNF-based and GNS-based DSSCs showed PCEs of 3.60% and 2.99%, respectively.

The porous expanded graphite (EG) obtained from graphite has a higher specific surface area and better conductivity. Pencil-lead is one kind of carbon. Wei *et al.* prepared carbon CEs for DSSCs by coating the mixed paste of expanded graphite (EG) and 5B pencil-lead carbon on FTO and then heating at 450 °C for one hour.[386] By optimizing the weight ratio of EG/5B pencil-lead to 1 : 1 in the CE carbon layer, the PCE of the DSSC reached 7.67% under irradiation of green light (525 nm, LED) with an intensity of 25 W $m^{-2}$.

The Ma group did comprehensive research on nine kinds of carbon materials, including activated carbon (Ca), carbon black (CB), conductive carbon (CC), carbon dye (Cd), carbon fiber (Cf), discarded toner of a printer (Cp), well-ordered mesoporous carbon (Com), carbon nanotube (CNT), and fullerene ($C_{60}$).[387] The photovoltaic results indicated that Com and Cd showed high catalytic activity, and the DSSCs gave a high PCE of 7.5%, which was comparable to the performance of Pt. The other carbon materials (Ca, CB, CC, Cf, and CNTs) showed decent catalytic activity, and the PCE values of the DSSCs ranged from 6.3% to 7.0%.

Lee *et al.* fabricated an all carbon CE for DSSCs by replacing the conventional thin Pt layer and FTO substrate with a large-surface-area polyaromatic hydrocarbon (LPAH) film and a graphite film.[91,388] The LPAH particles have a uniform size of ~10 nm, a more than 3-fold higher specific surface area, and 45% enhanced pore diameters compared with CB particles. The internal resistance of the cell was substantially reduced and the cell efficiency reached 8.63%, which was a 20.7% improvement compared to the case of Pt/FTO CE based DSSCs. Kumar *et al.* prepared graphitic carbon by the carbonization of sucrose and used it as CE in DSSCs.[389] The graphitic carbon from sucrose showed a faster reduction rate of $I_3^-$, compared with Pt CE. The DSSCs based on the graphitic carbon exhibited a high PCE of 9.96% and a FF of 0.72, which are higher than the PCE of 9.39% and FF of 0.67 of the cells with Pt CE.

The photovoltaic parameters of high-performance DSSCs based on carbon CEs are summarized in Table 2. The carbon materials demonstrate high catalytic activity, simple preparation, low cost, considerable stability, and are one of the most competitive candidates among Pt-free CE materials. However, most of the performances of DSSCs based on carbon CEs are slightly lower than those assembled with Pt CEs, which may come from various resistances associated with carbon CEs, such as contact resistance to the TCO substrate, bulk resistance through the thicker carbon CE, and diffusion resistance in the pores of CE. On the other hand, carbon CE requires a large dosage to attain the targeted catalytic activity, and suffers from poor adhesion to the substrate.

## 5. Polymer counter electrodes

Conductive polymers or, more precisely, intrinsic conducting polymers were discovered in 1977,[390,391] and are the fourth generation of polymers and have been developed from laboratory materials to mature industrial products.[392] Furthermore, the fundamental discovery of intrinsic conducting polymers was honored by a Nobel Prize won by Shirakawa, MacDiarmid, and Heeger in 2000.[393] Conductive polymers are organic polymers that conduct electricity. Such compounds may have metallic conductivity or can be semiconductors. The electrical properties can be fine-tuned using the methods of organic synthesis and by advanced dispersion techniques. One important advantage of

Open Access Article. Published on 25 August 2017. Downloaded on 4/25/2024 1:35:01 PM.
This article is licensed under a Creative Commons Attribution-NonCommercial 3.0 Unported Licence.

Table 2 Photovoltaic parameters of the liquid-junction DSSCs based on carbonaceous CEs

| CE materials | Substrate | Redox couple | Dye | FF | PCE/% | PCE (Pt)/% | Ref. |
|---|---|---|---|---|---|---|---|
| MWCNTs (CVD) | Asahi glass | $I_3^-/I^-$ | N719 | 0.73 | 10.04 | 8.80 | 118 |
| Au/GNP | FTO | $Co^{3+/2+}$ | LEG4 + ADEKA-1 | 0.771 | 14.30 | 13.8 | 223 |
| Carbon black | FTO | $I_3^-/I^-$ | N719 | 0.685 | 9.10 | | 265 |
| Carbon black + graphite | FTO | $I_3^-/I^-$ | N719 | 0.712 | 6.67 | | 266 |
| Carbon black | FTO | $I_3^-/I^-$ | N719 | 0.713 | 8.35 | 8.29 | 337 |
| Carbon black | FTO | $I_3^-/I^-$ | N719 | 0.656 | 7.20 | 7.60 | 338 |
| Carbon black | FTO | $Co^{3+/2+}$ | Y123 | 0.74 | 8.81 | | 339 |
| Carbon black + PEDOT | FTO | $T_2/T^-$ | C106 | 0.70 | 7.60 | 7.00 | 340 |
| Carbon nanofiber | FTO | $I_3^-/I^-$ | N719 | 0.70 | 7.00 | 7.10 | 348 |
| HACNF (hollow active carbon nanofiber) | FTO | $I_3^-/I^-$ | N719 | 0.64 | 7.21 | 7.69 | 349 |
| Pt/CF (1.0 wt%) | FTO | $Co^{3+/2+}$ | YD2-*o*-C8 | 0.68 | 8.97 | 9.41 | 350 |
| MWCNTs | FTO | $I_3^-/I^-$ | N719 | 0.64 | 7.67 | 7.83 | 355 |
| SWCNTs | FTO | $I_3^-/I^-$ | N719 | | 7.81 | | 356 |
| MWCNTs | FTO | $I_3^-/I^-$ | N719 | | 7.63 | | 356 |
| 3D-SWCNTs | FTO | $I_3^-/I^-$ | N719 | | 8.31 | 7.56 | 357 |
| Reduced graphene oxide | FTO | $I_3^-/I^-$ | N719 | 0.72 | 7.19 | 7.76 | 375 |
| NPG (N- and P-doped graphene) | FTO | $I_3^-/I^-$ | N719 | 0.72 | 8.57 | 7.58 | 376 |
| Honeycomb-like structured graphene | FTO | $I_3^-/I^-$ | N719 | 0.37 | 7.80 | | 377 |
| IGnPs (graphene nanoplatelets) | FTO | $Co^{3+/2+}$ | N719 | 0.71 | 10.42 | 9.92 | 378 |
| ERGO (electrically reduced graphene oxide) | ITO | $I_3^-/I^-$ | C106TBA | 0.74 | 9.54 | 9.14 | 379 |
| Au + GNP | FTO | $Co^{3+/2+}$ | YA422 | 0.74 | 10.65 | | 382 |
| Graphene | FTO | $Co^{3+/2+}$ | SM315 | 0.78 | 13.00 | | 383 |
| LPC (large porous carbon) | FTO | $I_3^-/I^-$ | N719 | 0.66 | 7.14 | | 384 |
| GNB (graphite nanoball) | FTO | $I_3^-/I^-$ | N719 | 0.67 | 7.88 | 8.38 | 385 |
| EG + 5BC (expanded graphite + 5B pencil, 1 : 1) | FTO | $I_3^-/I^-$ | N719 | 0.64 | 7.67 | | 386 |
| Cd (carbon dye) | FTO | $I_3^-/I^-$ | N719 | 0.70 | 7.50 | 7.50 | 387 |
| Com (ordered mesoporous carbon) | FTO | $I_3^-/I^-$ | N719 | 0.65 | 7.50 | 7.50 | 387 |
| LPAH (large-surface polyaromatic hydrocarbon) | Graphite | $I_3^-/I^-$ | N719 | 0.80 | 8.63 | 7.15 | 388 |
| Graphitic carbon from sucrose | FTO | $I_3^-/I^-$ | N719 | 0.72 | 9.96 | 9.39 | 389 |

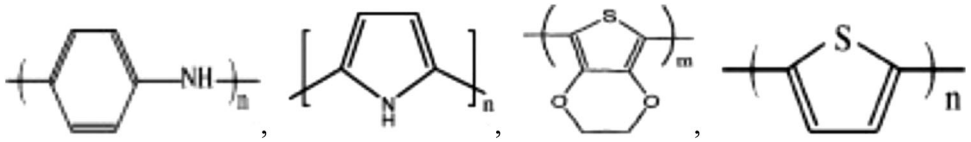


Fig. 21 The structures of typical conducting polymers from left to right: polyaniline, polypyrrole, poly(3,4-ethyelenedioxythiophene) (PEDOT) and polythiophene. Reprinted with permission from ref. 148. Copyright (2015) Elsevier.

conductive polymers is their processability, mainly by dispersion.[394] Most conductive polymers are derivatives of polyacetylene, polyaniline, polypyrrole or polythiophenes. The molecular structure feature (Fig. 21) of these polymers is conjugated double bonds for conduction.

Conductive polymers are potential candidates used as Pt-free CE materials in DSSCs due to their facile synthesis, porous structure, electrical conductivity, low cost, abundance, and favorable catalytic properties.[91,148,333,395]

### 5.1. Poly(3,4-ethylenedioxythiophene)

In the 1980s, a new polythiophene derivative, poly(3,4-ethylenedioxythiophene) (PEDOT), was invented at the Bayer Lab.[396,397] The molecular structure of PEDOT is shown in Fig. 21. Although PEDOT is an insoluble polymer, it exhibited excellent conductivity (300–500 S $cm^{-1}$),[393,398] which is much higher than that of polyaniline, polypyrrole, and polythiophene. Furthermore, its solubility issue was subsequently solved by doping with poly(styrene sulfonate) (PSS).[399] Because of its high conductivity, excellent transparency in visible light, and remarkable stability, PEDOT is a promising material for antistatic, electronic, and optoelectronic applications.[400,401] The water-soluble and easy processing PEDOT:PSS has become the industry leader in transparent conductive polymers.[402] Recently, it was reported that the conductivity of PEDOT:PSS reached more than 4600 S $cm^{-1}$.[403]

In 1998, Yohannes and Inganas fabricated an all-solid-state photoelectrochemical cell consisting of poly[3-(4-octylphenyl)-thiophene] (POPT) coated on ITO as the working electrode, amorphous poly(ethylene oxide) (POMOE) complexed with triiodide/iodide redox couple as the solid electrolyte, and electrochemically polymerized PEDOT on ITO as the counter electrode.[404] Although the efficiency of this solar cell was low, it demonstrated the catalytic activity of PEDOT for the reduction of triiodide. This signalled the feasibility of PEDOT as a CE material for DSSCs.

Owing to high conductivity, catalytic activity, electrochemical reversibility, and significant thermal and chemical stability,[405] in 2002, Saito *et al.* first explored PEDOT as CE for DSSCs by chemically polymerizing PEDOT on FTO.[406] They also prepared *p*-toluenesulfonate (TsO)-doped PEDOT and PSS-doped PEDOT. The PCE of the DSSCs with PEDOT-TsO CE was almost the same as that of the cell with Pt CE and was better than that of the device with PEDOT-PSS CE owing to the exposure of $PSS^-$ that

 This journal is © The Royal Society of Chemistry 2017

Open Access Article. Published on 25 August 2017. Downloaded on 4/25/2024 1:35:01 PM.
This article is licensed under a Creative Commons Attribution-NonCommercial 3.0 Unported Licence.

resulted in increased overpotential. Pringle *et al.* prepared PEDOT films on an ITO/PEN flexible substrate by using the electrodeposition technique. The results showed that a five sec deposition time was enough to achieve a highly effective and transparent PEDOT film. The DSSCs using this CE and organic liquid electrolyte produced a high PCE of 8.0%.[186]

The morphology of PEDOT affects the electrochemical properties of the CE and the photovoltaic performance of the devices. The nanoporous structure can be modified through process control. Ahmad *et al.* prepared PEDOT nanoporous layers on FTO by using electro-oxidative polymerization and using hydrophobic ionic liquids as a medium.[407] The as-prepared highly porous PEDOT films showed a conductivity of 195 S $cm^{-1}$. These films were used as CEs in DSSCs, yielding a PCE of 7.93%, which was close to that achieved with the classical Pt electrode (8.71%). Trevisan *et al.* used ZnO nanowire arrays as templates and electropolymerized PEDOT-nanotubes (NTs) on FTO.[408] The PEDOT-NT CE presented a performance as good as the conventional Pt CE, or even better, depending on the electrolyte used. The PEDOT-NT CEs showed improved performance, compared with their dense and flat counterparts. The DSSC with the PEDOT NT CE achieved a PCE of 8.3%, which was comparable to the DSSC with Pt CE (8.5%). Similarly, PEDOT-nanofibers (NFs) with diameters of 10–50 nm and a high conductivity of 83 S $cm^{-1}$ were prepared by using sodium dodecyl sulfate micelles as nanoreactors.[409] The PEDOT-NFs were spin-coated as a methanol-based colloidal dispersion. The DSSC based on the PEDOT-NF CE with low surface resistance and a highly porous surface achieved a high PCE of 9.2%, compared with bulk PEDOT (6.8%). It also surpassed the efficiency of Pt CEs (8.6%).

With $Co^{3+/2+}$ as the redox couple for DSSCs, the PEDOT CE can give a better result than the Pt CE. Tsao *et al.* prepared PEDOT CEs by electro-oxidative polymerization.[410] The DSSC with Y123-sensitized, Co-mediated and PEDOT-based CE yielded the highest PCE of 10.30%, which is due to the fact that PEDOT dramatically reduces the interfacial charge-transfer resistance and the mass transport limitations, resulting in superior PCE values. For the $T_2/T^-$ redox system, the use of PEDOT also leads to significant enhancement of photovoltaic properties. Burschka *et al.* achieved a record PCE of 7.9% for a T-mediated DSSC with PEDOT CE, and the efficiency was higher than that of the cell with a Pt electrode.[411]

Poly(3,4-propylenedioxythiophene) (PProDOT) supersedes Pt electrodes in DSSCs and gives better results due to its ultrahigh surface area and its ability to avoid the formation of any passivation layers at the electrode/electrolyte interface. To date, the PCE values of the DSSCs with PProDOT CEs are significantly higher than the data reported using many other types of CEs.[412–416] For instance, the cells using PProDOT CEs yielded a 20% improvement in PCE (9.9%) and a remarkable drop in $R_{CT}$ (2.5 Ω $cm^2$) as compared to the Pt electrode (8.24%, 50 Ω $cm^2$).[415] The record PCE values of the PProDOT-based DSSCs with I-based and Co-based redox couples are 9.25% and 10.08%, respectively. In addition, the PProDOT layer can be produced on flexible substrates, facilitating their use in flexible DSSCs.

Polythiophene (PTh) can also be used as a CE material in DSSCs. Bora *et al.* prepared a PTh/graphene (PTh/GR) composite by interfacial polymerization (shown in Fig. 22) and used it as CE for DSSCs.[417] The composite electrode showed higher electrocatalytic activity compared to the pristine PTh electrode for reduction of triiodide, and this is mainly due to its large active surface area and better charge transport. Higher $J_{SC}$ and higher FF values were observed in the case of PTh/GR based DSSCs compared to the PTh based device. This may be attributed to the incorporation of GR sheets that significantly

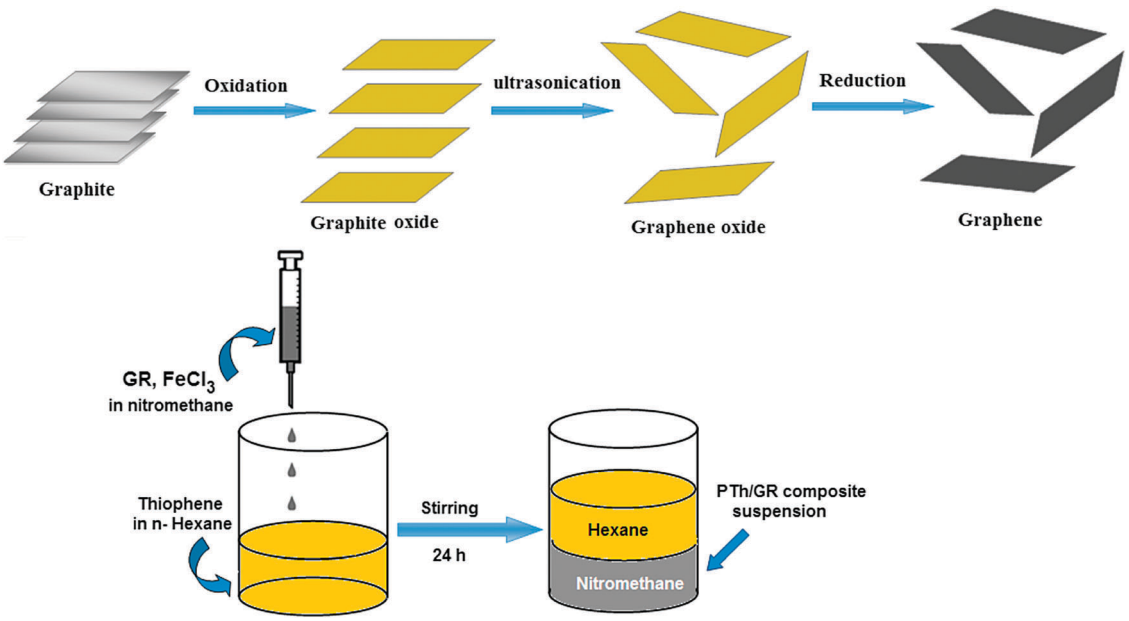


Fig. 22 Fabrication process of the PTh/GR composite. Reprinted with permission from ref. 417. Copyright (2015) Elsevier.

Open Access Article. Published on 25 August 2017. Downloaded on 4/25/2024 1:35:01 PM. This article is licensed under a Creative Commons Attribution-NonCommercial 3.0 Unported Licence.

increases the electron transport process within the PTh by reducing the resistance. The DSSCs with the composite electrode achieved a PCE of 4.8% and the device with conventional Pt electrode achieved a PCE of 5.1% under the same conditions.

### 5.2. Polyaniline

Polyaniline (PANI) is a conducting polymer. Although the compound was discovered over 150 years ago, PANI has captured intense attention from the scientific community since the early 1980s, which is due to the rediscovery of its high electrical conductivity. Amongst the family of conducting polymers and organic semiconductors, PANI is one of the most studied conducting polymers in the past 50 years.[418–421]

PANI is especially attractive because it is relatively inexpensive, has three distinct oxidation states with different colors, and has an acid/base doping response. The last property makes PANI an attraction for acid/base chemical vapor sensors, supercapacitors and biosensors. The different colors, charges and conformations of the multiple oxidation states also make the material promising for applications such as actuators, supercapacitors and electrochromics. It is suitable for the manufacture of electrically conducted yarns, antistatic coatings, electromagnetic shielding, and flexible electrodes.[422–426]

Among the various conducting polymers, polyaniline (PANI) is one of the most intensively studied counter electrode materials, owing to its low cost, easy synthesis, high conductivity, high thermal and chemical stability, and interesting redox properties.[427,428] Different varieties of PANI have been synthesized and used as CE materials for DSSCs. In general, synthesized PANI nanostructure should be a porous structure with a high surface area. Moreover, electrodeposited PANI exhibits superior performance because of its well-connected structure.

In 2008, the Wu group first reported the use of PANI as CE for DSSCs.[429] They synthesized microporous PANI nanoparticles (NPs) with size diameters of 100 nm by an aqueous oxidative polymerization reaction, with perchloride acid as a dopant in the presence of ammonium persulfate. The PANI CE exhibited higher electrocatalytic performance for the $I_3^-/I^-$ redox reaction than the Pt electrode, and achieved a PCE of 7.15%, over 0.25% higher than the PCE value of the Pt-based CE.

One-dimensional PANI nanostructures with different morphologies, like nanofibers, nanobelts, and nanotubes, have been synthesized.[407–409] For example, in order to improve the electrocatalytic performance of the PANI films, an oriented PANI nanowire array was *in situ* grown.[430] Since electron transportation along the PANI nanowires is fast, any exposed polymer parts will be effective for the catalytic reduction of the oxidized species in the electrolyte. The PANI nanowire array shows higher electrocatalytic activity for $Co^{3+/2+}$ redox reaction than the random PANI film, and even outperforms the Pt electrode. With the oriented PANI nanowire array as CE, a Co-mediated DSSC with a FNE29 dye achieved a PCE of 8.24%, much higher than the efficiency obtained using the random PANI film (5.97%) or the Pt cathode (6.78%). Hou *et al.* synthesized a polyaniline nanoribbon (PANI NR) CE with serrated, flexible and ultrathin nanostructures by *in situ* polymerization and by using electrospun vanadium pentoxide ($V_2O_5$) as template and oxidant, followed by acid etching.[431] Owing to its abundant active sites and good contact performance, the PANI NR CE showed high catalytic activity and the DSSC based on the PANI-NR CE achieved a PCE of 7.23%, which was comparable to that of the Pt-based DSSC (7.42%).

By appropriate methods, PANI can be prepared as transparent films, which can be used in bifacial solar cells, so as to improve the utilization efficiency of the incident light. By a facile *in situ* polymerization method, Tai *et al.* synthesized a highly uniform and transparent PANI film and used it as CE in DSSCs.[207] The electrode was used to fabricate a bifacial active transparent DSSC, which showed efficiencies of 6.54 and 4.26%, corresponding to front- and rear-side irradiation, respectively. Meanwhile, the efficiency of the device with the same photoanode and Pt CE was 6.69%. Compared to conventional Pt-based DSSCs, the design of the bifacial DSSC is conducive to utilize light from both sides. Wu devised a bifacial DSSC based on transparent PANI CE.[94] Owing to sunlight irradiation simultaneously from the front and the rear sides, more dye molecules are excited, which results in the enhancement of $J_{SC}$ and thus overall conversion efficiency. The photoelectric properties of PANI were improved by modifying with 4-aminothiophenol (4-ATP). The bifacial DSSC with 4-ATP/PANI CE achieved an overall conversion efficiency of 8.35%, which was increased by 24.6%, compared to the DSSC irradiated from the front only.

PSS, TsO (Ts = tosyl), $SO_4^{2-}$, $ClO_4^-$, $BF_4^-$ and $Cl^-$ have been used as dopants in the design of CEs.[412,432–434] Doping ions affect the morphologies, electrochemical properties, and doping/dedoping process of polymer films. Among them, the $SO_4^{2-}$-doped PANI film showed porous morphology, higher reduction current for the reduction of triiodide and a lower charge-transfer resistance (1.3 $\Omega$ $cm^2$) than the Pt CE. The DSSC with PANI-$SO_4$ CE achieved a PCE of 5.6%.[434] The sodium dodecyl sulfate (SDS)-doped PANI film exhibited the highest conductivity, which leads to a higher catalytic reduction of triiodide. DSSCs assembled with PANI-SDS CE gave a PCE of 7.0%, which was comparable to that of a conventional Pt CE (7.4%).[435]

Hexafluoro-isopropanol (HFIP) is a non-toxic, low boiling point (59 °C), mildly acidic and strong hydrogen-bonding solvent. Polymer films (PANI-$SO_4$-F or PEDOT-F) on FTO with high conductivity, strong adhesion, and good electrochemical activity can be fabricated simply by spin coating or casting from the corresponding solutions at room temperature. Chiang *et al.* made highly concentrated and stable PANI/HFIP and PEDOT/HFIP colloid solutions simply by dissolving the doped polymer powders in HFIP.[436] The DSSCs based on PANI-$SO_4$-F and PEDOT-F CEs, combining CYC-B11 sensitizer and triiodide/iodide electrolyte, achieved conversion efficiencies up to 8.8% and 9.0%, respectively. The device based on the conventional Pt electrode achieved an efficiency of 8.9% under the same conditions. Excellent photoelectric properties, easy preparation, and low cost render the PANI electrode a credible candidate for replacing Pt in DSSCs.

Superior catalytic activities, high conductivity, simple preparation, and low cost associated with PANI make it a credible

Open Access Article. Published on 25 August 2017. Downloaded on 4/25/2024 1:35:01 PM.
This article is licensed under a Creative Commons Attribution-NonCommercial 3.0 Unported Licence.

alternative CE for DSSCs. However, PANI is not an ideal CE material because it suffers from instability, self-oxidation, and carcinogenic properties.[91]

### 5.3. Polypyrrole

The first example of polypyrrole (PPy) was reported in 1963 by Weiss and his colleagues.[437] They described how the pyrolysis of tetraiodopyrrole produced highly conductive materials. Polypyrrole is a type of organic polymer formed by the polymerization of pyrrole. PPy films are yellow, but darken in air due to some oxidation. Doped films are blue or black, depending on the degree of polymerization and film thickness. They are amorphous, showing only weak diffraction. PPy is described as "quasi-one-dimensional" *vs.* one-dimensional since there is some crosslinking and chain hopping. Undoped and doped films are insoluble in solvents but swellable.[438] PPy is thermally stable in air up to 150 °C.[439,440]

PPy is an insulator, but its oxidized derivatives are good electrical conductors. The conductivity of the material depends on the conditions and reagents used in the oxidation. Conductivity ranges from 2 to 100 S $cm^{-1}$. PPy is mainly applied in electronic devices and chemical sensors.[441–443] PPy is a potential candidate to replace Pt CE because of its easy synthesis, good catalytic activity, low cost, high polymerization yield, and considerable environmental stability.[440,444–446]

Wu *et al.* first reported the application of PPy as CE material in DSSCs in 2008.[444] Before that, PPy as hole conductor was used in solid-state DSSCs.[447,448] In Wu's work,[444] PPy nanoparticles were synthesized by chemical polymerization, using iodine as initiator.[449] The as-prepared PPy was coated on FTO to construct PPy CE. SEM images show that PPy with porous morphology and particle diameter in the 40–60 nm range was uniformly and tightly covered on FTO. Cyclic voltammograms revealed that the PPy electrode has smaller $R_{CT}$ and higher electrocatalytic activity than the Pt electrode. The DSSC with the PPy CE achieved a PCE of 7.66%, while the device with Pt CE achieved a PCE of 6.90%.

Jeon *et al.* synthesized discrete spherical PPy nanoparticles with a uniform diameter of ~85 nm and a conductivity of ~10 S $cm^{-1}$ by chemical oxidative polymerization within micelles that have myristyl trimethyl ammonium bromide (MTAB) and decyl alcohol as the nanoreactors.[440] The surface resistivity of the PPy layer on the FTO glass decreased from 624 to 387 Ω $sq^{-1}$ after post-doping with concentrated HCl vapor for 1 min. The DSSCs based on PPy and HCl-doped PPy CEs achieved PCEs of 5.28 and 6.83%, respectively. Moreover, the cell efficiency was further enhanced to 7.73% by tuning electrolyte composition which is the highest efficiency to date with the use of PPy as CEs. Peng *et al.* presented a facile method to prepare free-standing PPy nanotube films by simply heating pulp-like homogeneous suspensions at low temperature, which can be used as a flexible FTO- and Pt-free CE for DSSCs.[445] The DSSCs based on these paper-like PPy membranes show an impressive conversion efficiency of 5.27%, which is about 84% of the cell with a conventional Pt/FTO CE (6.25%).

Hwang *et al.* synthesized ultrathin polypyrrole nanosheets (UPNSs) by chemical oxidation *via* organic single-crystal surface-induced polymerization (OCSP), using sodium decylsulfonate (SDSn) as a template (shown in Fig. 23).[446] These UPNSs have similar morphology as graphene sheets with higher surface area and active sites. The OCSP produced a two-dimensional structure with fewer grain boundaries. The UPNSs were deposited onto FTO for CEs in DSSCs. The UPNS CE had high transparency (94%) which is attributed to its nanoscale thickness. Post-doping treatment with HCl vapor increased conductivity to 39 S $cm^{-1}$, 26% greater than that of untreated UPNS electrodes (31 S $cm^{-1}$), and improved the catalytic activity of the electrodes. The Tafel polarization and impedance results support the enhancement of catalytic activity by HCl doping. The DSSC with the HCl-enhanced UPNS CEs showed a PCE of 6.8%, which is 19.3% greater than the untreated case and comparable to that of Pt CE-based DSSCs (7.8%). Furthermore, the UPNS is suitable for flexible applications, thanks to its high transparency, low temperature processing, and two-dimensional morphology.

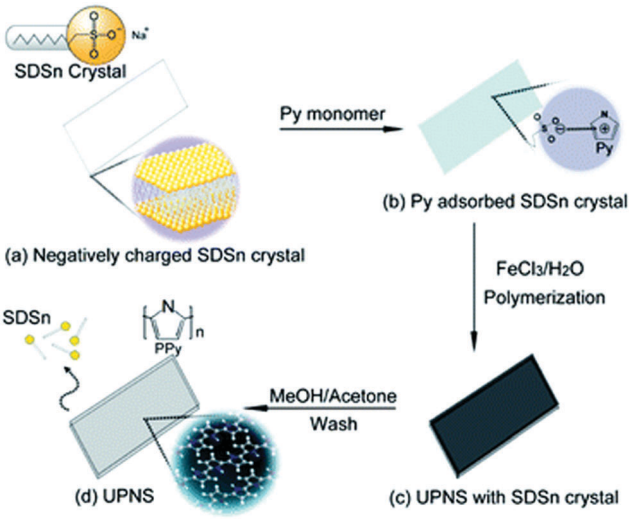


Fig. 23 A diagram of the UPNS preparation. Reprinted with permission from ref. 446. Copyright (2014) Royal Society of Chemistry.

There are copious amounts of research and applications of PPy as CE materials in DSSCs.[440,444–446,450–456] Amongst various conducting polymers known to us, PPy is of special interest because of its easy synthesis, excellent stability in air, low cost, and high polymerization yield.[333] The main issue for PPy CE is its higher $R_{CT}$, and the conductivity of the PPy film is also not good enough.[148] The performance of PPy CE is highly process dependent and it depends upon dopant, morphology, and choice of synthesis methods.

The photovoltaic parameters of DSSCs using conductive polymers as CEs are shown in Table 3. Conductive polymers are flexible, transparent, easily processed, and can be put into mass production easily. The properties of conductive polymers can be tuned easily. They show reasonable performance with respect to Pt counterparts. PEDOT (PProDOT) exhibits the best performance among conductive polymers, but its cost is comparable to that of Pt. While PPy based CEs are cheaper but the performance is slightly inferior to that of PEDOT. PANI-based CEs have more attractive prospect for their low cost and comparably better performance. Conducting polymer based

Open Access Article. Published on 25 August 2017. Downloaded on 4/25/2024 1:35:01 PM.
This article is licensed under a Creative Commons Attribution-NonCommercial 3.0 Unported Licence.

Table 3 Photovoltaic parameters of DSSCs based on polymer CEs (AM1.5, 100 mW $cm^{-2}$)

| CE materials | Dye | Redox couple | $J_{SC}$ (mA $cm^{-2}$) | $V_{OC}$ (mV) | FF | PCE (%) | Ref. |
|---|---|---|---|---|---|---|---|
| Transparent PEDOT (flexible) | N719 | $I_3^-/I^-$ | 14.10 | 787 | 0.73 | 8.00 | 186 |
| PEDOT | N719 | $I_3^-/I^-$ | 15.00 | 693 | 0.76 | 7.93 | 407 |
| PEDOT nanotube arrays | N719 | $I_3^-/I^-$ | 16.24 | 720 | 0.70 | 8.30 | 408 |
| PEDOT flat | N719 | $I_3^-/I^-$ | 15.83 | 730 | 0.69 | 7.90 | 408 |
| PEDOT nanofibers | N719 | $I_3^-/I^-$ | 17.50 | 724 | 0.73 | 9.20 | 409 |
| PEDOT | Y123 | $Co^{3+/2+}$ | 15.90 | 910 | 0.71 | 10.30 | 410 |
| PEDOT | Z907 | $T_2^-/T^-$ | 15.90 | 687 | 0.72 | 7.90 | 411 |
| PProDOT | N3 | $I_3^-/I^-$ | 16.80 | 715 | 0.59 | 7.08 | 412 |
| PProDOT-$Et_2$ | N3 | $I_3^-/I^-$ | 18.00 | 720 | 0.61 | 7.88 | 412 |
| PProDOT1 | N3 | $I_3^-/I^-$ | 16.40 | 770 | 0.72 | 9.12 | 413 |
| PProDOT2 | N3 | $I_3^-/I^-$ | 16.40 | 770 | 0.72 | 9.12 | 413 |
| PProDOT3 | N3 | $I_3^-/I^-$ | 17.00 | 761 | 0.71 | 9.25 | 413 |
| PEDOT | Y123 | $Co^{3+/2+}$ | 12.15 | 1027 | 0.69 | 8.62 | 414 |
| PProDOT1 | Y123 | $Co^{3+/2+}$ | 12.62 | 999 | 0.78 | 9.90 | 414 |
| PProDOT2 | Y123 | $Co^{3+/2+}$ | 11.95 | 1003 | 0.73 | 8.70 | 414 |
| PProDOT-$Et_2$ | Y123 | $Co^{3+/2+}$ | 11.51 | 1006 | 0.70 | 8.00 | 414 |
| PProDOT-$Me_2$ | Y123 | $Co^{3+/2+}$ | 12.33 | 1006 | 0.70 | 8.74 | 414 |
| PProDOT | Y123 | $Co^{3+/2+}$ | 13.06 | 998 | 0.77 | 10.08 | 415 |
| Microporous PANIN | N719 | $I_3^-/I^-$ | 14.60 | 714 | 0.69 | 7.15 | 429 |
| PANI nanowire arrays | FNE29 | $Co^{3+/2+}$ | 15.09 | 780 | 0.70 | 8.24 | 430 |
| PANI nanoribbons | N719 | $I_3^-/I^-$ | 17.92 | 720 | 0.56 | 7.23 | 431 |
| PANI-SDS | N719 | $I_3^-/I^-$ | 14.00 | 720 | 0.59 | 7.40 | 435 |
| PANI-$SO_4$-F(HFIP) | CYC-B11 | $I_3^-/I^-$ | 17.94 | 729 | 0.67 | 8.80 | 436 |
| PEDOT-F(HFIP) | CYC-B11 | $I_3^-/I^-$ | 18.50 | 723 | 0.67 | 9.00 | 436 |
| Spherical PPy | N719 | $I_3^-/I^-$ | 15.50 | 778 | 0.64 | 7.73 | 440 |
| Microporous PPy | N719 | $I_3^-/I^-$ | 15.01 | 740 | 0.69 | 7.66 | 444 |

CEs exhibit promising prospect when they are used with non-conventional electrolytes. They can play a dual role as substrate and catalyst. Therefore, replacing the TCO and Pt will account for more than half of the cost of the DSSCs.[148]

# 6. Transition metal compound counter electrodes

As alternatives to the noble metals, early transition metal compounds (TMCs), such as carbides and nitrides, have been used in the fields of ammonia synthesis and decomposition, hydrogenolysis, isomerization, methanation, hydroprocessing, among others. This is due to the fact that these transition metal compounds have electronic structures similar to noble metal Pt, with interstitial phases or interstitial compounds, and they show Pt-like behavior.[457–461] Consequently, it is not surprising that certain TMCs may replace platinum as CE materials in DSSCs. Since 2009, some metal compounds including carbides, nitrides, chalcogenides, oxides, phosphides, and so on have been applied in DSSCs as CEs to replace expensive Pt CE.

## 6.1. Carbides and nitrides

The catalytic activity of carbides was first explored between 1960 and 1970. This discovery led to similar findings for other early transition-metal carbides and nitrides.[457,462] The potential applications of transition-metal nitrides and carbides have been widely explored in material chemistry, in virtue of their unique physical and chemical properties, such as high electrical conductivity and thermal conductivity, good chemical stability,[463,464] catalytic activity,[465] as well as low-temperature superconductivity.[466] The synthesis of transition-metal nitrides provides interesting challenges because of the insertion of nitrogen into the interstitial sites of the metals. In general, transition-metal nitrides are conventionally produced by using metals, metal halides, or metal oxides that are thermally converted into nitrides by using high-temperature treatment with $N_2$ or $NH_3$, or into carbides by carbonation with $CH_4$.[333]

In 2009, Jiang *et al.* successfully synthesized highly ordered TiN nanotube arrays by the anodization of Ti foil, and subsequent nitridation in a $NH_3$ atmosphere, and used them as CE in DSSCs for the first time.[467] The TiN nanotube arrays as CEs resulted in lower $R_S$ and $R_{CT}$ at CE/electrolyte interfaces. The DSSC based on the TiN CE achieved a PCE of 7.73%, and the cell with conventional FTO/Pt CE achieved a PCE of 7.45%.

As for carbides, in 2010, Jang *et al.* prepared mesoporous tungsten carbides (WC) by polymer-derived (PD) and microwave-assisted (MW) methods, and used them as Pt-free CEs of DSSCs for the first time.[468] Although earlier in April of 2009, transition metal carbide TiC had been used in DSSCs, it was used in electrolytes, instead of counter electrodes.[469] The DSSCs with the mesoporous WC CEs by MW and PD methods achieved efficiencies of 7.01% and 6.61%, respectively, which were lower than that of the device with Pt CE (8.23%).[468] This can be attributed to the large particle size and low surface area of the two carbides. The Ma group thus embedded MoC and WC in ordered nanomesoporous carbon materials (MoC-OMC, WC-OMC) and spray coated on FTO glass.[470,471] The carbon dye (CD) was doped to improve the conductivity of the nanocomposites and $TiO_2$ powder (P25) was added to avoid particle aggregation and to improve the bonding. Owing to the high surface area of 611 $m^2$ $g^{-1}$ and 598 $m^2$ $g^{-1}$ of the two carbides, the DSSCs based on MoC-OMC and WC-OMC CEs achieved PCEs of 8.34% and 8.18%, respectively, while the cell

Open Access Article. Published on 25 August 2017. Downloaded on 4/25/2024 1:35:01 PM.
This article is licensed under a Creative Commons Attribution-NonCommercial 3.0 Unported Licence.

based on Pt CE achieved an efficiency of 7.89% under the same conditions.

Carbides (WC, MoC, NbC, TiC, VC, $Cr_3C_2$ and $Ta_4C_3$) are attractive CE materials for their properties of low cost, high catalytic activity, good selectivity, superior electrical conductivity, and good thermal stability. Moreover, N-doped carbides, such as TiC(N), VC(N), and NbC(N), show better catalytic activity and photovoltaic performance than the corresponding TiC, VC and NbC. The reason for the improved performance of carbide by N doping is not clear yet. The synergetic effect of N and C atoms may play an important role. Carbides and nitrides have more superior catalytic activity in S-mediated DSSCs than in I-mediated DSSCs, which is even better than Pt CE.[150,472–478]

Similar to the carbides, the nitrides of TiN, $Mo_2N$, MoN, $W_2N$, WN, $Fe_2N$, NiN, VN, NbN, CrN, and $Ta_4N_5$ were also introduced into DSSCs as CE materials.[125,150,467,479–488] Zhang *et al.* synthesized TiN sphere CEs by coating hierarchical micro/nano-$TiO_2$ paste onto Ti foil followed by a nitridation reaction.[479] Compared with particulate TiN and TiN flat CEs, the DSSCs with TiN sphere CE showed higher photovoltaic parameters in light of its hierarchical structure. After optimization, the highest PCE reached 7.83%, 30% higher than that of Pt CE based DSSCs (6.04%). Gao *et al.* prepared a surface-nitrided Ni foil and used it as CE in DSSCs, which showed a PCE of 5.68%, much lower than that of the Pt CE based DSSC (8.41%).[480] The low efficiency of the NiN CE based DSSC is attributed to the compact nitride film with a low surface area. To improve the surface area, the NiN particle with a mesoporous structure was prepared, and the DSSCs gave a high PCE of 8.31%, proving that a large surface area was a critical factor for high device performance. Further, they synthesized MoN, WN, and $Fe_2N$ by nitridation of the oxide ($MoO_2$, $WO_3$, $Fe_2O_3$) in a $NH_3$ atmosphere. The nitride-based DSSCs showed PCE values of 5.57% (MoN), 3.67% (WN), and 2.65% ($Fe_2N$).[481] Chen *et al.* successfully grew porous, single crystalline titanium nitride (TiN) nanoplates on carbon fibers (CF). The fiber-shaped DSSCs based on the TiN–CF CE achieved a high PCE of 7.20%, comparable or even superior to that of the DSSC based on Pt wire (6.23%).[482]

Wu *et al.* synthesized metal carbides, nitrides and oxides by a urea-metal route.[150] In their work, a metal chloride was dissolved in ethanol to form the metal orthoester. Then, different amounts of urea were added to the metal orthoester, producing a gel-like urea–metal precursor. After sintering the precursor, the target nitrides, carbides and oxides were thus obtained. The obtained carbides and nitrides by this method usually possess high purity (>99.5 wt%). The synthesized transition metal compounds included carbides: $Cr_3C_2$, N-doped VC [VC(N)], N-doped TiC [TiC(N)], $Mo_2C$, and N-doped NbC [NbC(N)]; nitrides: CrN, VN, TiN, MoN, and NbN; and oxides: $Cr_2O_3$, $V_2O_3$, $TiO_2$, $MoO_2$, $Nb_2O_5$, and $ZrO_2$. Also, commercial TiC, VC, ZrC, and ZrN were used to compare the catalytic properties of these carbides, nitrides, and oxides as CEs in DSSCs. Amongst these transition metal compounds, $Cr_3C_2$, CrN, VN, TiC, TiN, $V_2O_3$, VC(N), and TiC(N) all showed excellent catalytic activity for the reduction of triiodide in electrolytes. Further, VC was embedded in mesoporous carbon (VC-MC) by *in situ* synthesis. The DSSC with the $I_3^-/I^-$ electrolyte and the VC-MC CE achieved a high PCE of 7.63%, comparable to the DSSC with a Pt CE (7.50%). A comparison of the PCE values of DSSCs with different carbide, nitride and oxide CEs is shown in Fig. 24.

The carbon–nitrogen compound is an interesting material. It may share some merits with carbides, nitrides, graphite and graphene, and is a novel CE material used in DSSCs.[490–497] Ramasamy *et al.* synthesized an ordered mesoporous titanium nitride–carbon (OM TiN–C) nanocomposite with a surface area of 389 $m^2\ g^{-1}$ and uniform hexagonal mesopores of 5.5 nm *via* the soft-template method.[490] The DSSC with OM TiN–C as CE showed a PCE of 6.71% in the $T_2/T^-$ electrolyte system, while the DSSC with Pt CE showed an efficiency of 3.32%. Furthermore, in the $I_3^-/I^-$ electrolyte system, the PCEs of the devices are 8.41% and 8.0% for OM TiN–C and Pt CEs, respectively. The superior performance of the OM TiN–C CE resulted from the low charge transfer resistance, enhanced electrical conductivity, and abundance of active sites of the OM TiN–C nanocomposite. Xu *et al.* synthesized a hierarchical N–C and $Fe_3C$ nanocomposite ($Fe_3C$@N–C) by carbothermal reduction at 600 °C, using cyanamide ($NH_2CN$) as the nitrogen and carbon source.[491] By forming $Fe_3C$ at this temperature, the common problem of α-Fe formation was avoided as this material is unstable in the $I^-/I_3^-$ electrolyte.[492] An appropriate

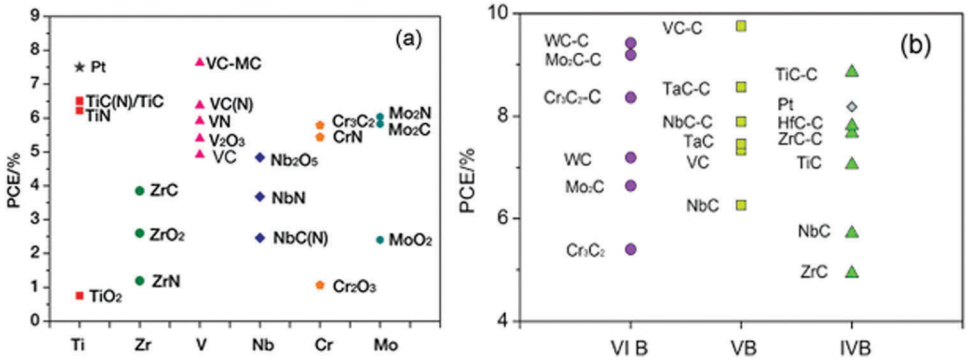


Fig. 24 The PCEs of the DSSCs with triiodide/iodide electrolyte and different TMC CEs. (a) Reprinted with permission from ref. 150. Copyright (2012) American Chemical Society. (b) Reprinted with permission from ref. 489. Copyright (2016) Elsevier.

Open Access Article. Published on 25 August 2017. Downloaded on 4/25/2024 1:35:01 PM.
This article is licensed under a Creative Commons Attribution-NonCommercial 3.0 Unported Licence.

amount of $NH_2CN$ prevented the aggregation of the $FeC_2O_4$ nanowires and generated a favorable carbon-coating. With the nanocomposite as CE, the $Fe_3C$@N–C-2.5 (ratio of $FeC_2O_4$/$CH_2N_2$ is 2.5) yielded the highest DSSC efficiency of 7.36%, which was higher than that of the cell with a Pt CE (7.15%). The good photovoltaic performance was attributed to the synergistic effect of the combination of N–C and $Fe_3C$ as well as 1-D configuration, which endows the nanostructures with more interfacial active sites, better catalytic performance and lowest charge-transfer resistance.

Lee *et al.* synthesized crystalline poly(triazine imide) based graphitic carbon nitride (g-CN) *via* a modified ionothermal method, and deposited it onto the counter electrodes along with a conductive additive and a sacrificial polymer binder.[493] The DSSC with this graphitic carbon nitride (g-CN) as CE exhibited a PCE of 7.8%, which is comparable to the cell with conventional Pt CE (7.9%). Wang *et al.* prepared a porous graphitic carbon nitride/graphene (g-$C_3N_4$/G) composite by the hydrothermal method and used it as the CE of DSSCs.[494] The incorporation of graphene nanosheets into g-$C_3N_4$ resulted in a 3D architecture with a high surface area, a porous structure, an efficient electron-transport network, and fast charge-transfer kinetics at g-$C_3N_4$/G interfaces. With g-$C_3N_4$/G as CE, the DSSC achieved an efficiency of 7.13%, which was comparable to the cell with a Pt CE (7.37%).

Balamurugan *et al.* designed and synthesized (shown in Fig. 25) a hybridized structure of iron nitride (FeN) core–shell nanoparticles grown on nitrogen-doped graphene (NG).[495] The FeN/NG core–shell nanohybrid material was successfully used as a CE in DSSCs. The interactions between the FeN core and the NG shell improved the electrochemical properties of the nanohybrids and led to superior electro-catalytic activity and high electrical conductivity. A DSSC based on the core–shell FeN/NG CE achieved a high PCE of 10.86%. The PCE value is superior to that of the device based on conventional Pt CE (9.93%) under the same experimental conditions. Such simple, cost-effective, and eco-friendly nanohybrids will provide a new pathway for the preparation of various core–shell structure nanohybrid materials and can be used in a wide range of applications, such as in solar cells, fuel cells, supercapacitors, Li-ion batteries, and biosensors.

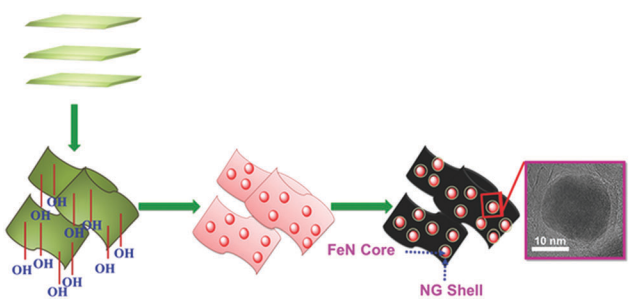


Fig. 25 Schematic illustration of the fabrication of core–shell FeN/NG nanohybrids. Reprinted with permission from ref. 495. Copyright (2015) John Wiley & Sons Ltd.

### 6.2. Chalcogenides

The term chalcogenide is more commonly reserved for sulfides, selenides, and tellurides, rather than oxides. Metal chalcogenides have various compositions, molecular structures, and distinctive properties, which render them a promising catalyst for the substitution of noble metal-based electrocatalysts used in fuel cells, electrolysis of water, and DSSCs. An important application of chalcogenides in PV technologies is as optical absorption materials in quantum dot-sensitized solar cells (QDSSCs).[498–501] Metal chalcogenides are also widely used as CEs in DSSCs.[333,502–508]

In 2009, Wang *et al.* deposited CoS on ITO/PEN films and used the sulfide as CE in DSSCs for the first time, and obtained an efficiency of 6.5% in conjunction with a Z907 sensitizer and a eutectic melt electrolyte.[502] Tuan *et al.* used $Co_9S_8$ nanocrystals as CE for DSSCs (with a size of 2 $cm^2$) and obtained an average PCE of 7.0%, slightly lower than that of Pt CE based DSSCs.[509] Ho *et al.* used a CoS nanorod array as CE in DSSCs, producing a PCE of 7.67%, similar to Pt CE-based DSSCs (7.70%).[505] Huo *et al.* deposited a sponge-like CoS/rGO hybrid on FTO by electrophoretic deposition and ion exchange deposition, followed by sodium borohydride and sulfuric acid solution treatment.[510] The addition of rGO improved the electrocatalytic activity for triiodide reduction, resulting in the better electrocatalytic property of CoS/rGO CEs compared to Pt CE. With CoS/rGO as CE, the DSSC achieved a PCE of 9.39%, which was increased by 27.93% compared with the DSSC with Pt CE (7.34%). Furthermore, Huo *et al.* prepared a transparent nanostructured CoS/rGO CE by a simple hydrothermal method.[503] The DSSC based on CoS/rGO CE with a thickness of 72 nm achieved a PCE of 9.82%, and a PCE of 8.38% was obtained for the Pt CE based DSSC under white light irradiation from the front and back.

Wu *et al.* synthesized $MoS_2$ and $WS_2$ and used them as CEs in DSSCs.[149] Both $MoS_2$ and $WS_2$ performed well for triiodide reduction, and the DSSCs with $MoS_2$ and $WS_2$ CEs yielded a PCE of 7.59% and 7.73%, respectively, comparable to the device with Pt CE (7.64%). In addition, both sulfide CEs surpass Pt in $T^-/T_2$ electrolyte based DSSCs. Ahn *et al.* converted a mesoporous interconnected $WO_3$ to edge-oriented $WS_2$ by a rapid sulfurization process at high temperature.[511] The oriented $WS_2$ exposed a large number of active edge sites and resulted in high catalytic activity toward triiodide reduction. With an optimized edge-oriented $WS_2$ as CE, the DSSC exhibited a PCE of 8.85%, which was higher than that of Pt (7.20%). Liang *et al.* directly grew ultrathin $MoS_2$ nanofilms with a thickness of only several stacked layers on transparent FTO by a one-step solution-phase process.[512] The $MoS_2$ nanofilms possessed excellent catalytic activity for triiodide reduction. With the $MoS_2$ nanofilm as CEs, the DSSC achieved an impressive PCE of 8.3%, which was higher than that of a Pt-based electrode (7.53%).

Chen *et al.* prepared semitransparent $FeS_2$ films on ITO/PEN. After modification, the DSSCs using $FeS_2$ CE showed a PCE of 7.31%.[209] Batabyal *et al.* used $Co_{8.4}S_8$, $Ni_3S_2$, and $Cu_{1.8}S$ as CEs in DSSCs, which produced PCE values of 6.50, 7.01, and 3.79%, respectively.[513] Meng *et al.* prepared NiS CEs by periodic potential reversal (PR) and potentiostatic (PS) techniques.

Open Access Article. Published on 25 August 2017. Downloaded on 4/25/2024 1:35:01 PM.
This article is licensed under a Creative Commons Attribution-NonCommercial 3.0 Unported Licence.

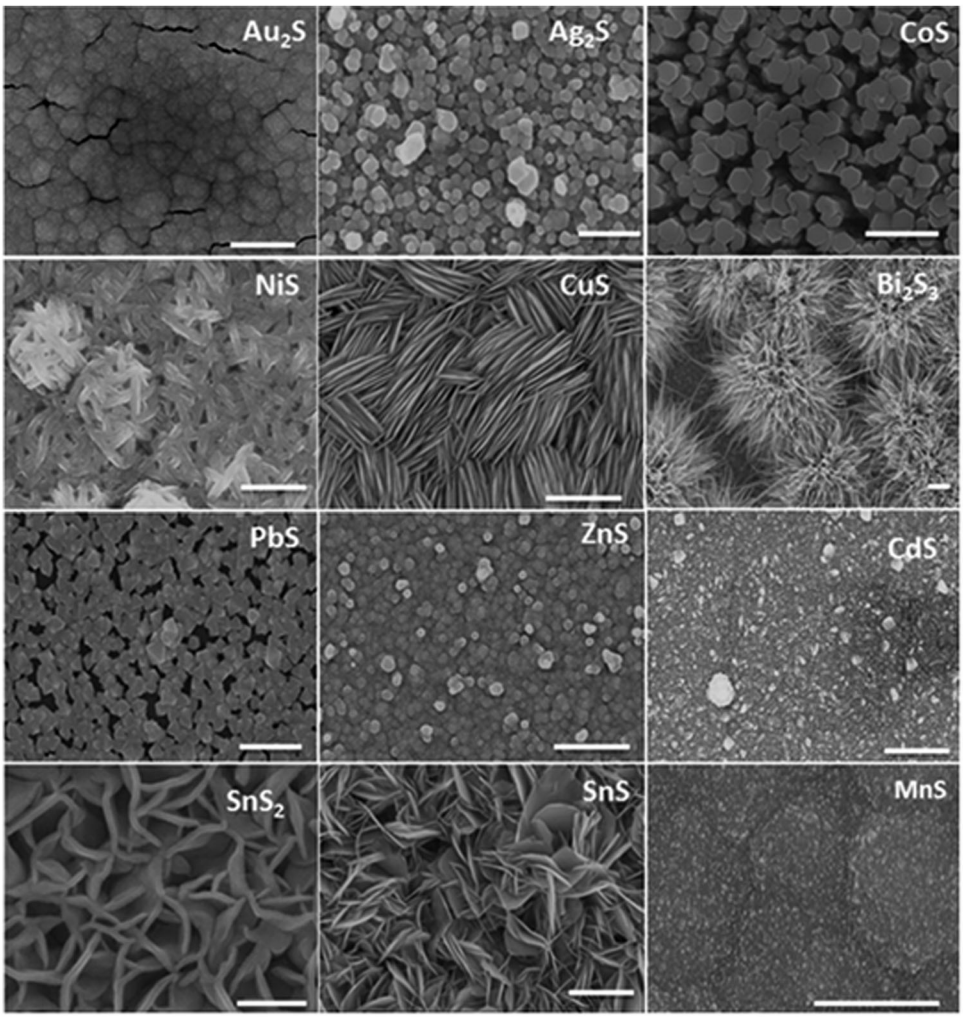


Fig. 26 Scanning electron microscopy images (false colored) of various metal-sulfides on glass substrates. The scale bar in each image corresponds to 500 nm. Reprinted with permission from ref. 515. Copyright (2015) John Wiley & Sons Ltd.

The DSSCs using PR-NiS and PS-NiS CEs showed PCE values of 6.83% (PR-NiS) and 3.22% (PS-NiS).[114] The NiS nanoarray film was prepared by a two-step low-temperature solution route, and the DSSCs using this sulfide CE achieved a PCE of 7.10%, compared to the Pt CE based DSSCs (7.35%).[514] Shinde *et al.* deposited a high crystalline and well-defined nanostructured NiS thin film on a flexible PET substrate by a simple and effective solution-based deposition (shown in Fig. 26).[515] The flexible DSSC with the NiS CE exhibited a high PCE of 9.50% (*vs.* 8.97% for the device with Pt CE). The Wu group deposited CoS and NiS on FTO by a simple electrodeposition method and the morphology of the films was tuned by adding different amounts of ammonia (shown in Fig. 27).[516] With the sulfide films as CEs, the DSSC achieved PCEs of 9.23% (CoS) and 9.65% (NiS), respectively. The values are obviously higher than that of DSSC with Pt CE (8.12%) under the same conditions.

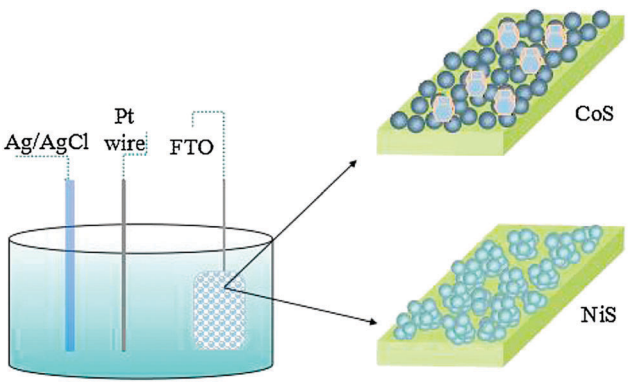


Fig. 27 A diagram of the electrodeposition process of CoS and NiS counter electrodes. Reprinted with permission from ref. 516. Copyright (2015) Elsevier.

The Tang group systematically studied metal selenides (M–Se; M = Co, Ni, Cu, Fe, Ru) as CEs for bifacial DSSCs.[517] Owing to superior charge-transfer ability at the interface, good electrocatalytic activity toward triiodide reduction, and optical transparency, the bifacial DSSCs based on MSe CEs yielded front and rear efficiencies of 7.64% and 5.05% for FeSe, 8.30% and 4.63% for $Co_{0.85}Se$, 7.85% and 4.37% for $Ni_{0.85}Se$, 6.43%

Open Access Article. Published on 25 August 2017. Downloaded on 4/25/2024 1:35:01 PM.
This article is licensed under a Creative Commons Attribution-NonCommercial 3.0 Unported Licence.

and 4.24% for $Cu_{0.50}Se$, and 9.22% and 5.90% for $Ru_{0.33}Se$, respectively, in comparison with 6.18% and 3.56% of the device based on pristine Pt CE. Furthermore, they prepared and compared transparent $Ni_{0.6}Se$, $Ni_{0.7}Se$ and $Ni_{0.85}Se$ CEs. The DSSC with $Ni_{0.85}Se$ CE achieved impressive PCEs of 7.85%, 4.37%, and 10.63% for irradiation from front, rear, and both, respectively, which were superior to the cell performances from Pt CE.[210] Based on the $Ni_{0.85}Se$/mirror CE, Jia *et al.* achieved a high DSSC efficiency of 10.19%.[214]

Gong *et al.* synthesized cobalt selenide ($Co_{0.85}Se$) and nickel selenide ($Ni_{0.85}Se$) *via* a facile one-step method.[518] The DSSCs with $Co_{0.85}Se$ and $Ni_{0.85}Se$ CEs produced PCE of 9.40% and 8.32%, respectively, while the device with Pt CE achieved a PCE of 8.64%. In another work, they used $NiSe_2$ as CE, and the DSSCs produced a PCE of 8.69%, higher than that of the Pt CE based DSSCs (8.04%).[519] Cui *et al.* used CoSe as CE for DSSCs and obtained a PCE of 7.30%, higher than that of the device with Pt CE (6.91%).[520] The Ma group prepared $NbSe_2$ nanosheets (NSs) and nanorods (NRs) *via* a facile and reductant-free solvothermal reaction. The DSSCs with the $NbSe_2$-NS and $NbSe_2$-NR CEs produced PCE values of 7.34 and 6.78%, close to that of Pt CE based DSSCs (7.9%).[521] The performance and structures of ternary nickel cobalt selenides can be optimized by tuning the Ni/Co molar ratio. Qian *et al.* optimized the compositions of the ternary compound and prepared a three-dimensional dandelion-like $Ni_{0.33}Co_{0.67}Se$ microsphere CE, which delivered a high DSSC efficiency of 9.01% compared to the Pt catalyst (8.30%).[522] Recently, Li *et al.* prepared tubular-structured orthorhombic $CoSe_2$ by a facile precursor transformation method.[523] Owing to the structural features of functional shells and well-defined interior voids, the $CoSe_2$ showed a high PCE of 9.34% as a CE for DSSCs, superior to that of Pt CE (8.15%). Very recently, the Wu group successfully synthesized $CoSe_2$ by a facile electrochemical deposition. The DSSC based on the $CoSe_2$ CE achieved a record PCE of 10.17%, which was increased by 21.9% compared to the cell based on Pt CE (8.35%).[524]

Guo *et al.* synthesized metal tellurides of CoTe and $NiTe_2$ by a composite-hydroxide-mediated (CHM) method. The tellurides were used as CEs in DSSCs, yielding PCE values of 6.92% and 7.21%, respectively, comparable to the device using Pt CE (7.04%).[525] Patil *et al.* prepared self-standing CoTe nanotubes *via* anion exchange in aqueous solution at room temperature.[526] The DSSC with the CoTe CE showed a PCE of 8.10%, which is highly comparable to that of the device with Pt CE (8.20%). The Wu group synthesized CoTe/RGO by the hydrothermal method and used it as CE in DSSCs.[508] The CoTe/RGO has a larger surface area, good electrocatalytic activity and a lower $R_{CT}$ of 2.94 $\Omega$ $cm^2$, resulting in a high PCE of 9.17%, outperforming the device with Pt CE (8.17%).

### 6.3. Oxides

Differently from the carbides, nitrides and chalcogenides, transition metal oxides are less used as CEs to replace Pt. However, Ma *et al.* synthesized $WO_2$ nanorods with excellent catalytic activity, and the iodide electrolyte based DSSCs with $WO_2$ CE showed a high PCE of 7.25%, close to that of the DSSC with Pt CE (7.57%).[527] Moreover, the $WO_2$ performed better than Pt in the $T_2/T^-$ electrolyte system, and obtained a DSSC efficiency of 4.66%.[528] Similar to $WO_2$, $WO_{2.72}$ also showed higher catalytic activity, and the corresponding DSSC produced a high PCE of 8.03%, close to that of the Pt CE based DSSCs (8.08%).[529] $WO_3$ was also prepared, and the DSSC with $WO_3$ CE showed a low PCE of 4.67%.[529]

Lin *et al.* synthesized $NbO_2$ with excellent catalytic activity for triiodide reduction, resulting in a high DSSC efficiency of 7.88%, surpassing the DSSC using Pt CE (7.65%).[530] Hou *et al.* prepared $RuO_2$ nanocrystals *via* hydrothermal and sintering processes and used them as CE in DSSCs,[531] getting an efficiency of 7.22% and exceeding the efficiency of the Pt-based DSSC (7.17%). Wang *et al.* synthesized $Fe_3O_4$ with hierarchical structures and used it as CE in DSSCs.[532] A PCE of 7.65% was achieved for the DSSC with the $Fe_3O_4$ CE, which was superior to that with pyrolytic Pt (6.88%) and close to the DSSC with sputtered Pt (7.87%). Ahmad *et al.* synthesized monolithic copper oxide nanorods (CuO-NRs) and doped them into active super hydrophobic acetylene black (AB) nanocrystals *via* a fast solvation method.[533] Owing to the superior catalytic activity of CuO-NRs and the good electrical conductivity of AB, the CuO-NRs/AB based DSSC exhibited a high PCE of 8.05%, in contrast to AB (6.51%) and pristine Pt (6.96%) CE based DSSCs.

Zhou *et al.* prepared 1D $W_{18}O_{49}$ nanofibers by a solvothermal anisotropic growth route.[534] The interlaced $W_{18}O_{49}$ NFs offered a desired network structure for heterogeneous electrocatalysis and exhibited multiple superior properties by offering abundant active sites, interlaced highways for electron transport and broad pore structures for thorough contact with the electrolyte solution. The semitransparent $W_{18}O_{49}$ NF CEs enabled the DSSCs to achieve a high PCE of 8.58%, close to that of 8.78% for the Pt-based CE.

### 6.4. Others

Wu *et al.* directly coated a $Ni_2P$ nanolayer with a porous nanosphere structure on FTO by pulse-reverse deposition. Owing to the significant improvement of ion transport, the efficiency of DSSCs based on $Ni_2P$ CE was increased to 7.32%.[535] Wu *et al.* prepared a monolayer of $Ni_5P_4$ clusters with a mesoporous structure on FTO by cyclic voltammetric deposition. The mesoporous $Ni_5P_4$ exhibited good electrocatalytic activity towards triiodide reduction, low charge-transfer resistance and diffusion impedance. The PCE of the DSSC based on the $Ni_5P_4$ CE reached 7.6%, which was higher than that of the device with Pt nanocluster CE (7.2%).[536]

Earth abundant silicon compounds, including $Si_3N_4$, $SiO_2$, $SiS_2$, and $SiSe_2$, were introduced as CEs in DSSCs.[537] Using a conducting binder, PEDOT:PSS, various silicon-based composites were coated on the ITO. In a composite film, silicon based nanoparticles provided electrocatalytic ability and plenty of electrocatalytic active sites for triiodine ion reduction. PEDOT:PSS not only acted as a good conducting binder for silicon-based nanoparticles, but also provided a continuous polymer matrix to increase electron transportation. The composite films containing 5 wt% $Si_3N_4$ ($Si_3N_4$-5) and 5 wt% $SiSe_2$ ($SiSe_2$-5)

Open Access Article. Published on 25 August 2017. Downloaded on 4/25/2024 1:35:01 PM.
This article is licensed under a Creative Commons Attribution-NonCommercial 3.0 Unported Licence.

possessed excellent electrocatalytic activity and rendered a high efficiency of 8.2% to DSSCs, which was comparable to the Pt electrode (efficiency of 8.5%).

It is generally believed that silver or silver-based compounds are not suitable as CE materials for DSSCs as a result of the corrosion of the $I_3^-/I^-$ redox couple in electrolytes. However, $Ag_2S$ can be used in DSSCs because of its high carrier concentration and tiny solubility product constant. He *et al.* fabricated a $Ag_2S$ CE for DSSCs which exhibited efficient electrocatalytic activity for triiodide reduction.[538] The DSSC with $Ag_2S$ CE displayed a PCE of 8.40%, higher than that the device with Pt CE (8.11%). Moreover, the devices also showed the characteristics of fast activity onset, high multiple start/stop capability and good irradiation stability.

Multicomponent compounds, in particular multicomponent sulfides, such as CZTS,[504,539] CZTSe,[539,540] $CuInS_2$,[541,542] $NiCo_2S_4$,[543] $NiMoS_4$,[544] $Ag_8GeS_6$,[545] and so on,[546,547] could provide more alternatives and tune physicochemical properties due to the presence of multiple cations. The Lin group prepared copper zinc tin sulfide (CZTS) nanocrystals using a solution synthesis method and got CZTSe after Se vapor treatments.[522] Using the two multiple compounds as CEs in DSSCs, they achieved PCE values of 3.62% for CZTS CE and 7.37% for CZTSe CE. Wu *et al.* investigated the influence of the CZTSe layer thickness on the catalyst activity and found that 1.2 μm was the optimal thickness,[541] getting a DSSC efficiency of 7.82%. He *et al.* prepared a $Ag_8GeS_6$ CE for DSSCs *via* a colloidal synthesis process. The $Ag_8GeS_6$ electrode displayed lower charge transfer resistance, better chemical stability and higher catalytic activity toward triiodide reduction. The DSSC with $Ag_8GeS_6$ CE displayed a PCE of 8.10%, superior to that of the device with the Pt CE (8.02%).

The photovoltaic parameters of the DSSCs based on excellent carbide, nitride chalcogenide, oxide and other CEs are summarized in Table 4. Although the study of transition metal compounds as CE materials lags behind that of carbon materials and conductive polymers in time, transition metal compounds have become a hot research area for CEs of DSSCs in recent years owing to their material diversity, low cost and Pt-like catalytic activity. They can be prepared by simple synthesis and can be easily modified. However, the performance of the TMC-based DSSC is relatively lower than that of the devices with other Pt-free CE materials, which may be ascribed to the poor conductivity of TMCs and the unreliable electron transportation between the TMC nanoparticles and conducting substrates.

Table 4 Photovoltaic parameters of DSSCs based on transition metal compound CEs. (FTO substrate, $I_3^-/I^-$ redox electrolyte, N719 dye, irradiation intensity 100 mW $cm^{-2}$, AM1.5)

| CE materials | $J_{SC}$ (mA $cm^{-2}$) | $V_{OC}$ (mV) | FF | PCE (%) | PCE (Pt)/% | Ref. |
|---|---|---|---|---|---|---|
| TiN nanotube | 15.78 | 760 | 0.64 | 7.73 | 7.45 | 467 |
| Mesoporous WC | 14.17 | 763 | 0.65 | 7.01 | 8.23 | 468 |
| WC-OMC | 14.59 | 804 | 0.70 | 8.18 | 7.89 | 471 |
| MoC-OMC | 15.50 | 787 | 0.68 | 8.34 | 7.89 | 471 |
| TiN sphere | 16.57 | 759 | 0.62 | 7.83 | 6.04 | 479 |
| Mesoporous NiN | 15.76 | 766 | 0.69 | 8.31 | 7.93 | 480 |
| TiN–Carbon fiber | 19.35 | 640 | 0.58 | 7.20 | 6.23 | 482 |
| VC-Mesoporous carbon | 13.11 | 808 | 0.72 | 7.63 | 7.50 | 150 |
| OM TiN–C | 15.30 | 820 | 0.67 | 8.41 | 8.00 | 490 |
| $Fe_3C$@N–C | 14.97 | 741 | 0.66 | 7.36 | 7.15 | 491 |
| g-CN | 15.40 | 749 | 0.68 | 7.80 | 7.90 | 493 |
| g-$C_3N_4$/G | 14.91 | 723 | 0.66 | 7.13 | 7.37 | 494 |
| FeN/N-doped graphene | 18.83 | 740 | 0.78 | 10.86 | 9.93 | 495 |
| CoS nanorods | 16.31 | 710 | 0.66 | 7.67 | 7.70 | 505 |
| $Co_9S_8$ nanocrystals | 14.21 | 710 | 0.69 | 7.00 | 7.13 | 509 |
| CoS/rGO | 19.42 | 764 | 0.63 | 9.39 | 7.34 | 510 |
| Transparent CoS/rGO | 18.90 | 767 | 0.677 | 9.82 | 8.38 | 503 |
| $MoS_2$ | 13.84 | 760 | 0.73 | 7.59 | 7.64 | 149 |
| $WS_2$ | 14.13 | 780 | 0.70 | 7.73 | 7.64 | 149 |
| $MoS_2$ nanofilm | 16.96 | 740 | 0.66 | 8.28 | 7.53 | 512 |
| $FeS_2$ on ITO/PEN | 15.14 | 710 | 0.68 | 7.31 | 7.52 | 209 |
| NiS nanoarray | 15.18 | 708 | 0.66 | 7.10 | 7.35 | 514 |
| CoS | 19.26 | 759 | 0.631 | 9.23 | 8.12 | 516 |
| NiS | 19.47 | 758 | 0.654 | 9.65 | 8.12 | 516 |
| FeSe | 17.10 | 733 | 0.61 | 7.64 | 6.18 | 517 |
| $Co_{0.85}Se$ | 16.74 | 742 | 0.668 | 8.3 | 6.18 | 517 |
| $Ni_{0.85}Se$ | 16.67 | 740 | 0.636 | 7.85 | 6.18 | 517 |
| $Ru_{0.33}Se$ | 18.93 | 715 | 0.681 | 9.22 | 6.18 | 517 |
| $Ni_{0.85}Se$ (both irradiation) | 24.34 | 737 | 0.593 | 10.63 | 8.78 | 210 |
| $Ni_{0.85}Se$/mirror | 18.44 | 791 | 0.698 | 10.19 | 8.13 | 214 |
| $Co_{0.85}Se$ | 16.98 | 738 | 0.75 | 9.40 | 8.64 | 518 |
| $Ni_{0.85}Se$ | 15.63 | 739 | 0.72 | 8.32 | 8.64 | 518 |
| $NiSe_2$ | 15.94 | 734 | 0.743 | 8.69 | 8.04 | 519 |
| CoSe | 13.72 | 747 | 0.713 | 7.30 | 6.91 | 520 |
| $NbSe_2$ nanosheets | 15.04 | 770 | 0.63 | 7.34 | 7.90 | 521 |
| $Ni_{0.33}Co_{0.67}Se$ microsphere | 17.29 | 789 | 0.67 | 9.01 | 8.30 | 522 |
| Tubular orthorhombic $CoSe_2$ | 17.35 | 771 | 0.70 | 9.34 | 8.15 | 523 |
| $CoSe_2$ | 17.65 | 809 | 0.712 | 10.17 | 8.35 | 524 |
| $NiTe_2$ | 14.13 | 790 | 0.65 | 7.21 | 7.04 | 525 |
| CoTe nanotubes | 21.40 | 620 | 0.60 | 8.10 | 8.20 | 526 |
| CoTe/RGO | 17.41 | 770 | 0.69 | 9.18 | 8.17 | 508 |
| $WO_2$ | 14.02 | 808 | 0.64 | 7.25 | 7.59 | 527 |
| $WO_{2.72}$ | 14.90 | 770 | 0.70 | 8.03 | 8.08 | 529 |
| $NbO_2$ | 13.90 | 810 | 0.70 | 7.88 | 7.65 | 530 |
| $RuO_2$ | 16.51 | 813 | 0.54 | 7.22 | 7.17 | 531 |
| $Fe_3O_4$ | 16.67 | 693 | 0.63 | 7.65 | 6.88 | 532 |
| CuO-NRs/AB | 15.94 | 770 | 0.65 | 8.05 | 6.96 | 533 |
| $W_{18}O_{49}$ | 17.39 | 0.73 | 0.68 | 8.58 | 8.78 | 534 |
| $Ni_2P$ | 13.25 | 750 | 0.73 | 7.32 | 7.15 | 535 |
| $Ni_5P_4$ | 14.70 | 720 | 0.72 | 7.60 | 7.20 | 536 |
| $SiSe_2$/PEDOT:PSS | 16.98 | 720 | 0.67 | 8.20 | 8.50 | 537 |
| $Si_3N_4$/PEDOT:PSS | 16.11 | 760 | 0.67 | 8.18 | 8.50 | 537 |
| $Ag_2S$ | 16.79 | 757 | 0.66 | 8.40 | 8.11 | 538 |
| $Cu_2ZnSnSe_4$ | 15.54 | 782 | 0.66 | 7.82 | 7.56 | 540 |
| $Ag_8GeS_6$ | 16.59 | 746 | 0.65 | 8.10 | 8.02 | 545 |

## 7. Hybrid counter electrodes

In order to improve the performance and adaptability of CEs, much attention has been paid to developing hybrids or composite CEs. The hybrids are materials consisting of two or more components. The performance of the hybrids could be improved by taking advantage of the synergetic effects that arise from different components of the hybrids. Currently, hybrids have become one of the popular CEs.

As the CEs for DSSCs, the hybrids can be divided into Pt-loaded and Pt-free hybrids. For Pt-free hybrid CEs, carbon materials, conductive polymers, and transition metal compounds (TMCs) are often used as basic components of the hybrids. As illustrated in Fig. 28, there are usually three classes of two-component (TMCs/carbon, carbon/polymers and polymers/TMCs) hybrids.

Open Access Article. Published on 25 August 2017. Downloaded on 4/25/2024 1:35:01 PM.
This article is licensed under a Creative Commons Attribution-NonCommercial 3.0 Unported Licence.

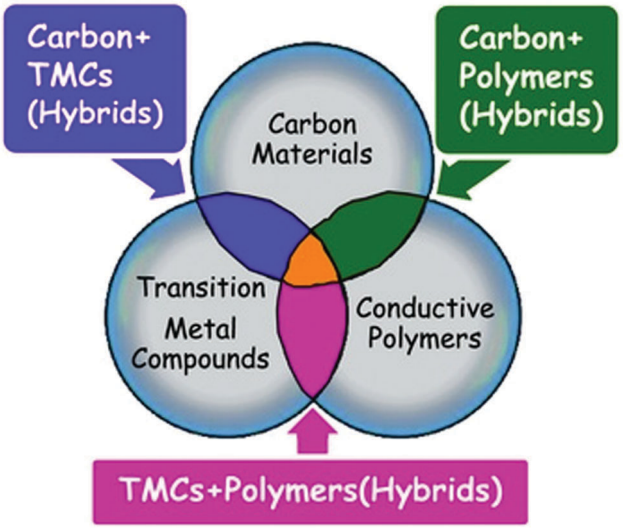


Fig. 28 Three classes of Pt-free hybrid CE materials fabricated with different components. Reprinted with permission from ref. 91. Copyright (2014) John Wiley & Sons Ltd.

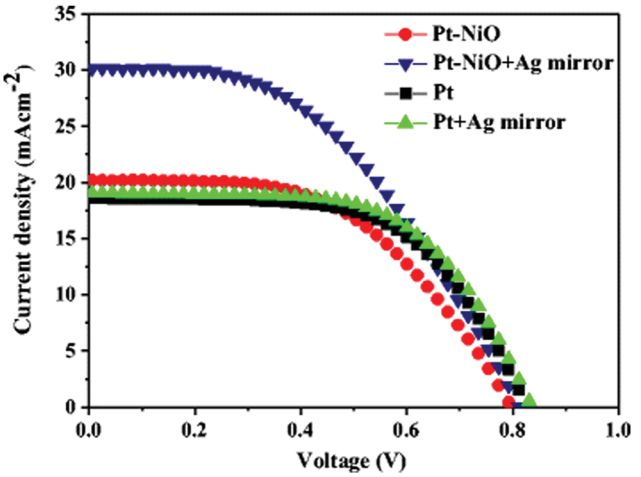


Fig. 29 Photocurrent–voltage ($J$–$V$) curves of the DSSCs with Pt–NiO and Pt counter electrodes. Reprinted with permission from ref. 538. Copyright (2015) Springer-Verlag Berlin Heidelberg.

### 7.1. Platinum-loaded hybrids

In 2009, the Wu group prepared a Pt/carbon black CE for DSSCs by reducing $H_2PtCl_6$ with $NaBH_4$ in carbon black.[548] The Pt/CB hybrid CE had high electrocatalytic activity for triiodide reduction. With the Pt/CB (1.5 wt% Pt) hybrid CE, the DSSC achieved a PCE of 6.72%, which was higher than that of the device with Pt CE (6.63%). Guo *et al.* prepared a nanohybrid consisting of Pt nanoparticles and carbon nanotubes (Pt/MWCNTs) *via* a sulfur-assisted route. The DSSC with the Pt/MWCNT CEs produced a PCE of 7.69%, while the device with Pt CE achieved a PCE of 6.31%.[549] Wu *et al.* prepared binary composite Pt/TiC, Pt/$WO_2$, and Pt/VN CEs for DSSCs, and obtained PCE values of 7.63, 6.94, and 6.80%, respectively. Moreover, the Pt/TiC CE was used in large-area DSSCs, producing a PCE of 4.94%.[550] Wang *et al.* prepared a ternary composite of Pt/$TiO_2$/$WO_2$ with higher catalytic activity, and the DSSCs based on the ternary CE yielded a PCE of 7.23%.[551] Miao *et al.* deposited Pt particles on vertically ordered silicon nanowires (SiNWs) and got a Pt/SiNW hybrid CE for DSSCs. After optimization, the DSSC achieved a PCE of 8.30%, better than the device with Pt CEs (7.67%).[552]

Chen *et al.* used as-synthesized carbon nanotube aerogel (CNA) as CE for DSSCs and produced a PCE of 8.35%, higher than the DSSCs with MWCNT CE (5.95%) and conventional Pt CE (7.39%). 3.75 wt% Pt was loaded on CNA to form a Pt/CNA composite (3.75 wt% Pt) CE. Owing to the improved electrocatalytic activity, reduced charge-transfer resistance, and increased diffusion, the PCE was further increased to 9.04%.[553] Zhu *et al.* deposited Pt nanoparticles on a carbon sphere (CS) surface to form hybrid Pt/CS. A large-scale, highly effective, and flexible CE was fabricated with this hybrid on the ITO-PEN substrate for flexible DSSCs. The flexible Pt/CS CE exhibited higher catalytic activity toward $Co^{3+/2+}$ couple regeneration than Pt and CS CEs. The excellent catalytic activity of Pt/CS can be attributed to the low activation energy ($E_a$) for $Co^{3+/2+}$ redox reaction. The flexible DSSC with the Pt/CS CE achieved a PCE of 9.02%.[554] The Wu group fabricated a high-performance Pt/NiO hybrid CE for DSSCs. Pt/NiO hybrid CEs showed high catalytic activity and low charge transfer resistance. The DSSC with the Pt/NiO hybrid CEs achieved a PCE of 8.40%, which is lower than that of the DSSC with conventional Pt CE (9.15%). However, owing to the extremely high transparency of Pt/NiO CE, when adding an Ag mirror behind the back side of the DSSC, the PCE was enhanced to 11.27% (Fig. 29).[555]

### 7.2. TMCs/carbon hybrids

For TMCs/carbon hybrids, carbon materials are often used as the supports while TMCs serve as the catalysts. A series of TMCs embedded in mesoporous carbon (MC), such as TiN/MC,[490] MoC/MC,[471] WC/MC,[91] TaO/MC,[91] TaC/MC,[471] $WO_2$/MC,[116,528] $HfO_2$/MC,[556] $MoS_2$/C[557] and VC/MC,[150] were developed.[476] The surface areas of the hybrids were greatly increased from several tens to several hundreds $m^2\ g^{-1}$ after the incorporation of TMCs into MC. DSSCs using these carbon-based hybrid CEs presented PCEs of 8.41%, 8.34%, 8.18%, 8.09%, 7.93%, 7.76%, 7.75%, 7.69%, and 7.63% respectively. The PCE values are higher than those of the corresponding TMC and MC electrodes alone, which can be attributed to the synergetic effects between different components of the hybrids.

Reduced graphene oxide (RGO) is an intermediate state between graphene oxide (GO) and graphene. It has oxygen-containing groups (–COOH, –OH and =O) and lattice defects, which are usually regarded as the catalytic active sites and can interact with other components. In this regard, RGO is more suitable than the reduced and defect-free graphene for CEs in DSSCs. Wang *et al.* prepared a series of TMCs/RGO nanohybrids, such as $NiS_2$/RGO, $Ta_3N_5$/RGO and TaON/RGO.[558–560] I-Meditated DSSCs with N719 dye produced PCEs: $NiS_2$/RGO (8.55%) > Pt (8.15%) > $NiS_2$ (7.02%) > RGO (3.14%); Co-mediated DSSCs with FNE29 dye produced PCEs: $Ta_3N_5$/RGO (7.85%) > Pt (7.59%) > RGO (4.55%) > $Ta_3N_5$ (2.89%)

Open Access Article. Published on 25 August 2017. Downloaded on 4/25/2024 1:35:01 PM. This article is licensed under a Creative Commons Attribution-NonCommercial 3.0 Unported Licence.

and Pt (7.91%) > TaON/RGO (7.65%) > RGO (4.62%) > TaON (2.54%).

By utilizing metal chlorides as metal sources and phenolic resin as a carbon source, Guo *et al.* synthesized carbon supported transition metal carbide hybrids: $Cr_3C_2$/C, $Mo_2C$/C, WC/C, VC/C, NbC/C, TaC/C, and TiC/C.[473] As CEs, the carbon supported carbide hybrids showed high catalytic activities towards $Co^{3+/2+}$ redox couple regeneration. The DSSCs based on the TiC/C, VC/C, and WC/C composite CEs displayed PCE values of 8.85%, 9.75% and 9.42%, respectively, which were much higher than those of the counterparts with TiC, VC and WC CEs. The Cui group prepared metal nitride (MoN, TiN, VN) nanoparticle/N-doped reduced graphene oxide (NG) hybrid materials and used them as CEs for DSSCs.[561] The synergistic effects of high concentration of active sites and electronic/ionic mixed conducting networks offer a promising electrocatalytic feature for triiodide reduction. The PCE values of the devices with VN/NG, TiN/NG and MoN/NG CEs were 6.28%, 7.50% and 7.91% respectively, which were comparable with that of Pt devices (7.86%).

Guo *et al.* synthesized an $In_{2.77}S_4$@conductive carbon ($In_{2.77}S_4$@CC) hybrid *via* a two-step method.[562] The $In_{2.77}S_4$@CC hybrid electrode showed superior electrocatalytic activity for the reduction of triiodide. The DSSC with the $In_{2.77}S_4$@CC hybrid CE exhibited a high PCE of 8.71%, comparable to the commercial Pt-based DSSC (PCE = 8.75%). Wang *et al.* investigated a composite CE of rosin carbon/$Fe_3O_4$ with stunning morphology and used it as CE in DSSCs. The DSSC assembled with the composite showed a high PCE of 8.11%, which was superior to pure rosin carbon CE (7.0%) and pure $Fe_3O_4$ CE (6.61%) and was comparable to the traditional sputtered Pt CE (8.37%).[563] As shown in Fig. 30, Zhou *et al.* prepared nano-micro composite catalysts (NMCCs) composed of highly dispersed $Fe_3O_4$ nanoparticles on RGO sheets (namely $Fe_3O_4$@RGO-NMCC) as CEs in DSSCs.[564] The $Fe_3O_4$@RGO-NMCC CE exhibited improved catalytic activity. The DSSCs on rigid and flexible substrates with $Fe_3O_4$@RGO-NMCC CEs achieved high PCEs of up to 9% and 8%, respectively. The superior performance of $Fe_3O_4$@RGO-NMCC is ascribed to faster electron hopping between $Fe^{2+}$ and $Fe^{3+}$ and free electron transport by broad RGO sheets.

### 7.3. Carbon/polymer hybrids

Graphene, RGO, CNTs, CB, PEDOT-PSS, PPy and PANI are usually used as components of the carbon/polymer hybrids. In 2008, Hong *et al.* deposited a graphene/PEDOT:PSS composite film on an ITO substrate by spin coating at room temperature.[565] The composite film with a 60 nm thickness and 1 wt% graphene exhibited high transmittance (>80%) and high electrocatalytic activity. With the composite film as CE, the DSSCs achieved a PCE of 4.5%. The Wu group electrodeposited a PEDOT:PSS/graphene composite film on FTO by the one-step electrochemical polymerization method and used it as CE in DSSCs.[566] The graphene/PEDOT:PSS CE has low charge-transfer resistance and high catalytic activity. The DSSC with the PEDOT:PSS/graphene CE showed a PCE of 7.86%, which was higher than that of the DSSC with Pt CE (7.31%).

Gong *et al.* incorporated graphene oxide (GO) into PPy and then GO/PPy was reduced to RGO/PPy.[567] Owing to the incorporation of RGO sheets as conductive channels in the RGO/PPy hybrid, the resultant hybrid electrode exhibited an excellent catalytic activity for triiodide reduction, $R_{CT}$ values decreased from 15.5 Ω cm$^2$ to 5.0 Ω cm$^2$, $J_{SC}$ values of the corresponding DSSC increased from 14.27 to 15.81 mA cm$^{-2}$, and PCE values increased from 7.11% to 8.14%. Liu *et al.* synthesized a class of M/PPy/C hybrids (M = Co, Fe, and Ni) for the CE of DSSCs.[568] The DSSCs with M/PPy/C CEs achieved PCE values of 7.64 (Co/PPy/C), 7.44 (Ni/PPy/C), and 5.07% (Fe/PPy/C), while the DSSCs using a bare carbon CE achieved a PCE of 6.26%. The good performance of the devices based on Ni/PPy/C and Co/PPy/C is due to the high activity of the Ni–$N_2$ and Co–$N_2$ sites through the entrapment of the metal atoms in the PPy matrix.

Li *et al.* prepared a composite film of carbon black nanoparticles and sulfonated-polythiophene (CB-NPs/s-PT) on a flexible titanium foil and used it as the CE of DSSCs.[569] The CB-NPs provided a large number of catalytic active sites and the s-PT as a conductive binder improved the inter-particle linkage and adhesion. The flexible CB-NPs/s-PT composite film possessed good catalytic ability and rapid reduction kinetic rate constant of $I_3^-$. The cell with a CB-NPs/s-PT CE exhibited a high efficiency of 9.02%, while the cell with a Pt CE showed an efficiency of 8.36% under the same conditions.

Carbon material was the most common component to form composite CEs. A variety of carbon/carbon hybrids with excellent properties have been developed. Zheng *et al.* prepared the RGO/SWCNT (20 wt% SWCNTs) composite by using the

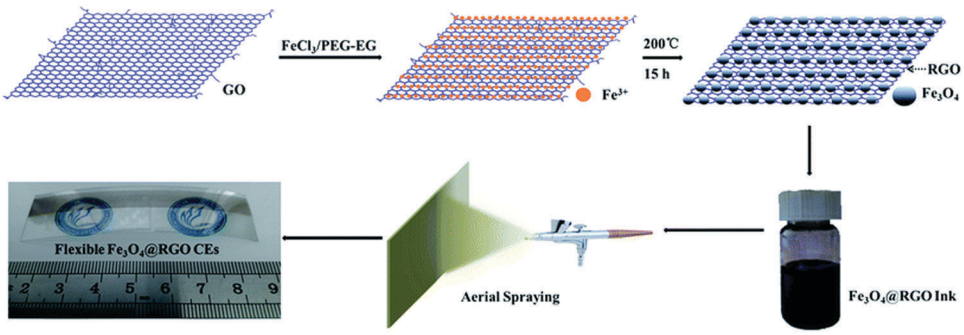


Fig. 30 Schematic diagrams for preparing $Fe_3O_4$@RGO nano-micro composite CEs by a one-pot solvothermal approach and aerial spraying. Reprinted with permission from ref. 564. Copyright (2016) Royal Society of Chemistry.

Open Access Article. Published on 25 August 2017. Downloaded on 4/25/2024 1:35:01 PM.
This article is licensed under a Creative Commons Attribution-NonCommercial 3.0 Unported Licence.

gel-coating method.[570] The fresh DSSC with the RGO/SWCNT CE produced a $V_{OC}$ of 0.86 V and a PCE of 8.37%, which are higher than those of Pt-based DSSCs (0.77 V, 7.79%). The $V_{OC}$ of DSSCs with RGO/SWCNTs further increased up to 0.90 V after aging for one week. The enhanced $V_{OC}$ and PCE can be attributed to the synergetic effects of RGO with a high surface area and SWCNTs with high conductivity. Mesoscopic carbon nanoparticles are interconnected *via* CNTs to form medusa-like CNTs/MC hybrids.[571] The high surface area MC produced more catalytic sites and the CNTs as electrical bridges generated fast electrical transfer networks. DSSCs with CNTs/MC hybrid CE achieved a PCE of 8.4% and remarkable chemical stability that rivals DSSCs with Pt CE (8.3%). Joshi *et al.* prepared nickel-embedded CNT-coated electrospun carbon nanofiber (Ni-CNT/CNF) hybrids by combining electrospinning and a CVD technique.[572] The DSSC based on the Ni-CNT/CNF hybrid CEs yielded a PCE of 7.96%, comparable to DSSCs with Pt CE (8.32%).

Arbab *et al.* synthesized a hybrid based on multiwalled carbon nanotubes and activated charcoal (AC/MWCNTs) by an enzymatic dispersion method.[573] The hybrid possessed the synchronized structures of highly conductive MWCNT and porous AC, which led to high electrocatalytic activity and a low $R_{CT}$ of 0.60 Ω cm$^2$. The resultant DSSC achieved an impressive efficiency of 10.05% with a high fill factor (83%), outperforming the device with Pt CE.

### 7.4. Polymer/TMC hybrids

In 2007, Muto *et al.* coated a viscous mixture of $TiO_2$ nanoparticles and PEDOT:PSS on a plastic substrate.[574] The composite $TiO_2$/PEDOT:PSS showed high catalytic activity and was used as CE in a full-plastic DSSC, yielding a PCE of 4.38%. By simple mechanical mixing of TiN and PEDOT:PSS under ultrasonication, TiN nanoparticles (TiN(P)), TiN nanorods (TiN(R)) and TiN mesoporous spheres (TiN(S)) were incorporated into PEDOT:PSS.[575] TiN(P) were well-dispersed in the PEDOT:PSS matrix, the size of TiN(R) was ~20 nm, and the TiN(S) with a spherical diameter of 170 nm and a TiN nanoparticle size of about 15 nm were linked by PEDOT:PSS. Owing to higher uniformity compared to TiN(R)/PEDOT:PSS and TiN(S)/PEDOT:PSS, TiN(P)/PEDOT-PSS provided more catalytic sites for triiodide reduction. The DSSC with TiN(P)/PEDOT:PSS CE produced a PCE of 7.06%, which was higher than those of Pt (6.57%), TiN(R)/PEDOT:PSS (6.89%) and TiN(S)/PEDOT:PSS (6.19%) CEs. Furthermore, these TiN/PEDOT:PSS based devices showed much higher PCEs than pristine PEDOT:PSS, TiN(P), TiN(R) and TiN(S) based devices.

Yue *et al.* prepared a PPy/PEDOD:PSS hybrid film and used it as CE in DSSCs.[576] Due to its high surface area and rough surface, the hybrid film showed a high catalytic activity, yielding a PCE of 7.60%, comparable to the DSSCs with a sputtered Pt CE (7.73%). Ahmad *et al.* also obtained a similar result.[407,414] Tsai *et al.* doped an organic acid, 1*S*-(+)-camphorsulfonic acid, with the conductive polymer poly(*o*-methoxyaniline) to form a hybrid (CSA/POMA) and used it as CE in DSSCs.[577] The optimal CSA/POMA (16 wt% CSA) electrodes exhibited increased surface roughness, increased crystallinity and decreased impedance.

Table 5 Photovoltaic parameters of DSSCs based on hybrid CEs. (FTO substrate, $I_3^-/I^-$ redox electrolyte, N719 dye, irradiation intensity 100 mW cm$^{-2}$, AM1.5)

| CE materials | $J_{SC}$ (mA cm$^{-2}$) | $V_{OC}$ (mV) | FF | PCE (%) | PCE (Pt)/% | Ref. |
|---|---|---|---|---|---|---|
| Pt/MWCNTs | 16.27 | 755 | 0.63 | 7.69 | 6.31 | 549 |
| Pt/TiC | 16.47 | 719 | 0.65 | 7.68 | 7.16 | 550 |
| Pt/$TiO_2$/$WO_2$ | 12.54 | 830 | 0.70 | 7.23 | 7.03 | 551 |
| Pt/SiNW | 17.19 | 731 | 0.66 | 8.30 | 7.67 | 552 |
| Pt/CNA | 16.57 | 779 | 0.70 | 9.04 | 7.39 | 553 |
| Pt/CS flexible Co electrolyte | 14.24 | 859 | 0.74 | 9.05 | 8.42 | 554 |
| Pt/NiO/Ag mirror | 30.10 | 810 | 462 | 11.27 | 9.64 | 555 |
| TiN/MC | 15.30 | 820 | 0.67 | 8.41 | 8.00 | 490 |
| MoC/OMC | 15.50 | 787 | 0.68 | 8.34 | 7.89 | 471 |
| WC/OMC | 14.59 | 804 | 0.70 | 8.18 | 7.89 | 471 |
| $NiS_2$/RGO | 16.55 | 749 | 0.69 | 8.55 | 8.15 | 558 |
| TiC/C | 14.91 | 847 | 0.70 | 8.85 | 8.18 | 473 |
| VC/C | 15.86 | 840 | 0.73 | 9.75 | 8.18 | 473 |
| WC/C | 15.52 | 842 | 0.72 | 9.42 | 8.18 | 473 |
| TiN/NG | 14.16 | 796 | 0.66 | 7.50 | 7.86 | 561 |
| MoN/NG | 14.62 | 772 | 0.70 | 8.00 | 7.86 | 561 |
| $In_{2.77}S_4$@CC | 17.34 | 750 | 0.67 | 8.71 | 8.75 | 562 |
| Carbon/$Fe_3O_4$ | 16.01 | 750 | 0.68 | 8.11 | 8.37 | 563 |
| $Fe_3O_4$@RGO-NMCC | 17.00 | 760 | 0.70 | 9.04 | 9.46 | 564 |
| PEDOT:PSS/graphene | 15.70 | 770 | 0.65 | 7.86 | 7.31 | 566 |
| RGO/PPy | 15.81 | 725 | 0.71 | 8.14 | 8.34 | 567 |
| Co/PPy/C | 14.21 | 717 | 0.75 | 7.64 | 6.26 | 568 |
| Ni/PPy/C | 14.16 | 720 | 0.73 | 7.44 | 6.26 | 568 |
| CB-NPs/s-PT | 17.21 | 764 | 0.69 | 9.02 | 8.36 | 569 |
| RGO/SWCNT | 12.81 | 860 | 0.76 | 8.37 | 7.79 | 570 |
| CNTs/MC | 16.20 | 749 | 0.69 | 8.40 | 8.30 | 571 |
| Ni-CNT/CNF | 15.83 | 800 | 0.63 | 7.96 | 8.32 | 572 |
| AC/MWCNTs | 16.07 | 753 | 0.83 | 10.05 | 9.30 | 573 |
| TiN/PEDOT:PSS | 14.45 | 727 | 0.67 | 7.06 | 6.57 | 575 |
| PPy/PEDOD:PSS | 14.27 | 750 | 0.71 | 7.60 | 7.73 | 576 |
| CSA/POMA | 18.35 | 740 | 0.65 | 8.76 | 8.01 | 577 |

The DSSC based on the CSA/POMA CE exhibited an efficiency of 8.76%, which was higher than that of DSSCs with Pt CE.

Photovoltaic parameters of some DSSCs based on hybrid CEs are listed in Table 5. The performance of most of the hybrid-based DSSCs outperforms that of the devices with their corresponding components. The superior performance of hybrid CEs can be simply attributed to the synergetic effects of the different components in the hybrids. However, the exact reason for the superior electrochemical property of the hybrids in DSSCs is not fully elaborated, and the role of each part of the hybrid needs to be clarified, and quantitative mechanism analysis is still far away. In any case, the hybrids open up new routes for the development of high-performance and low-cost DSSCs.

## 8. Summary and outlook

Dye-sensitized solar cells, efficient in converting solar energy into electric energy with low cost, easy preparation, high efficiency and environment benignity, are becoming one of the typical representatives of the third generation solar cells. With a focus on the PV technology's golden triangle issues, namely, efficiency, cost and stability, and on the basis of DSSCs' three key components, namely, photoanodes, electrolytes and counter electrodes, the scientists have devoted a great

 This journal is © The Royal Society of Chemistry 2017

Open Access Article. Published on 25 August 2017. Downloaded on 4/25/2024 1:35:01 PM.
This article is licensed under a Creative Commons Attribution-NonCommercial 3.0 Unported Licence.

deal of endeavor and important progress has been achieved since 1991.

The counter electrode is a key component and has a significant influence on both the photovoltaic performance and the device cost of DSSCs. As a counter electrode, it must possess high conductivity and good catalytic activity for electrolyte regeneration, as well as good stability. The platinum metal well satisfies all the requirements for CEs and has been the most frequently used CE material. However, the high cost and lack of stability limit its application widely. Amongst the Pt-free CEs, carbonaceous materials are the widest researched CE materials. The highest PCE (14.3%) of DSSCs is based on the FTO/Au/GNP (graphene nanoplatelet). The low cost, simple preparation and good stability render carbon materials stronger competitors. The main drawback of the carbon-based CE is its relatively low conductivity and catalytic activity compared to the Pt electrode, as well as the large dosage required to attain the targeted catalytic activity, and its poor adhesion to substrates. Conductive polymers are flexible, transparent, easily processed, and easily property tuned. Among conductive polymers, PEDOT exhibits the best performance, but its cost is high. The PPy-based CE is cheaper but the performance is inferior to that of PEDOT. The PANI-based CE has more attractive prospects thanks to its low cost and comparably better performance. The study of the TMC CE has begun later than other Pt-free CEs and it has become a hot research area in recent years owing to its material diversity, Pt-like catalytic activity, and easy preparation and modification. However, the performance of the TMC-based DSSC is relatively lower than that of the devices with other Pt-free CE materials, which might be explained by its poor conductivity for TMCs and electron transportation at interface of TMCs and substrates. Most hybrid-based DSSCs outperform the devices based on their corresponding components, which is attributed to the synergetic effects. The exact reason for the superior performance of the hybrids is not fully elaborated.

It is believed that a power conversion efficiency as high as 15% for monolithic DSSCs could be achieved in near future. As a crucial component of the DSSCs, the counter electrode plays an important role in realizing this important target. We have tried to give an objective evaluation of counter electrode materials. Future development should focus on designing new ideas, using new methods and developing new materials; should aim at main requirements: conductivity, catalytic activity, stability, efficiency, cost and cleanness; should be concerned with the regulation mechanism for photoinduced charge carrier generation, evolution and transportation; should investigate into the interaction rules among photoanodes, electrolytes, and counter electrodes, including each component in counter electrodes.

## Conflicts of interest

There are no conflicts to declare.

## Acknowledgements

The authors acknowledge the joint financial support by the National Natural Science Foundation of China (no. 91422301, U1205112, 90922028, 51472094, 51002053, 50842027) and the specialized research fund for the doctoral program of Higher University, Ministry of Education, China (no. 20123501110001).

## References

1 General Assembly. Transforming our world: the 2030 Agenda for Sustainable Development, https://sustainabledevelopment.un.org/post2015/transformingourworld, accessed 21 October 2015.
2 W. M. Adams, The Future of Sustainability: Re-thinking Environment and Development in the Twenty-first Century, Report of the IUCN Renowned Thinkers Meeting, 29–31 January 2006. Retrieved on: 2009-02-16.
3 Wikipedia, Sustainable development, available from: https://en.wikipedia.org/wiki/ File: Sustainable_development.svg.
4 R. E. Smalley, *Abstr. Paper Am. Chem. Soc.*, 2003, **226**, U24.
5 L. Steve, Renewable Energy World, U.N. Secretary-General: Renewables Can End Energy Poverty, http://www.renewableenergyworld.com/articles/2011/08/u-n-secretary-general-renewables-can-end-energy-poverty.html, accessed 25 August 2011.
6 M. S. Dresselhaus and I. L. Thomas, *Nature*, 2001, **414**, 332–337.
7 A. Witze, *Nature*, 2007, **445**, 14–17.
8 R. F. Service, *Science*, 2005, **309**, 548–551.
9 J. Potocnik, *Science*, 2007, **315**, 810–811.
10 J. Wu, Z. Lan, J. Lin, M. Huang, Y. Huang, L. Fan and G. Luo, *Chem. Rev.*, 2015, **115**, 2136–2173.
11 REN21.2016, *Renewables 2016 Global Status Report*, REN21 Secretariat, Paris, 2016.
12 IRENA, *Renewable Energy and Jobs-Annual Review 2015*, International Renewable Energy Agency, Masdar, 2015.
13 V. Smil, *General Energetics: Energy in the Biosphere and Civilization*, John Wiley, New York, 1991, p. 240.
14 V. Smil, *Energy at the crossroad*, Organisation for Economic Co-operation and Development, Paris, 2006, p. 12.
15 O. Morton, *Nature*, 2006, **443**, 19–22.
16 N. S. Lewis and D. G. Nocera, *Proc. Natl. Acad. Sci. U. S. A.*, 2006, **103**, 15729–15735.
17 A. H. Weston, *Energy*, 2006, **31**, 1685–1702.
18 Q. Schiermeier, J. Tollefson, T. Scully, A. Witze and O. Morton, *Nature*, 2008, **454**, 816–823.
19 A. L. Hammond, *Science*, 1972, **177**, 1088.
20 A. L. Hammond, *Science*, 1972, **178**, 732.
21 N. S. Lewis, *Science*, 2007, **315**, 798–801.
22 A. Lopez, B. Roberts, D. Heimiller, N. Blair and G. Porro, *US Renewable Energy Technical Potentials: A GIS-Based Analysis*, National Renewable Energy Laboratory, Colorado, 2012, p. 20.
23 E. Becquerel, *Comptes Rendus*, 1839, **9**, 561.
24 R. Williams, *J. Chem. Phys.*, 1960, **32**, 1505–1514.
25 C. E. Fritts, *Am. J. Sci.*, 1883, **26**, 465.
26 E. Albert, *Ann. Phys.*, 1905, **17**, 891.

Open Access Article. Published on 25 August 2017. Downloaded on 4/25/2024 1:35:01 PM. This article is licensed under a Creative Commons Attribution-NonCommercial 3.0 Unported Licence.

27 D. Chapin, C. Fuller and G. Pearson, *J. Appl. Phys.*, 1954, **25**, 676.
28 D. J. Flood, *Mod. Phys. Lett. B*, 2001, **15**, 561–570.
29 S. Chu and A. Majumdar, *Nature*, 2012, **488**, 294–303.
30 M. A. Green, *Prog. Photovoltaics*, 2001, **9**, 123–135.
31 M. A. Green, *Sol. Energy*, 2004, **76**, 3–8.
32 G. Conibeer, *Mater. Today*, 2007, **10**, 42–50.
33 D. M. Bagnall and M. Boreland, *Energy Policy*, 2008, **36**, 4390–4396.
34 B. K. Kim and L. White, *J. Nanoelectron. Optoelectron.*, 2012, **7**, 454–459.
35 M. Green, K. Emery, Y. Hishikawa, W. Warta and E. Dunlop, *Prog. Photovoltaics*, 2014, **22**, 1–9.
36 W. A. Badawy, *J. Adv. Res.*, 2015, **6**, 123–132.
37 A. Polman, M. Knight, E. Garnett, B. Ehrler and W. Sinke, *Science*, 2016, **352**, aad4424.
38 D. Cusano, *Solid-State Electron.*, 1963, **6**, 217–232.
39 B. O'Regan and M. Gratzel, *Nature*, 1991, **353**, 737–740.
40 R. M. Swanson, *Prog. Photovoltaics*, 2006, **14**, 443–453.
41 J. D. Farmer and F. Lafond, *Research Policy*, 2016, **45**, 647–665.
42 B. Mary, *Snapshot of Global PV Markets*, International Energy Agency Power Systems Programme (IEA PVPS), Paris, 2014, p. 4.
43 M. Wang, C. Gratzel, S. Zakeeruddin and M. Gratzel, *Energy Environ. Sci.*, 2012, **5**, 9394–9405.
44 W. Hoffmann, *Sol. Energy Mater. Sol. Cells*, 2006, **90**, 3285–3311.
45 P. Wurfel, *Physics of Solar Cells: From Basic Principles to Advanced Concepts*, Wiley-VCH, Weinheim, 2005.
46 National Renewable Energy Laboratory (NREL), Best Research-Cell Efficiencies (04-14-2017), available from: https://commons.wikimedia.org/wiki/File:Best_Research-Cell_Efficiencies.png.
47 M. Gratzel, *Nature*, 2001, **414**, 338–344.
48 C. Longo and M. De Paoli, *J. Braz. Chem. Soc.*, 2003, **14**, 889–901.
49 K. Kalyanasundaram and M. Gratzel, *Coord. Chem. Rev.*, 1998, **77**, 347–414.
50 H. Gerischer, M. E. Michel-Beyerle, F. Rebentrost and H. Tributsch, *Electrochim. Acta*, 1968, **13**, 1509–1515.
51 K. Kalyanasundaram, *Sol. Cells*, 1985, **15**, 93–156.
52 A. Hagfeldtt and M. Gratzel, *Chem. Rev.*, 1995, **95**, 49–68.
53 H. Gerischer and H. Tributsch, *Ber. Bunsenges. Phys. Chem.*, 1968, **72**, 437–445.
54 M. Dare-Edwards, J. Goodenough, A. Hamnet, K. Seddon and R. Wright, *J. Chem. Soc., Faraday Trans.*, 1983, **79**, 2027–2041.
55 H. Tsubomura, M. Matsumura, Y. Noyamaura and T. Amamyiya, *Nature*, 1976, **261**, 402–403.
56 W. Clark and N. Sutin, *J. Am. Chem. Soc.*, 1977, **99**, 4676–4682.
57 G. Hasselman, D. Watson, J. Stromberg, D. Bocian, D. Holten, J. Lindsey and G. Meyer, *J. Phys. Chem. B*, 2006, **110**, 25430–25440.
58 M. Matsumura, Y. Nomura and H. Tsubomura, *Bull. Chem. Soc. Jpn.*, 1977, **50**, 2533–2537.
59 N. Alonso, M. Beley, P. Chartier and V. Ern, *Rev. Phys. Appl.*, 1981, **16**, 5–10.
60 J. Desilvestro, M. Gratzel, L. Kavan, J. Moser and J. Augustynski, *J. Am. Chem. Soc.*, 1985, **107**, 2988–2990.
61 D. Duonghong, N. Serpone and M. Gratzel, *Helv. Chim. Acta*, 1984, **67**, 1012–1018.
62 N. Vlachopoulos, P. Liska, J. Augustynski and M. Gratzel, *J. Am. Chem. Soc.*, 1988, **110**, 1216–1220.
63 M. Gratzel, *Inorg. Chem.*, 2005, **44**, 6841–6851.
64 M. Gratzel, *Prog. Photovoltaics*, 2000, **8**, 171–185.
65 A. Hagfeldt and M. Gratzel, *Acc. Chem. Res.*, 2000, **33**, 269–277.
66 L. Goncalves, V. Bermudez, H. Ribeiroa and A. Mendes, *Energy Environ. Sci.*, 2008, **1**, 655–667.
67 M. Gratzel, *Acc. Chem. Res.*, 2009, **42**, 1788–1798.
68 A. Hagfeldt, G. Boschloo, L. Sun, L. Kloo and H. Pettersson, *Chem. Rev.*, 2010, **110**, 6595–6663.
69 M. Ragoussia and T. Torres, *Chem. Commun.*, 2015, **51**, 3957–3972.
70 S. Ardo and G. Meyer, *Chem. Soc. Rev.*, 2009, **38**, 115–164.
71 G. Boschloo and A. Hagfeldt, *Acc. Chem. Res.*, 2009, **42**, 1819–1826.
72 K. Tennakone, G. Kumara, I. Kottegoda and V. Perera, *Chem. Commun.*, 1999, 15–16.
73 K. Sayama, H. Suguhara and H. Arakawa, *Chem. Mater.*, 1998, **10**, 3825–3832.
74 C. Kelly and G. Meyer, *Coord. Chem. Rev.*, 2001, **211**, 295–315.
75 G. Meyer, *J. Chem. Educ.*, 1997, **74**, 652–656.
76 R. Shanti, F. Bella, Y. Salim, S. Chee and K. Ramesh, *Mater. Des.*, 2016, **108**, 560–569.
77 N. Farhana, M. Khanmirzaei, S. Ramesh and K. Ramesh, *J. Appl. Polym. Sci.*, 2017, **134**, 45091.
78 F. Bella, S. Galliano, C. Gerbaldi and G. Viscardi, *Energies*, 2016, **9**, 384.
79 M. Imperiyka, A. Ahmad, S. Hanifah and F. Bella, *Physica B*, 2014, **450**, 151–154.
80 F. Bella, C. Gerbaldi, C. Barolo and M. Gratzel, *Chem. Soc. Rev.*, 2015, **44**, 3431–3473.
81 F. Bella, S. Galliano, M. Falco, G. Viscardi, C. Barolo, M. Gratzel and C. Gerbaldi, *Green Chem.*, 2017, **19**, 1043–1051.
82 F. Bella, S. Galliano, M. Falco, G. Viscardi, C. Barolo, M. Gratzel and C. Gerbaldi, *Chem. Sci.*, 2016, **7**, 4880–4890.
83 S. Zhang, G. Dong, B. Lin, J. Qu, N. Yuan, J. Ding and Z. Gu, *Sol. Energy*, 2016, **127**, 19–27.
84 S. Galliano, F. Bella, C. Gerbaldi, M. Falco, G. Viscardi, M. Gratzel and C. Barolo, *Energy Technol.*, 2017, **5**, 300–311.
85 U. Bach, D. Lupo, P. Comte, J. E. Moser, F. Weissortel, J. Salbeck, H. Spreitzer and M. Gratzel, *Nature*, 1998, **395**, 583–585.
86 J. Wu, Z. Lan, S. Hao, P. Li, J. Lin, M. Huang, L. Fang and Y. Huang, *Pure Appl. Chem.*, 2008, **80**, 2241–2258.
87 B. Li, L. Wang, B. Kang, P. Wang and Y. Qiu, *Sol. Energy Mater. Sol. Cells*, 2006, **90**, 549–573.
88 S. Weinberg, *The Discovery of Subatomic Particles Revised Edition*, Cambridge University Press, 2003, p. 81.

Open Access Article. Published on 25 August 2017. Downloaded on 4/25/2024 1:35:01 PM.
This article is licensed under a Creative Commons Attribution-NonCommercial 3.0 Unported Licence.

89 M. Faraday, *On Electrical Decomposition*, Philosophical Transactions of the Royal Society, 1834.
90 S. Thomas, T. Deepak, G. Anjusree, T. Arun, S. Naira and A. Nair, *J. Mater. Chem. A*, 2014, **2**, 4474–4490.
91 S. Yun, A. Hagfeldt and T. Ma, *Adv. Mater.*, 2014, **26**, 6210–6237.
92 L. Wang, M. Al-Mamun, P. Liu, Y. Wang, H. Yang, H. Wang and H. Zhao, *NPG Asia Mater.*, 2015, **7**, e226.
93 N. Papageorgiou, W. Maier and M. Gratzel, *J. Electrochem. Soc.*, 1997, **144**, 876–884.
94 J. Wu, Y. Li, Q. Tang, G. Yue, J. Lin, M. Huang and L. Meng, *Sci. Rep.*, 2014, **4**, 4028.
95 J. Trancik, S. Barton and J. Hone, *Nano Lett.*, 2008, **8**, 982–987.
96 N. Papageorgiou, *Coord. Chem. Rev.*, 2004, **248**, 1421–1446.
97 K. Li, Z. Yu, Y. Luo, D. Li and Q. Meng, *J. Mater. Sci. Technol.*, 2007, **23**, 577–582.
98 A. Hauch and A. Georg, *Electrochim. Acta*, 2001, **46**, 3457–3466.
99 F. Fabregat-Santiago, J. Bisquert, E. Palomares, L. Otero, D. Kuang, S. Zakeeruddin and M. Gratzel, *J. Phys. Chem. C*, 2007, **111**, 6550–6560.
100 B. Zhang, D. Wang, Y. Hou, S. Yang, X. Yang, J. Zhong, J. Liu, H. Wang, P. Hu, H. Zhao and H. Yang, *Sci. Rep.*, 2013, **3**, 1836–1843.
101 N. Koide, A. Islam, Y. Chiba and L. Han, *J. Photochem. Photobiol., A*, 2006, **182**, 296–305.
102 D. Pysch, A. Mette and S. Glunz, *Sol. Energy Mater. Sol. Cells*, 2007, **91**, 1698–1706.
103 X. Yin, Z. Xue and B. Liu, *J. Power Sources*, 2011, **196**, 2422–2426.
104 C. Chen, C. Chen and T. Wei, *Electrochim. Acta*, 2010, **55**, 1687–1695.
105 S. Park, H. Boo and T. Chung, *Anal. Chim. Acta*, 2006, **556**, 46–57.
106 T. Murakami and M. Gratzel, *Inorg. Chim. Acta*, 2008, **361**, 572–580.
107 Z. Tang, J. Wu, M. Zheng, J. Huo and Z. Lan, *Nano Energy*, 2013, **2**, 622–627.
108 M. Wu, C. Chen, Y. Chen and H. Shih, *Electrochim. Acta*, 2016, **215**, 50–56.
109 X. Zheng, J. Deng, N. Wang, D. Deng, W. Zhang, X. Bao and C. Li, *Angew. Chem.*, 2014, **53**, 7023–7027.
110 M. Moharanal and A. Mallik, *Electrochim. Acta*, 2013, **98**, 1–10.
111 C. Zhong, W. Hua and Y. Cheng, *J. Power Sources*, 2011, **196**, 8064–8072.
112 C. Yoon, R. Vittal, J. Lee, W. Chae and K. Kim, *Electrochim. Acta*, 2008, **53**, 2890–2896.
113 T. Hsieh, H. Chen, C. Kung, C. Wang, R. Vittal and K. Ho, *J. Mater. Chem.*, 2012, **22**, 5550–5559.
114 H. Sun, D. Qin, S. Huang, X. Guo, D. Li, Y. Luo and Q. Meng, *Energy Environ. Sci.*, 2011, **4**, 2630–2637.
115 J. Huo, M. Zheng, Y. Tu, J. Wu, L. Hu and S. Dai, *Electrochim. Acta*, 2015, **159**, 166–173.
116 V. Dao and H. Choi, *ACS Appl. Mater. Interfaces*, 2016, **8**, 1004–1010.
117 M. Song, K. Chaudhari, J. Park, D. Yang, J. Kim, M. Kim, K. Lim, J. Ko and J. Yu, *Appl. Energy*, 2012, **100**, 132–137.
118 J. Nam, Y. Park, B. Kim and J. Lee, *Scr. Mater.*, 2010, **62**, 148–150.
119 Y. Xue, Y. Ding, J. Niu, Z. Xia, A. Roy, H. Chen, J. Qu, Z. Wang and L. Dai, *Sci. Adv.*, 2015, **1**(8), e1400198.
120 A. Scalia, F. Bella, A. Lamberti, S. Bianco, C. Gerbaldi, E. Tresso and C. Pirri, *J. Power Sources*, 2017, **359**, 311–321.
121 Y. Xiao and G. Han, *J. Power Sources*, 2015, **294**, 8–15.
122 J. Huo, J. Wu, M. Zheng, Y. Tu and Z. Lan, *RSC Adv.*, 2015, **5**, 83029–83035.
123 R. Moraes, E. Saito, D. Leite, M. Massi and A. Sobrinho, *Appl. Surf. Sci.*, 2016, **364**, 229–234.
124 X. Cheng, Z. Zhou, Z. Hou, W. Zhou and S. Wu, *Sci. Adv. Mater.*, 2013, **5**, 1193–1198.
125 K. Soo, M. Park, J. Kim, S. Park, Y. Dong, S. Yu, J. Kim, J. Park, J. Choi and J. Lee, *Sci. Rep.*, 2015, **5**, 10450.
126 Y. Hsu, G. Chen and R. Lee, *J. Polym. Res.*, 2014, **21**, 440.
127 B. Anothumakkool, I. Agrawal, S. Bhange, R. Soni, O. Game, S. Ogale and S. Kurungot, *ACS Appl. Mater. Interfaces*, 2016, **8**, 553–562.
128 J. Halme, P. Vahermaa, K. Miettunen and P. Lund, *Adv. Mater.*, 2010, **22**, E210–E234.
129 A. Listorti, B. O'Regan and J. Durrant, *Chem. Mater.*, 2011, **23**, 3381–3399.
130 P. Barnes, K. Miettunen, X. Li, A. Anderson, T. Bessho, M. Gratzel and B. O'Regan, *Adv. Mater.*, 2013, **25**, 1881–1922.
131 S. Fantacci and F. De Angelis, *Coord. Chem. Rev.*, 2011, **255**, 2704–2726.
132 A. Mishra, M. Fischer and P. Bauerle, *Angew. Chem.*, 2009, **48**, 2474–2499.
133 J. Ondersma and T. Hamann, *Coord. Chem. Rev.*, 2013, **257**, 1533–1543.
134 H. Dunn and L. Peter, *J. Phys. Chem. C*, 2009, **113**, 4726–4731.
135 W. Liu, L. Hu, Z. Huo and S. Dai, *Prog. Chem.*, 2009, **21**, 1085–1093.
136 D. Zheng, M. Ye, X. Wen, N. Zhang and C. Lin, *Sci. Bull.*, 2015, **60**, 850–863.
137 M. Nazeeruddin, E. Baranoff and M. Gratzel, *Sol. Energy*, 2011, **85**, 1172–1178.
138 X. Yang, M. Yanagida and L. Han, *Energy Environ. Sci.*, 2013, **6**, 54–66.
139 N. Koide and L. Han, *Rev. Sci. Instrum.*, 2004, **75**, 2828–2831.
140 D. Aoki, T. Aoki, H. Saito, S. Magaino and K. Takagi, *Electrochim. Acta*, 2012, **80**, 640–646.
141 K. Takagi, S. Magaino, H. Saito, T. Aoki and D. Aoki, *J. Photochem. Photobiol., C*, 2013, **14**, 1–12.
142 C. Seaman, *Sol. Energy*, 1982, **29**, 291–298.
143 P. Sommeling, H. Riele, J. Roosmalen, A. Schonecker, J. Kroon, J. Wienke and A. Hinsch, *Sol. Energy Mater. Sol. Cells*, 2000, **62**, 399–410.
144 R. Nicholson and S. Irving, *Anal. Chem.*, 1964, **36**, 706–723.
145 R. Nicholson, *Anal. Chem.*, 1965, **37**, 1351–1355.
146 J. Heinze, *Angew. Chem.*, 1984, **23**, 831–847.
147 Y. Xiao, J. Lin, W. Wang, S. Tai, G. Yue and J. Wu, *Electrochim. Acta*, 2013, **90**, 468–474.

Open Access Article. Published on 25 August 2017. Downloaded on 4/25/2024 1:35:01 PM.
This article is licensed under a Creative Commons Attribution-NonCommercial 3.0 Unported Licence.

148 K. Saranya, M. Rameez and A. Subramania, *Eur. Polym. J.*, 2015, **66**, 207–227.
149 M. Wu, Y. Wang, X. Lin, N. Yu, L. Wang, A. Hagfeldt and T. Ma, *Phys. Chem. Chem. Phys.*, 2011, **13**, 19298–19301.
150 M. Wu, X. Lin, Y. Wang, L. Wang, W. Guo, D. Qu, X. Peng, A. Hagfeldt, M. Gratzel and T. Ma, *J. Am. Chem. Soc.*, 2012, **134**, 3419–3428.
151 F. Fabregat-Santiago, J. Bisquert, L. Cevey, P. Chen, M. Wang, S. Zakeeruddin and M. Gratzel, *J. Am. Chem. Soc.*, 2008, **131**, 558–562.
152 L. Han, N. Koide, Y. Chiba, A. Islam, R. Komiya, F. Nobuhiro, A. Fukui and R. Yamanaka, *Appl. Phys. Lett.*, 2005, **86**, 213501.
153 Q. Wang, J. Moser and M. Gra1tzel, *J. Phys. Chem. B*, 2005, **109**, 14945–14953.
154 Z. Huang, G. Natu, Z. Ji, P. Hasin and Y. Wu, *J. Phys. Chem. C*, 2011, **115**, 25109–25114.
155 W. Liu, D. Kou, M. Cai, L. Hu and S. Dai, *Prog. Chem.*, 2012, **24**, 722–736.
156 L. Peter, *J. Phys. Chem. C*, 2007, **111**, 6601–6612.
157 G. Schlichthorl, N. Park and A. Frank, *J. Phys. Chem. B*, 1999, **103**, 782–791.
158 J. van de Lagemaat, N. Park and A. Frank, *J. Phys. Chem. B*, 2000, **104**, 2044–2052.
159 F. Cao, G. Oskam, G. Meyer and P. Searson, *J. Phys. Chem.*, 1996, **100**, 17021–17027.
160 L. Dloczik, O. Ileperuma, I. Lauermann, L. Peter, E. Ponomarev, G. Redmond, N. Shaw and I. Uhlendorf, *J. Phys. Chem. B*, 1997, **101**, 10281–10289.
161 J. Kruger, R. Plass, M. Gratzel, P. Cameron and L. Peter, *J. Phys. Chem. B*, 2003, **107**, 7536–7539.
162 G. Schlichthorl, S. Huang, J. Sprague and A. Frank, *J. Phys. Chem. B*, 1997, **101**, 8141–8155.
163 R. Kern, R. Sastrawan, J. Ferber, R. Stangl and J. Luther, *Electrochim. Acta*, 2002, **47**, 4213–4225.
164 L. Han, N. Koide, Y. Chiba, A. Islam and T. Mitate, *C. R. Chim.*, 2006, **9**, 645–651.
165 J. Bisquert, *J. Phys. Chem. B*, 2002, **106**, 325–333.
166 M. Adachi, M. Sakamoto, J. Jiu, Y. Ogata and S. Isoda, *J. Phys. Chem. B*, 2006, **110**, 13872–13880.
167 Q. Wang, S. Ito, M. Gratzel, F. Fabregat-Santiago, I. Mora-Sero, J. Bisquert, T. Bessho and H. Imai, *J. Phys. Chem. B*, 2006, **110**, 25210–25221.
168 L. Peter and K. Wijayantha, *Electrochim. Acta*, 2000, **45**, 4543–4551.
169 T. Oekermann, D. Zhang, T. Yoshida and H. Minoura, *J. Phys. Chem. B*, 2004, **108**, 2227–2235.
170 W. Liu, L. Hu, S. Dai, L. Guo, N. Jiang and D. Kou, *Electrochim. Acta*, 2010, **55**, 2338–2343.
171 D. Hecht, L. Hu and G. Irvin, *Adv. Mater.*, 2011, **23**, 1482–1513.
172 T. Minami, *Semicond. Sci. Technol.*, 2005, **20**, S35.
173 Z. Chen, W. Li, R. Li, Y. Zhang, G. Xu and H. Cheng, *Langmuir*, 2013, **29**, 13836–13842.
174 B. Yoo, K. Kim, D. Lee, M. Ko, H. Lee, Y. Kim, W. Kim and N. Park, *J. Mater. Chem.*, 2010, **20**, 4392–4398.
175 T. Kawashima, T. Ezure, K. Okada, H. Matsui, K. Goto and N. Tanabe, *J. Photochem. Photobiol., A*, 2004, **164**, 199–202.
176 C. Sima, C. Grigoriu and S. Antohe, *Thin Solid Films*, 2010, **519**, 595–597.
177 B. Yoo, K. Kim, D. Lee, M. Ko, H. Lee, Y. Kim, W. Kimc and N. Park, *J. Mater. Chem.*, 2010, **20**, 4392–4398.
178 I. Zumeta, J. Ayllon, B. Gonzalez, X. Domenech and E. Vigil, *Sol. Energy Mater. Sol. Cells*, 2009, **93**, 1728–1732.
179 B. Yoo, K. Kim, S. Lee, W. Kim and N. Park, *Sol. Energy Mater. Sol. Cells*, 2008, **92**, 873–877.
180 W. MacDonald, M. Looney, D. MacKerron, R. Eveson, R. Adam, K. Hashimoto and K. Rakos, *J. Soc. Inf. Disp.*, 2007, **15**, 1075–1083.
181 Q. Qin and R. Zhang, *Electrochim. Acta*, 2013, **89**, 726–731.
182 S. Agarkar, V. Dhas, S. Muduli and S. Ogale, *RSC Adv.*, 2012, **2**, 11645–11649.
183 V. Zardetto, F. Di Giacomo, D. Garcia-Alonso, W. Keuning, M. Creatore, C. Mazzuca, A. Reale, A. Di Carlo and T. Brown, *Adv. Energy Mater.*, 2013, **3**, 1292–1298.
184 M. De Paoli, A. Nogueira, D. Machado and C. Longo, *Electrochim. Acta*, 2001, **46**, 4243–4249.
185 F. Pichot, S. Ferrere, R. Pitts and B. Gregg, *J. Electrochem. Soc.*, 1999, **146**, 4324–4326.
186 J. Pringle, V. Armel and D. MacFarlane, *Chem. Commun.*, 2010, **46**, 5367–5369.
187 J. An, W. Guo and T. Ma, *Small*, 2012, **8**, 3427–3431.
188 K. Sun, I. Sahito, J. Noh, S. Yeo, J. Im, S. Yi, Y. Kim and S. Jeong, *J. Mater. Chem. A*, 2016, **4**, 458–465.
189 W. Dow, G. Liao, S. Huang and S. Chen, *J. Mater. Chem.*, 2010, **20**, 3600–3609.
190 S. Cherng, C. Chen, W. Dow, C. Lin and S. Chen, *Electrochem. Solid-State Lett.*, 2011, **14**, P13–P15.
191 J. Lin, W. Wang, Y. Lin and S. Chou, *ACS Appl. Mater. Interfaces*, 2014, **6**, 3357–3364.
192 F. Bella, D. Pugliese, L. Zolin and C. Gerbaldi, *Electrochim. Acta*, 2017, **237**, 87–93.
193 A. Lamberti, A. Virga, A. Angelini, A. Ricci, E. Descrovi, M. Cocuzza and F. Giorgis, *RSC Adv.*, 2015, **5**, 4404.
194 S. Roelofs, A. Van Den Berg and M. Odijk, *Lab Chip*, 2015, **15**, 3428.
195 F. Bella, A. Lamberti, S. Bianco, E. Tresso, C. Gerbaldi and C. Pirri, *Adv. Mater. Technol.*, 2016, **1**, 1600002.
196 T. Ma, X. Fang, M. Akiyama, K. Inoue, H. Noma and E. Abe, *J. Electroanal. Chem.*, 2004, **574**, 77–83.
197 M. Toivola, F. Ahlskog and P. Lund, *Sol. Energy Mater. Sol. Cells*, 2006, **90**, 2881–2893.
198 S. Balasingam, M. Kangw and Y. Jun, *Chem. Commun.*, 2013, **49**, 11457–11475.
199 K. Miettunen, J. Halme and P. Lund, *Wiley Interdiscip. Rev.: Energy Environ.*, 2013, **2**, 104–120.
200 N. Vyas, C. Charbonneau, M. Carnie, D. Worsley and T. Watson, *ECS Trans.*, 2013, **53**, 29–37.
201 A. F. Kanta and A. Decroly, *Electrochim. Acta*, 2011, **56**, 10276–10282.
202 G. Man, N. Park, S. Kwang, H. Soon and K. Kim, *Chem. Lett.*, 2005, 804.

Open Access Article. Published on 25 August 2017. Downloaded on 4/25/2024 1:35:01 PM.
This article is licensed under a Creative Commons Attribution-NonCommercial 3.0 Unported Licence.

203 M. Paulose, K. Shankar, O. Varghese, G. Mor, B. Hardin and C. Grimes, *Nanotechnology*, 2006, **17**, 1446–1448.
204 L. Chen, C. Hsieh, Y. Lee and H. Teng, *ACS Appl. Mater. Interfaces*, 2013, **5**, 11958–11964.
205 S. Ito, S. Zakeeruddin, P. Comte, P. Liska, D. Kuang and M. Gratzel, *Nat. Photonics*, 2008, **2**, 693–698.
206 J. Bisquert, *Nat. Photonics*, 2008, **2**, 648–649.
207 Q. Tai, B. Chen, F. Guo, S. Xu, H. Hu, B. Sebo and X. Zhao, *ACS Nano*, 2011, **5**, 3795–3799.
208 S. Xu, Y. Luo, G. Liu, G. Qiao, W. Zhong, Z. Xiao, Y. Luo and H. Ou, *Electrochim. Acta*, 2015, **156**, 20–28.
209 Y. Wang, D. Wang, Y. Jiang, H. Chen, C. Chen, K. Ho, H. Chou and C. Chen, *Angew. Chem., Int. Ed.*, 2013, **52**, 6694–6698.
210 Y. Duan, Q. Tang, B. He, R. Li and L. Yu, *Nanoscale*, 2014, **6**, 12601–12608.
211 P. Chen, C. Li, C. Lee, R. Vittal and K. Ho, *Nano Energy*, 2015, **12**, 374–385.
212 Y. Fu, Z. Lv, S. Hou, H. Wu, D. Wang, C. Zhang and D. Zou, *Adv. Energy Mater.*, 2012, **2**, 37–41.
213 S. Gao, Z. Lan, W. Wu, L. Que, J. Wu and J. Lin, *Polym. Adv. Technol.*, 2014, **25**, 1560–1564.
214 J. Jia, J. Wu, Y. Tu, J. Huo, M. Zheng and J. Lin, *J. Alloys Compd.*, 2015, **640**, 29–33.
215 J. Dong, J. Wu, J. Jia, J. Ge, Q. Bao, C. Wang and L. Fan, *Appl. Surf. Sci.*, 2017, **401**, 1–6.
216 W. Kylberg, F. Castro, P. Chabrecek, U. Sonderegger, B. Chu, F. Nuesch and R. Hany, *Adv. Mater.*, 2011, **23**, 1015–1019.
217 X. Fan, F. Wang, Z. Chu, L. Chen, C. Zhang and D. Zou, *Appl. Phys. Lett.*, 2007, **90**, 073501.
218 J. Usagawa, S. Pandey, Y. Ogomi, S. Noguchi, Y. Yamaguchi and S. Hayase, *Prog. Photovoltaics*, 2013, **21**, 517–524.
219 T. Miyasaka, *J. Phys. Chem. Lett.*, 2011, **2**, 262–269.
220 Y. Xiao, J. Wu, G. Yue, J. Lin, M. Huang, L. Fan and Z. Lan, *Electrochim. Acta*, 2011, **58**, 621–627.
221 X. Fan, F. Wang, Z. Chu, L. Chen and C. Zhang, and D. Zoua, *Appl. Phys. Lett.*, 2007, **90**, 073501.
222 M. Murayama and T. Mori, *J. Phys. D: Appl. Phys.*, 2007, **40**, 1664–1668.
223 K. Kakiage, Y. Aoyama, T. Yano, K. Oya, J. Fujisawa and M. Hanaya, *Chem. Commun.*, 2015, **51**, 15894–15897.
224 Z. Lan and J. Wu, *Prog. Chem.*, 2010, **22**, 2248–2253.
225 H. Weerasinghe, F. Huang and Y. Cheng, *Nano Energy*, 2013, **2**, 174–189.
226 K. Fan, R. Li, J. Chen, W. Shi and T. Peng, *Sci. Adv. Mater.*, 2013, **5**, 1596–1626.
227 T. Brown, F. Rossi, F. Giacomo, G. Mincuzzi, V. Zardetto, A. Realea and A. Carlo, *J. Mater. Chem. A*, 2014, **2**, 10788–10817.
228 F. Rossi, L. Gaspare, A. Reale, A. Carlo and T. Brown, *J. Mater. Chem. A*, 2013, **1**, 12941–12947.
229 T. Yamaguchi, N. Tobe, D. Matsumoto, T. Nagai and H. Arakawa, *Sol. Energy Mater. Sol. Cells*, 2010, **94**, 812–816.
230 N. Fu, Y. Fang, Y. Duan, X. Zhou, X. Xiao and Y. Lin, *ACS Nano*, 2012, **6**, 9596–9605.
231 Y. Xiao, J. Wu, G. Yue, J. Lin, M. Huang, L. Fan and Z. Lan, *J. Power Sources*, 2012, **208**, 197–202.
232 Y. Xiao, J. Wu, G. Yue, J. Lin, M. Huang, Z. Lan and L. Fan, *Electrochim. Acta*, 2012, **85**, 432–437.
233 Y. Xiao, J. Wu, G. Yue, J. Lin, M. Huang, L. Fan and Z. Lan, *RSC Adv.*, 2012, **2**, 10550–10555.
234 J. Wu, Y. Xiao, Q. Tang, G. Yue, J. Lin, M. Huang, Y. Huang, L. Fan, Z. Lan and S. Yin, *Adv. Mater.*, 2012, **24**, 1884–1888.
235 Y. Liu, M. Li, H. Wang, J. Zheng, H. Xu, Q. Ye and H. Shen, *J. Phys. D: Appl. Phys.*, 2010, **43**, 205103.
236 G. Kauffman, J. Thurner and D. Zatko, *Inorg. Synth.*, 1967, **9**, 182–185.
237 P. Loferski, US Geological Survey Minerals Yearbook-2014: Platinum-group metals, USGS Mineral Resources Program, US Department of the Interior, retrieved 11 July 2016.
238 M. Wu and T. Ma, *J. Phys. Chem. C*, 2014, **118**, 16727–16742.
239 Q. Tang, J. Duan, Y. Duan, B. He and L. Yua, *Electrochim. Acta*, 2015, **178**, 886–899.
240 M. Nazeerudin, A. Kay, I. Rodicio, R. Humpbry-Baker, E. Miiller, P. Liska, N. Vlachopoulos and M. Gratzel, *J. Am. Chem. Soc.*, 1993, **115**, 6382–6390.
241 X. Fang, T. Ma, G. Guan, M. Akiyama, T. Kida and E. Abe, *J. Electroanal. Chem.*, 2004, **570**, 257–263.
242 L. Chen, W. Tan, J. Zhang, X. Zhou, X. Zhang and Y. Lin, *Electrochim. Acta*, 2010, **55**, 3721–3726.
243 P. Li, J. Wu, J. Lin, M. Huang, Z. Lan and Q. Li, *Electrochim. Acta*, 2008, **53**, 4161–4166.
244 G. Wang, R. Lin, Y. Lin, X. Li, X. Zhou and X. Xiao, *Electrochim. Acta*, 2005, **50**, 5546–5552.
245 M. Ikegami, K. Miyoshi, T. Miyasaka, K. Teshima, T. Wei, C. Wan and Y. Wang, *Appl. Phys. Lett.*, 2007, **90**, 153122.
246 E. Olsen, G. Hagen and S. Lindquist, *Sol. Energy Mater. Sol. Cells*, 2000, **63**, 267–273.
247 V. Dao and H. Choi, *Electrochim. Acta*, 2013, **93**, 287–292.
248 M. Song, K. Chaudhari, J. Park, D. Yang, J. Kim, M. Kim, K. Lim, J. Ko and J. Yu, *Appl. Energy*, 2012, **100**, 132–137.
249 Y. Lee, C. Chen, L. Chong, C. Chen, Y. Liu and C. Chi, *Electrochem. Commun.*, 2010, **12**, 1662–1665.
250 H. Jeong, Y. Pak, Y. Hwang, H. Song, K. Lee, H. Ko and G. Y. Jung, *Small*, 2012, **8**, 3757–3761.
251 H. Zhang, W. Zhou, Y. Du, P. Yang and C. Wang, *Electrochem. Commun.*, 2010, **12**, 882–885.
252 H. Lee and M. Horn, *Thin Solid Films*, 2013, **540**, 208–211.
253 J. Kim, J. Kang, U. Jeong and H. Kim, and H. Lee, *ACS Appl. Mater. Interfaces*, 2013, **5**, 3176–3181.
254 J. Wu, Z. Tang, Y. Huang, M. Huang, H. Yu and J. Lin, *J. Power Sources*, 2014, **257**, 84–89.
255 J. Chen, B. Lim, E. Lee and Y. Xia, *Nano Today*, 2009, **4**, 81–95.
256 M. Subhramannia and V. Pillai, *J. Mater. Chem.*, 2008, **18**, 5858–5870.
257 J. Tiwari, F. Pan and K. Lin, *New J. Chem.*, 2009, **33**, 1482–1485.
258 W. Yang, Y. Wang, J. Li and X. Yang, *Energy Environ. Sci.*, 2010, **3**, 144–149.
259 H. Kawasaki, T. Yao, T. Suganuma, K. Okumura, Y. Iwaki, T. Yonezawa, T. Kikuchi and R. Arakawa, *Chem. – Eur. J.*, 2010, **16**, 10832–10843.

Open Access Article. Published on 25 August 2017. Downloaded on 4/25/2024 1:35:01 PM.
This article is licensed under a Creative Commons Attribution-NonCommercial 3.0 Unported Licence.

260 Y. Xiao and G. Han, *Org. Electron.*, 2016, **37**, 239–244.
261 G. Calogero, P. Calandra, A. Irrera, A. Sinopoli, I. Citro and G. Marco, *Energy Environ. Sci.*, 2011, **4**, 1838–1844.
262 A. Yella, H. Lee, H. Tsao, C. Yi, A. Chandiran, M. Nazeeruddin, E. Diau, C. Yeh, S. Zakeeruddin and M. Gratzel, *Science*, 2011, **334**, 629–635.
263 K. Kakiage, Y. Aoyama, T. Yano, T. Otsuka, T. Kyomen, M. Unno and M. Hanaya, *Chem. Commun.*, 2014, **50**, 6379–6381.
264 K. Kakiage, Y. Aoyama, T. Yano, K. Oya, T. Kyomen and M. Hanaya, *Chem. Commun.*, 2015, **51**, 6315–6317.
265 T. Murakami, S. Ito, Q. Wang, M. Nazeeruddin, T. Bessho, I. Cesar, P. Liska, R. Humphry-Baker, P. Comte, P. Pechy and M. Gratzel, *J. Electrochem. Soc.*, 2006, **153**, A2255–2261.
266 A. Kay and M. Gratzel, *Sol. Energy Mater. Sol. Cells*, 1996, **44**, 99–117.
267 M. Wang, N. Chamberland, J. Breau, J. Moser, R. Humphry-Baker, B. Marsan, S. Zakeeruddin and M. Gratzel, *Nat. Chem.*, 2010, **2**, 385–389.
268 S. Feldt, E. Gibson, E. Gabrielsson, L. Sun, G. Boschloo and A. Hagfeldt, *J. Am. Chem. Soc.*, 2010, **132**, 16714–16724.
269 S. Sapp, C. Elliott, C. Contado, S. Caramori and C. Bignozzi, *J. Am. Chem. Soc.*, 2002, **124**, 11215–11222.
270 A. Hartmann, M. Neilson, R. Lamb and K. Watanabe, and J. Scott, *Appl. Phys. A: Mater. Sci. Process.*, 2000, **70**, 239–242.
271 T. Eom, W. Sari, K. Choi, W. Shin, J. Kim, D. Lee, K. Kim, H. Sohn and S. Kim, *Electrochem. Solid-State Lett.*, 2009, **12**, D85–D88.
272 Y. Noh, B. Yu, K. Yoo, M. Ko and O. Song, *Korean J. Met. Mater.*, 2012, **50**, 243–247.
273 J. Han, K. Yoo, M. Ko, B. Yu, Y. Noh and O. Song, *Met. Mater. Int.*, 2012, **18**, 105–108.
274 Y. Noh and O. Song, *Korean J. Met. Mater.*, 2013, **51**, 71–76.
275 D. Yun, H. Ra, S. Jo, W. Maeng, S. Lee, S. Park, J. Jang, K. Cho and S. Rhee, *ACS Appl. Mater. Interfaces*, 2012, **4**, 4588–4594.
276 J. Seok, K. Ryu, J. Lee, I. Jeong, N. Lee, J. Baik, J. Kim, M. Ko, K. Kim and M. Kim, *Phys. Chem. Chem. Phys.*, 2015, **17**, 3004–3008.
277 G. An, H. An and H. Ahn, *J. Electroanal. Chem.*, 2016, **775**, 280–285.
278 G. An, B. Koo and H. Ahn, *Phys. Chem. Chem. Phys.*, 2016, **18**, 6587–6594.
279 G. An, J. Sohn and H. Ahn, *J. Mater. Chem. A*, 2016, **4**, 2049–2054.
280 M. Zhang, E. Uchaker, S. Hu, Q. Zhang, T. Wang, G. Cao and J. Li, *Nanoscale*, 2013, **5**, 12342–12349.
281 G. An and H. Ahn, *J. Power Sources*, 2014, **272**, 828–836.
282 Y. Noh, K. Yoo, J. Kim, O. Song and M. Ko, *Curr. Appl. Phys.*, 2013, **13**, 1620–1624.
283 K. Mokurala, A. Kamble, P. Bhargava and S. Mallick, *J. Electron. Mater.*, 2015, **44**, 4400–4404.
284 Y. Noh and O. Song, *Electron. Mater. Lett.*, 2014, **10**, 981–984.
285 J. Sun, C. Tang, J. Xu, X. Yin, S. Nie, H. Wang, K. Sun, S. Cho and H. Gong, *Int. J. Hydrogen Energy*, 2015, **40**, 10194–10199.
286 M. Rahman, R. Kojima, M. Fihry, Y. Kimura and M. Niwano, *Jpn. J. Appl. Phys.*, 2010, **49**, 122302.
287 Y. Noh and O. Song, *Electron. Mater. Lett.*, 2014, **10**, 271–273.
288 Y. Noh and O. Song, *Korean J. Met. Mater.*, 2013, **51**, 603–606.
289 Y. Noh and O. Song, *Korean J. Met. Mater.*, 2014, **52**, 557–560.
290 H. Snaith, A. Moule, C. Klein, K. Meerholz, R. Friend and M. Gratzel, *Nano Lett.*, 2007, **7**, 3372–3376.
291 J. Xia, C. Yuan and S. Yanagida, *ACS Appl. Mater. Interfaces*, 2010, **2**, 2136–2139.
292 R. Street, W. Wong, S. Ready, M. Chabinyc, A. Arias, S. Limb, A. Salleo and R. Lujan, *Mater. Today*, 2006, **9**, 32–37.
293 M. Al-Mamun, J. Kim, K. Lee, Y. Ko, J. Lee, I. In, J. Lee, Y. Sung and S. Kim, *Synth. Met.*, 2013, **177**, 77–81.
294 G. Margulis, M. Christoforo, D. Lam, Z. Beiley, A. Bowring, C. Bailie, A. Salleo and M. McGehee, *Adv. Energy Mater.*, 2013, **3**, 1657–1663.
295 B. Hardin, W. Gaynor, I. Ding, S. Rim, P. Peumans and M. McGehee, *Org. Electron.*, 2011, **12**, 875–879.
296 T. Tokuno, M. Nogi, J. Jiu, T. Sagahara and K. Suganuma, *Langmuir*, 2012, **28**, 9298–9302.
297 Y. Sun, B. Mayers, T. Herricks and Y. Xia, *Nano Lett.*, 2003, **3**, 955–960.
298 T. Tokuno, M. Nogi, M. Karakawa, J. Jiu, T. Nge, Y. Aso and K. Suganuma, *Nano Res.*, 2011, **4**, 1215–1222.
299 L. Hu, H. Kim, J. Lee, P. Peumans and Y. Cui, *ACS Nano*, 2010, **4**, 2955–2963.
300 Z. Yu, Q. Zhang, L. Li, Q. Chen, X. Niu, J. Liu and Q. Pei, *Adv. Mater.*, 2011, **23**, 664–668.
301 R. Zhu, C. Chung, K. Cha, W. Yang, Y. Zheng, H. Zhou, T. Song, C. Chen, P. Weiss, G. Li and Y. Yang, *ACS Nano*, 2011, **5**, 9877–9882.
302 B. Liu and Z. Wang, *RSC Adv.*, 2016, **6**, 47185–47191.
303 M. Al-Mamun, J. Kim, Y. Sung, J. Lee and S. Kim, *Chem. Phys. Lett.*, 2013, **561**, 115–119.
304 B. He, X. Meng and Q. Tang, *ACS Appl. Mater. Interfaces*, 2014, **6**, 4812–4818.
305 B. He, X. Meng, Q. Tang, P. Li, S. Yuan and P. Yang, *J. Power Sources*, 2014, **260**, 180–185.
306 J. Wan, G. Fang, H. Yin, X. Liu, D. Liu, M. Zhao, W. Ke, H. Tao and Z. Tang, *Adv. Mater.*, 2014, **26**, 8101–8106.
307 S. Peng, J. Shi, J. Pei, Y. Liang, F. Cheng and J. Liang, and J. Chen, *Nano Res.*, 2009, **2**, 484–492.
308 Q. Yang, P. Yang, J. Duan, X. Wang, L. Wang, Z. Wang and Q. Tang, *Electrochim. Acta*, 2016, **190**, 85–91.
309 Q. Tang, H. Zhang, Y. Meng, B. He and L. Yu, *Angew. Chem.*, 2015, **54**, 11448–11452.
310 H. Cai, Q. Tang, B. He and P. Li, *J. Power Sources*, 2014, **258**, 117–121.
311 V. Dao, Y. Choi, K. Yong, L. Larina, O. Shevaleevskiy and H. Choi, *J. Power Sources*, 2015, **274**, 831–838.
312 V. Stamenkovic, B. Mun, M. Arenz, K. Mayrhofer, C. Lucas, G. Wang, P. Ross and N. Markovic, *Nat. Mater.*, 2007, **6**, 241–247.

Open Access Article. Published on 25 August 2017. Downloaded on 4/25/2024 1:35:01 PM.
This article is licensed under a Creative Commons Attribution-NonCommercial 3.0 Unported Licence.

313 V. Stamenkovic, B. Fowler, B. Mun, G. Wang, P. Ross, C. Lucas and N. Markovic, *Science*, 2007, **315**, 493–497.
314 C. Wang, N. Markovic and V. Stamenkovic, *ACS Catal.*, 2012, **2**, 891–898.
315 Y. Duan, Q. Tang, J. Liu, B. He and L. Yu, *Angew. Chem.*, 2014, **126**, 14797–14802.
316 H. Cai, Q. Tang, B. He, R. Li and L. Yu, *Nanoscale*, 2014, **6**, 15127–15133.
317 J. Liu, Q. Tang, B. He and L. Yu, *J. Power Sources*, 2015, **282**, 79–86.
318 S. Kukunuri, S. Karthicka and S. Sampath, *J. Mater. Chem. A*, 2015, **3**, 17144–17153.
319 P. Yang and Q. Tang, *Electrochim. Acta*, 2015, **182**, 827–833.
320 P. Yang and Q. Tang, *Appl. Surf. Sci.*, 2016, **362**, 28–34.
321 S. Kim, K. Park, J. Yuma and Y. Sung, *J. Photochem. Photobiol., A*, 2007, **189**, 301–306.
322 A. Nozik and R. Memming, *J. Phys. Chem.*, 1996, **100**, 13061–13078.
323 J. Liu, Q. Tang and B. He, *J. Power Sources*, 2014, **268**, 56–62.
324 X. Chen, Q. Tang, B. He, L. Lin and L. Yu, *Angew. Chem.*, 2014, **53**, 10799–10803.
325 P. Karthik, A. Himaja and S. Singh, *Carbon Lett.*, 2014, **15**, 219–237.
326 Wikipedia, Allotropes of carbon, available from: https://en.wikipedia.org/wiki/Allotropes_of_carbon#/media/File:Eight_Allotropes_of_Carbon.png.
327 H. Kroto, J. Heath, S. O'Brien, R. Curl and R. Smalley, *Nature*, 1985, **318**, 162–163.
328 S. Iijima, *Nature*, 1991, **354**, 56–58.
329 K. Novoselov, A. Geim, S. Morozov, D. Jiang, Y. Zhang, S. Dubonos, I. Grigorieva and A. Firsov, *Science*, 2004, **306**, 666–669.
330 R. Costa, F. Lodermeyer, R. Casillas and D. Guldi, *Energy Environ. Sci.*, 2014, **7**, 1281–1296.
331 L. Wang, H. Liu, R. Konic, J. Misewich and S. Wang, *Chem. Soc. Rev.*, 2013, **42**, 8134–8156.
332 P. Poudel and Q. Qiao, *Nano Energy*, 2014, **4**, 157–175.
333 J. Theerthagiri, A. Senthil, J. Madhavan and T. Maiyalagan, *ChemElectroChem*, 2015, **2**, 928–945.
334 H. Shiraza and F. Astaraie, *J. Mater. Chem. A*, 2015, **3**, 20849–20862.
335 J. Roy-Mayhew and I. Aksay, *Chem. Rev.*, 2014, **114**, 6323–6348.
336 J. Lim, S. Ryu, J. Kim and Y. Jun, *Nanoscale Res. Lett.*, 2013, **8**, 1–5.
337 C. Wu, T. Chang, H. Teng and Y. Lee, *Energy*, 2016, **115**, 513–518.
338 J. Kim and S. Rhee, *Electrochim. Acta*, 2012, **83**, 264–270.
339 I. Liu, Y. Hou, C. Li and Y. Lee, *J. Mater. Chem. A*, 2017, **5**, 240–249.
340 J. Zhang, H. Long, S. Miralles, J. Bisquert, F. Fabregat-Santiago and M. Zhang, *Phys. Chem. Chem. Phys.*, 2012, **14**, 7131–7136.
341 R. Baan, *Inhalation Toxicol.*, 2007, **19**, 213–228.
342 E. Zussman, X. Chen, W. Ding, L. Calabri, D. Dikin, J. Quintana and R. Ruoff, *Carbon*, 2005, **43**, 2175–2185.
343 M. Inagaki, Y. Yang and F. Kang, *Adv. Mater.*, 2012, **24**, 2547–2566.
344 Q. Ngo, T. Yamada, M. Suzuki, Y. Ominami, A. Cassell, L. Jun, M. Meyyappan and C. Yang, *IEEE Trans. Nanotechnol.*, 2007, **6**, 688–695.
345 C. Wei and D. Srivastava, *Appl. Phys. Lett.*, 2004, **85**, 2208–2210.
346 C. Pike, C. Grabner and A. Harkins, *J. Visualized Exp.*, 2009, **27**, e1040.
347 P. Joshi, L. Zhang, Q. Chen, D. Galipeau, H. Fong and Q. Qiao, *ACS Appl. Mater. Interfaces*, 2010, **2**, 3572–3577.
348 G. Veerappan, W. Kwon and S. Rhee, *J. Power Sources*, 2011, **196**, 10798–10805.
349 S. Park, B. Kim and W. Lee, *J. Power Sources*, 2013, **239**, 122–127.
350 H. Guo, Y. Zhu, W. Li, H. Zheng, K. Wu, K. Ding, B. Ruan, A. Hagfeldt, T. Ma and M. Wu, *Electrochim. Acta*, 2015, **176**, 997–1000.
351 X. Wang, Q. Li, J. Xie, Z. Jin, J. Wang, Y. Li, K. Jiang and S. Fan, *Nano Lett.*, 2009, **9**, 3137–3141.
352 M. Volder, S. Tawfick, R. Baughman and A. Hart, *Science*, 2013, **339**, 535–539.
353 V. Popov, *Mater. Sci. Eng., R*, 2004, **43**, 61–102.
354 K. Suzuki, M. Yamaguchi, M. Kumagai and S. Yanagida, *Chem. Lett.*, 2003, **32**, 28–29.
355 W. Lee, E. Ramasamy, D. Lee and J. Song, *ACS Appl. Mater. Interfaces*, 2009, **1**, 1145–1149.
356 X. Mei, S. Cho, B. Fan and J. Ouyang, *Nanotechnology*, 2010, **21**, 395202.
357 J. Ma, C. Li, F. Yu and J. Chen, *ChemSusChem*, 2014, **7**, 3304–3311.
358 A. Geim and K. Novoselov, *Nat. Mater.*, 2007, **6**, 183–191.
359 C. Banks, T. Davies, G. Wildgoose and R. Compton, *Chem. Commun.*, 2005, 829–841.
360 C. Lee, X. Wei, J. Kysar and J. Hone, *Science*, 2008, **321**, 385–388.
361 D. Dreyer, R. Ruoff and C. W. Bielawski, *Angew. Chem.*, 2010, **49**, 9336–9344.
362 Y. Zhu, S. Murali, W. Cai, X. Li, J. Suk, J. Potts and R. Ruoff, *Adv. Mater.*, 2010, **22**, 3906–3924.
363 A. Balandin, S. Ghosh, W. Bao, I. Calizo, D. Teweldebrhan, F. Miao and C. Lau, *Nano Lett.*, 2008, **8**, 902–907.
364 A. Ranjbartoreh, B. Wang, X. Shen and G. Wang, *J. Appl. Phys.*, 2011, **109**, 014306.
365 X. Du, I. Skachko, A. Barker and E. Andrei, *Nat. Nanotechnol.*, 2008, **3**, 491–495.
366 J. Chen, C. Jang, S. Xiao, M. Ishigami and M. Fuhrer, *Nat. Nanotechnol.*, 2008, **3**, 206–209.
367 S. Unarunotai, Y. Murata, C. Chialvo, N. Mason, I. Petrov, R. Nuzzo, J. Moore and J. Rogers, *Adv. Mater.*, 2010, **22**, 1072–1077.
368 A. Peigney, C. Laurent, E. Flahaut, R. Bacsa and A. Rousset, *Carbon*, 2001, **39**, 507–514.
369 J. McAllister, J. Li, D. Adamson, H. Schniepp, A. Abdala, J. Liu, M. Herrera-Alonso, D. Milius, R. Car, R. Prudhomme and I. Aksay, *Chem. Mater.*, 2007, **19**, 4396–4404.

Open Access Article. Published on 25 August 2017. Downloaded on 4/25/2024 1:35:01 PM. This article is licensed under a Creative Commons Attribution-NonCommercial 3.0 Unported Licence.

370 S. Stankovich, D. Dikin, G. Dommett, K. Kohlhaas, E. Zimney, E. Stach, R. Piner and S. Nguyen, *Nature*, 2006, **442**, 282–286.
371 R. Nair, P. Blake, A. Grigorenko, K. Novoselov, T. Booth and T. Stauber, *Science*, 2008, **320**, 1308.
372 Z. Lu, G. Xu, C. He, T. Wang, L. Yang, Z. Yang and D. Ma, *Carbon*, 2015, **84**, 500–508.
373 Y. Xu, H. Bai, G. Lu, C. Li and G. Shi, *J. Am. Chem. Soc.*, 2008, **130**, 5856–5857.
374 J. Roy-Mayhew, D. Bozym, C. Punckt and I. Aksay, *ACS Nano*, 2010, **4**, 6203–6211.
375 H. Zheng, C. Neo, X. Mei, J. Qiu and J. Ouyang, *J. Mater. Chem.*, 2012, **22**, 14465–14474.
376 C. Yu, Z. Liu, X. Meng, B. Lu, D. Cui and J. Qiu, *Nanoscale*, 2016, **8**, 17458–17464.
377 H. Wang, K. Sun, F. Tao, D. Stacchiola and Y. Hu, *Angew. Chem.*, 2013, **125**, 9380–9384.
378 I. Jeon, H. Kim, I. Choi, K. Lim, J. Ko, J. Kim, H. Choi, M. Ju, J. Lee and H. Kim, *Nano Energy*, 2015, **13**, 336–345.
379 X. Xu, D. Huang, K. Cao, M. Wang, S. Zakeeruddin and M. Gratzel, *Sci. Rep.*, 2013, **3**, 1489.
380 L. Kavan, J. Yum and M. Gratzel, *Nano Lett.*, 2011, **11**, 5501–5506.
381 L. Kavan, J. Yum, M. Nazeeruddin and M. Gratzel, *ACS Nano*, 2011, **5**, 9171–9178.
382 J. Yang, P. Ganesan, J. Teuscher, T. Moehl, Y. Kim, C. Yi, P. Comte, K. Pei, T. Holcombe, M. Nazeeruddin, J. Hua, S. Zakeeruddin, H. Tian and M. Gratzel, *J. Am. Chem. Soc.*, 2014, **136**, 5722–5730.
383 S. Mathew, A. Yella, P. Gao, R. Humphry-Baker, B. Curchod, N. Ashari-Astani, I. Tavernelli, U. Rothlisberger, M. Nazeeruddin and M. Gratzel, *Nat. Chem.*, 2014, **6**, 242–247.
384 P. Srinivasu, S. Singh, A. Islam and L. Han, *Int. J. Photoenergy*, 2011, 617439.
385 Y. Li, C. Li, M. Yeh, K. Huang, P. Chen, R. Vittal and K. Ho, *Electrochim. Acta*, 2015, **179**, 211–219.
386 Y. Wei, Q. Jin and T. Ren, *Solid-State Electron.*, 2011, **63**, 76–82.
387 M. Wu, X. Lin, T. Wang, J. Qiu and T. Ma, *Energy Environ. Sci.*, 2011, **4**, 2308–2315.
388 B. Lee, D. Buchholz and R. Chang, *Energy Environ. Sci.*, 2012, **5**, 6941–6952.
389 R. Kumar, S. Nemala, S. Mallick and P. Bhargava, *Opt. Mater.*, 2017, **64**, 401–405.
390 C. Chiang, C. Fincher, Y. Park, A. Heeger, H. Shirakawa, E. Louis, S. Gau and A. MacDiarmid, *Phys. Rev. Lett.*, 1977, **39**, 1098–1101.
391 H. Shirakawa, E. Louis, A. MacDiarmid, C. Chiang and A. Heeger, *Chem. Commun.*, 1977, 578–580.
392 S. Kirchmeyer and K. Reuter, *J. Mater. Chem.*, 2005, **15**, 2077–2088.
393 L. Groenendaal, F. Jonas, D. Freitag, H. Pielartzik and J. Reynolds, *Adv. Mater.*, 2000, **12**, 481–494.
394 T. Skotheim and J. Reynold, *Handb. Conduct. Polym.*, CRC Press, 1998.
395 S. Yun, J. Freitas, A. Nogueira, Y. Wang, S. Ahmad and Z. Wang, *Prog. Polym. Sci.*, 2016, **59**, 1–40.
396 G. Heywang and F. Jonas, *Adv. Mater.*, 1992, **4**, 116–118.
397 F. Jonas and L. Schrader, *Synth. Met.*, 1991, **41**, 831–836.
398 L. Hu, D. Hecht and G. Gruner, *Appl. Phys. Lett.*, 2009, **94**, 081103.
399 F. Jonas, W. Krafft and B. Muys, *Macromol. Symp.*, 1995, **100**, 169–173.
400 R. Po, C. Carbonera, A. Bernardi, F. Tinti and N. Camaioni, *Sol. Energy Mater. Sol. Cells*, 2012, **100**, 97–114.
401 R. Sondergaard, M. Hosel, D. Angmo, T. Larsen-Olsen and F. Krebs, *Mater. Today*, 2012, **15**, 36–49.
402 J. Saghaei, A. Fallahzadeh and T. Saghaei, *Org. Electron.*, 2015, **24**, 188–194.
403 B. Worfolk, S. Andrews, S. Park, J. Reinspach, N. Liu, M. Toney, S. Mannsfeld and Z. Bao, *Proc. Natl. Acad. Sci. U. S. A.*, 2015, **112**, 14138–14143.
404 T. Yohannes and O. Inganas, *Sol. Energy Mater. Sol. Cells*, 1998, **51**, 193–202.
405 W. Wei, H. Wang and Y. Hu, *Int. J. Energy Res.*, 2014, **38**, 1099–1111.
406 Y. Saito, T. Kitamura, Y. Wada and S. Yanagida, *Chem. Lett.*, 2002, 1060–1061.
407 S. Ahmad, J. Yum, Z. Xianxi, M. Gratzel, H. Butt and M. Nazeeruddin, *J. Mater. Chem.*, 2010, **20**, 1654–1658.
408 R. Trevisan, M. Dobbelin, P. Boix, E. Barea, R. Tena-Zaera and B. Mora-Sero, *Adv. Energy Mater.*, 2011, **1**, 781–784.
409 T. Lee, K. Do, Y. Lee, S. Jeon, C. Kim, J. Ko and S. Im, *J. Mater. Chem.*, 2012, **22**, 21624–21629.
410 S. Ahmad, T. Bessho, F. Kessler, E. Baranoff, J. Frey, C. Yi, M. Gratzel and M. Nazeeruddin, *Phys. Chem. Chem. Phys.*, 2012, **14**, 10631–10639.
411 H. Tsao, J. Burschka, C. Yi, F. Kessler, M. Nazeeruddin and M. Gratzel, *Energy Environ. Sci.*, 2011, **4**, 4921–4924.
412 J. Burschka, V. Brault, S. Ahmad, L. Breau, M. Nazeeruddin, B. Marsan, S. Zakeeruddin and M. Gratzel, *Energy Environ. Sci.*, 2012, **5**, 6089–6097.
413 K. Lee, P. Chen, C. Hsu, J. Huang, W. Ho, H. Chen and K. Ho, *J. Power Sources*, 2009, **188**, 313–318.
414 S. Ahmad, J. Yum, H. Butt, M. Nazeeruddin and M. Gratzel, *ChemPhysChem*, 2010, **11**, 2814–2819.
415 J. Yum, E. Baranoff, F. Kessler, T. Moehl, S. Ahmad, T. Bessho, A. Mar-chioro, E. Ghadiri, J. Moser, C. Yi, M. Nazeeruddin and M. Gratzel, *Nat. Commun.*, 2012, **3**, 631–638.
416 E. Amasawa, N. Sasagawa, M. Kimura and M. Taya, *Adv. Energy Mater.*, 2014, **4**, 1400379.
417 C. Bora, C. Sarkar, K. Mohan and S. Dolui, *Electrochim. Acta*, 2015, **157**, 225–231.
418 A. MacDiarmid, *Angew. Chem., Int. Ed.*, 2001, **40**, 2581–2590.
419 H. Letheby, *J. Chem. Soc.*, 1862, **15**, 161–163.
420 J. Chiang and A. MacDiarmid, *Synth. Met.*, 1986, **1**, 193–205.
421 A. Heeger, *Rev. Mod. Phys.*, 2001, **73**, 681–700.
422 G. Wu, K. More, C. Johnston and P. Zelenay, *Science*, 2011, **332**, 443–447.

 This journal is © The Royal Society of Chemistry 2017

Open Access Article. Published on 25 August 2017. Downloaded on 4/25/2024 1:35:01 PM. This article is licensed under a Creative Commons Attribution-NonCommercial 3.0 Unported Licence.

423 C. Wu and T. Bein, *Science*, 1994, **264**, 1757–1759.
424 S. Bhadra, D. Khastgir, N. Singha and J. Lee, *Prog. Polym. Sci.*, 2009, **34**, 783–810.
425 J. Stejskal and R. Gilbert, *Pure Appl. Chem.*, 2002, **74**, 857–867.
426 A. Syed and M. Dinesan, *Talanta*, 1991, **38**, 815–837.
427 A. MacDiarmid, *Angew. Chem.*, 2001, **113**, 2649–2659.
428 E. Kang, K. Neoh and K. Tan, *Prog. Polym. Sci.*, 1998, **23**, 277–324.
429 Q. Li, J. Wu, Q. Tang, Z. Lan, P. Li, J. Lin and L. Fan, *Electrochem. Commun.*, 2008, **10**, 1299–1302.
430 H. Wang, Q. Feng, F. Gong, Y. Li, G. Zhou and Z. Wang, *J. Mater. Chem. A*, 2013, **1**, 97–104.
431 W. Hou, Y. Xiao, G. Han, D. Fu and R. Wu, *J. Power Sources*, 2016, **322**, 155–162.
432 Y. Saito, W. Kubo, T. Kitamura, Y. Wada and S. Yanagida, *J. Photochem. Photobiol., A*, 2004, **164**, 153–157.
433 J. Xia, N. Masaki, K. Jiang and S. Yanagida, *J. Mater. Chem.*, 2007, **17**, 2845–2850.
434 Z. Li, B. Ye, X. Hu, X. Ma, X. Zhang and Y. Deng, *Electrochem. Commun.*, 2009, **11**, 1768–1771.
435 Y. Qiu, S. Lu, S. Wang, X. Zhang, S. He and T. He, *J. Power Sources*, 2014, **253**, 300–304.
436 C. Chiang, S. Chen and C. Wu, *Org. Electron.*, 2013, **14**, 2369–2378.
437 R. McNeill, R. Siudak, J. Wardlaw and D. Weiss, *Aust. J. Chem.*, 1963, **16**, 1056–1075.
438 T. Vernitskaya and O. Efimov, *Russ. Chem. Rev.*, 1997, **66**, 443–457.
439 J. Xia, L. Chen and S. Yanagida, *J. Mater. Chem.*, 2011, **21**, 4644–4649.
440 S. Jeon, C. Kim, J. Ko and S. Im, *J. Mater. Chem.*, 2011, **21**, 8146–8151.
441 J. Janata and M. Josowicz, *Nat. Mater.*, 2003, **2**, 19–24.
442 Y. Huang, H. Li, Z. Wang, M. Zhu, Z. Pei, Q. Xue, Y. Huang and C. Zhi, *Nano Energy*, 2016, **22**, 422–438.
443 X. Zhang, J. Zhang, W. Song and Z. Liu, *J. Phys. Chem. B*, 2006, **110**, 1158–1165.
444 J. Wu, Q. Li, L. Fan, Z. Lan, P. Li, J. Lin and S. Hao, *J. Power Sources*, 2008, **181**, 172–176.
445 T. Peng, W. Sun, C. Huang, W. Yu, B. Sebo, Z. Dai, S. Guo and X. Zhao, *ACS Appl. Mater. Interfaces*, 2014, **6**, 14–17.
446 D. Hwang, D. Song, S. Jeon, T. Han, Y. Kang and S. Im, *J. Mater. Chem. A*, 2014, **2**, 859–865.
447 T. Kitamura, M. Maitani, M. Matsuda, Y. Wada and S. Yanagida, *Chem. Lett.*, 2001, 1054–1055.
448 R. Cervini and Y. Cheng, G Simon, *J. Phys. D: Appl. Phys.*, 2004, **37**, 13–20.
449 E. Kang, T. Tan, K. Neoh and Y. Ong, *Polymer*, 1986, **27**, 1958–1962.
450 S. Lu, S. Wang, R. Han, T. Feng, L. Guo, X. Zhang, D. Liu and T. He, *J. Mater. Chem. A*, 2014, **2**, 12805–12811.
451 T. Makris, V. Dracopoulos, T. Stergiopoulos and P. Lianos, *Electrochim. Acta*, 2011, **56**, 2004–2008.
452 X. Zhang, S. Wang, S. Lu, J. Su and T. He, *J. Power Sources*, 2014, **246**, 491–498.
453 K. Keothongkham, S. Pimanpang, W. Maiaugree, S. Saekow, W. Jarernboon and V. Amornkitbamrung, *Int. J. Photoenergy*, 2012, 671326.
454 P. Veerender, V. Saxena, P. Jha, S. Koiry, A. Gusain, S. Samanta, A. Chauhan, D. Aswal and S. Gupta, *Org. Electron.*, 2012, **13**, 3032–3039.
455 J. Xu, M. Li, L. Wu, Y. Sun, L. Zhu, S. Gu, L. Liu, Z. Bai, D. Fang and W. Xu, *J. Power Sources*, 2014, **257**, 230–236.
456 C. Bu, Q. Tai, Y. Liu, S. Guo and X. Zhao, *J. Power Sources*, 2013, **221**, 78–83.
457 R. Levy and M. Boudart, *Science*, 1973, **181**, 547–549.
458 E. Furimsky, *Appl. Catal., A*, 2003, **240**, 1–28.
459 C. Giordano and M. Antonietti, *Nano Today*, 2011, **6**, 366–380.
460 J. Hargreaves, *Coord. Chem. Rev.*, 2013, **257**, 2015–2031.
461 R. Ningthoujam and N. Gajbhiye, *Prog. Mater. Sci.*, 2015, **70**, 50–154.
462 C. Giordano, C. Erpen, W. Yao and M. Antonietti, *Nano Lett.*, 2008, **8**, 4659–4663.
463 K. Kamiya and T. Nishijima, *J. Am. Ceram. Soc.*, 1990, **73**, 2750–2752.
464 D. Choi and P. Kumta, *J. Am. Ceram. Soc.*, 2005, **88**, 2030–2035.
465 S. Kaskel, K. Schlichte and T. Kratzke, *J. Mol. Catal. A: Chem.*, 2004, **208**, 291–298.
466 B. Sacepe, C. Chapelier, T. Baturina, V. Vinokur, M. Baklanov and M. Sanquer, *Phys. Rev. Lett.*, 2008, **101**, 157006.
467 Q. Jiang, G. Li and X. Gao, *Chem. Commun.*, 2009, 6720–6722.
468 J. Jang, D. Ham, E. Ramasamy, J. Lee and J. Lee, *Chem. Commun.*, 2010, **46**, 8600–8602.
469 C. Lee, K. Lee, P. Chen and K. Ho, *Sol. Energy Mater. Sol. Cells*, 2009, **93**, 1411–1416.
470 L. Yang, L. Wu, M. Wu, G. Xin, H. Lin and T. Ma, *Electrochem. Commun.*, 2010, **12**, 1000–1003.
471 M. Wu, X. Lin, A. Hagfeldt and T. Ma, *Angew. Chem., Int. Ed.*, 2011, **50**, 3520–3524.
472 S. Yun, L. Wang, C. Zhao, Y. Wang and T. Ma, *Phys. Chem. Chem. Phys.*, 2013, **28**, 4286–4290.
473 S. Yun, M. Wu, Y. Wang, J. Shi, X. Lin, A. Hagfeldt and T. Ma, *ChemSusChem*, 2013, **6**, 411–416.
474 A. Ko, J. Oh, Y. Lee, S. Han and K. Park, *Mater. Lett.*, 2011, **65**, 2220–2223.
475 M. Wu, L. Mu, Y. Wang, Y. Lin, H. Guo and T. Ma, *J. Mater. Chem. A*, 2013, **1**, 7519–7524.
476 S. Yun, H. Zhang, H. Pu, J. Chen, A. Hagfeldt and T. Ma, *Adv. Energy Mater.*, 2013, **3**, 1407–1412.
477 S. Pimanpang, M. Towannang, P. Kumlangwan, W. Maiaugree, K. Ratchaphonsaenwong, V. Harnchana, W. Jarenboon and V. Amornkitbamrung, *Electron. Mater. Lett.*, 2015, **11**, 643–649.
478 V. Paranthaman, S. Muthu, P. Alagarsamy, H. Ming and R. Perumalsamy, *Electrochim. Acta*, 2016, **211**, 375–384.
479 X. Zhang, X. Chen, S. Dong, Z. Liu, X. Zhou, J. Yao, S. Pang, H. Xu, Z. Zhang, L. Lia and G. Cui, *J. Mater. Chem. A*, 2012, **22**, 6067–6071.

Open Access Article. Published on 25 August 2017. Downloaded on 4/25/2024 1:35:01 PM.
This article is licensed under a Creative Commons Attribution-NonCommercial 3.0 Unported Licence.

480 Q. Jiang, G. Li, S. Liu and X. Gao, *J. Phys. Chem. C*, 2010, **114**, 13397–13401.
481 G. Li, J. Song, G. Pan and X. Gao, *Energy Environ. Sci.*, 2011, **4**, 1680–1683.
482 L. Chen, H. Dai, Y. Zhou, Y. Hu, T. Yu, J. Liu and Z. Zou, *Chem. Commun.*, 2014, **50**, 14321–14324.
483 J. He, J. Pringle and Y. Cheng, *J. Phys. Chem. C*, 2014, **118**, 16818–16824.
484 S. Park, Y. Cho, M. Choi, H. Choi, J. Kang, J. Um, J. Choi, H. Choe and Y. Sung, *Surf. Coat. Technol.*, 2014, **259**, 560–569.
485 M. Wu, H. Guo, Y. Lin, K. Wu, T. Ma and A. Hagfeldt, *J. Phys. Chem. C*, 2014, **118**, 12625–12631.
486 Z. Wen, S. Cui, H. Pu, S. Mao, K. Yu, X. Feng and J. Chen, *Adv. Mater.*, 2011, **23**, 5445–5450.
487 M. Wu, Q. Zhang, J. Xiao, C. Ma, X. Lin, C. Miao, Y. He, Y. Gao, A. Hagfeldt and T. Ma, *J. Mater. Chem.*, 2011, **21**, 10761–10766.
488 G. Li, F. Wang, Q. Jiang, X. Gao and P. Shen, *Angew. Chem., Int. Ed.*, 2010, **49**, 3653–3656.
489 H. Guo, Q. Han, C. Gao, H. Zheng, Y. Zhu and M. Wu, *J. Power Sources*, 2016, **332**, 399–405.
490 E. Ramasamy, C. Jo, A. Anthonysamy, I. Jeong, J. Kim and J. Lee, *Chem. Mater.*, 2012, **24**, 1575–1582.
491 H. Xu, C. Zhang, Z. Wang, S. Pang, X. Zhou, Z. Zhang and G. Cui, *J. Mater. Chem. A*, 2014, **2**, 4676–4681.
492 J. Briscoe and S. Dunn, *Adv. Mater.*, 2016, **28**, 3802–3813.
493 W. Lee, Y. Jun, J. Park and G. Stucky, *J. Mater. Chem. A*, 2015, **3**, 24232–24236.
494 G. Wang, J. Zhang, S. Kuang and W. Zhang, *Chem. – Eur. J.*, 2016, **22**, 11763–11769.
495 J. Balamurugan, T. Thanh, N. Kim and J. Lee, *Adv. Mater. Interfaces*, 2016, **3**, 1500348.
496 N. Baro and S. Ramaprabhu, *J. Nanosci. Nanotechnol.*, 2016, **16**, 9583–9590.
497 G. Wang, S. Kuang, J. Zhang, S. Hou and S. Nian, *Electrochim. Acta*, 2016, **187**, 243–248.
498 S. Ruhle, M. Shalom and A. Zaban, *ChemPhysChem*, 2010, **11**, 2290–2304.
499 P. Kamat, *Acc. Chem. Res.*, 2012, **45**, 1906–1915.
500 H. Jun, M. Careem and A. Arof, *Renewable Sustainable Energy Rev.*, 2013, **22**, 148–167.
501 I. Hwang and K. Yong, *ChemElectroChem*, 2015, **2**, 634–653.
502 M. Wang, A. Anghel, B. Marsan, C. Ha, N. Pootrakulchote, S. Zakeeruddin and M. Gratzel, *J. Am. Chem. Soc.*, 2009, **131**, 15976–15977.
503 J. Huo, J. Wu, M. Zheng and Z. Lan, *Electrochim. Acta*, 2016, **187**, 210–217.
504 X. Xin, M. He, W. Han, J. Jung and Z. Lin, *Angew. Chem., Int. Ed.*, 2011, **50**, 11739–11742.
505 C. Kung, H. Chen, C. Lin, K. Huang, R. Vittal and K. Ho, *ACS Nano*, 2012, **6**, 7016–7025.
506 S. Peng, L. Li, H. Tan, R. Cai, W. Shi, C. Li, S. Mhaisalkar, M. Srinivasan, S. Ramakrishna and Q. Yan, *Adv. Funct. Mater.*, 2014, **24**, 2155–2162.
507 Z. Jin, M. Zhang, M. Wang, C. Feng and Z. Wang, *Acc. Chem. Res.*, 2017, **50**, 895–904.
508 J. Jia, J. Wu, J. Dong and J. Lin, *Electrochim. Acta*, 2015, **185**, 184–189.
509 S. Chang, M. Lu, Y. Tung and H. Tuan, *ACS Nano*, 2013, **7**, 9443–9451.
510 J. Huo, J. Wu, M. Zheng and Z. Lan, *J. Power Sources*, 2015, **293**, 570–576.
511 S. Ahn and A. Manthiram, *Adv. Energy Mater.*, 2016, **6**, 1501814.
512 J. Liang, J. Li, H. Zhu, Y. Han, Y. Wang, C. Wang, Z. Jin, G. Zhang and J. Liu, *Nanoscale*, 2016, **8**, 16017–16025.
513 H. Mulmudi, S. Batabyal, M. Rao, R. Prabhakar, N. Mathews, Y. Lam and S. Mhaisalkar, *Phys. Chem. Chem. Phys.*, 2011, **13**, 19307–19309.
514 W. Zhao, X. Zhu, H. Bi, H. Cui, S. Sun and F. Huang, *J. Power Sources*, 2013, **242**, 28–32.
515 D. Shinde, S. Patil, K. Cho, D. Ahn, N. Shrestha, R. Mane, J. Lee and S. Han, *Adv. Funct. Mater.*, 2015, **25**, 5739–5747.
516 J. Huo, J. Wu, M. Zheng, Y. Tu and Z. Lan, *Electrochim. Acta*, 2015, **180**, 574–580.
517 Y. Duan, Q. Tang, J. Liu, B. He and L. Yu, *Angew. Chem., Int. Ed.*, 2014, **53**, 14569–14574.
518 F. Gong, H. Wang, X. Xu, G. Zhou and Z. Wang, *J. Am. Chem. Soc.*, 2012, **134**, 10953–10958.
519 F. Gong, X. Xu, Z. Li, G. Zhou and Z. Wang, *Chem. Commun.*, 2013, **49**, 1437–1439.
520 Z. Zhang, S. Pang, H. Xu, Z. Yang, X. Zhang, Z. Liu, X. Wang, X. Zhou, S. Dong and X. Chen, *RSC Adv.*, 2013, **3**, 16528–16533.
521 J. Guo, Y. Shi, C. Zhu, N. Wang and T. Ma, *J. Mater. Chem. A*, 2013, **1**, 11874–11879.
522 X. Qian, H. Li, L. Shao, X. Jiang and L. Hou, *ACS Appl. Mater. Interfaces*, 2016, **8**, 29486–29495.
523 H. Li, X. Qian, C. Zhu, X. Jiang, L. Shao and L. Hou, *J. Mater. Chem. A*, 2017, **5**, 4513–4526.
524 J. Jia, J. Wu, J. Dong, Q. Bao, L. Fan and J. Lin, *Sol. Energy*, 2017, **151**, 61–67.
525 J. Guo, Y. Shi, Y. Chu and T. Ma, *Chem. Commun.*, 2013, **49**, 10157–10159.
526 S. Patil, E. Kim, N. Shrestha, J. Chang, J. Lee and S. Han, *ACS Appl. Mater. Interfaces*, 2015, **7**, 25914–25922.
527 M. Wu, X. Lin, A. Hagfeldt and T. Ma, *Chem. Commun.*, 2011, **47**, 4535–4537.
528 M. Wu, X. Lin, L. Wang, W. Guo, Y. Wang, J. Xiao, A. Hagfeldt and T. Ma, *J. Phys. Chem. C*, 2011, **115**, 22598–22602.
529 H. Zhou, Y. Shi, L. Wang, H. Zhang, C. Zhao, A. Hagfeldt and T. Ma, *Chem. Commun.*, 2013, **49**, 7626–7628.
530 X. Lin, M. Wu, Y. Wang, A. Hagfeldt and T. Ma, *Chem. Commun.*, 2011, **47**, 11489–11491.
531 Y. Hou, Z. Chen, D. Wang, B. Zhang, S. Yang, H. Wang, P. Hu, H. Zhao and H. Yang, *Small*, 2014, **10**, 484–492.
532 L. Wang, Y. Shi, H. Zhang, X. Bai, Y. Wang and T. Ma, *J. Mater. Chem. A*, 2014, **2**, 15279–15283.
533 W. Ahmad, L. Chu, M. Al-bahrani, Z. Yang, S. Wang, L. Li and Y. Gao, *RSC Adv.*, 2015, **5**, 35635–35642.
534 H. Zhou, Y. Shi, Q. Dong, Y. Wang, C. Zhu, L. Wang, N. Wang, Y. Wei, S. Tao and T. Ma, *J. Mater. Chem. A*, 2014, **2**, 4347–4354.

 This journal is © The Royal Society of Chemistry 2017

Open Access Article. Published on 25 August 2017. Downloaded on 4/25/2024 1:35:01 PM.
This article is licensed under a Creative Commons Attribution-NonCommercial 3.0 Unported Licence.

535 M. Wu and J. Wu, *Chem. Commun.*, 2013, **49**, 10971–10973.
536 M. Wu, C. Chung and Z. Ceng, *RSC Adv.*, 2015, **5**, 4561–4567.
537 C. Li, Y. Tsai and K. Ho, *ACS Appl. Mater. Interfaces*, 2016, **8**, 7037–7046.
538 Q. He, S. Huang, J. Zai, N. Tang, B. Li, Q. Qiao and X. Qian, *Chem. – Eur. J.*, 2015, **21**, 15153–15157.
539 J. Wang, X. Xin and Z. Lin, *Nanoscale*, 2011, **3**, 2040–3048.
540 S. Yuan, Z. Zhou, Z. Hou, W. Zhou, R. Yao, Y. Zhao and S. Wu, *Chem. – Eur. J.*, 2013, **19**, 10107–10110.
541 J. Yang, C. Bao, J. Zhang, T. Yu, H. Huang, Y. Wei, H. Gao, G. Fu, J. Liu and Z. Zou, *Chem. Commun.*, 2013, **49**, 2028–2030.
542 R. Yao, Z. Zhou, Z. Hou, X. Wang, W. Zhou and S. Wu, *ACS Appl. Mater. Interfaces*, 2013, **5**, 3143–3148.
543 J. Lin and S. Chou, *Electrochem. Commun.*, 2013, **37**, 11–14.
544 X. Zheng, J. Guo, Y. Shi, F. Xiong, W. Zhang, T. Ma and C. Li, *Chem. Commun.*, 2013, **49**, 9645–9647.
545 Q. He, T. Qian, J. Zai, Q. Qiao, S. Huang, Y. Li and M. Wang, *J. Mater. Chem. A*, 2015, **3**, 20359–20365.
546 Z. Shi, K. Deng and L. Li, *Sci. Rep.*, 2015, **5**, 9317.
547 A. Banerjee, K. Upadhyay, S. Bhatnagar, M. Tathavadekar, U. Bansode, S. Agarkar and S. Ogale, *RSC Adv.*, 2014, **4**, 8289–8294.
548 P. Li, J. Wu, J. Lin, M. Huang, Y. Huang and Q. Li, *Sol. Energy*, 2009, **83**, 845–849.
549 J. Guo, B. Zhang, Y. Hou, S. Yang, X. Yang and H. Yang, *J. Mater. Chem. A*, 2013, **1**, 1982–1986.
550 M. Wu, Y. Wang, X. Lin, W. Guo, K. Wu, Y. Lin, H. Guo and T. Ma, *J. Mater. Chem. A*, 2013, **1**, 9672–9679.
551 Y. Wang, C. Zhao, M. Wu, W. Liu and T. Ma, *Electrochim. Acta*, 2013, **105**, 671–676.
552 F. Miao, B. Tao and P. Chu, *Electrochim. Acta*, 2013, **96**, 61–65.
553 H. Chen, T. Liu, J. Ren, H. He, Y. Cao, N. Wang and Z. Guo, *J. Mater. Chem. A*, 2016, **4**, 3238–3244.
554 Y. Zhu, C. Gao, Q. Han, Z. Wang, Y. Wang, H. Zheng and M. Wu, *J. Catal.*, 2017, **346**, 62–69.
555 Z. Lan, L. Que, W. Wu and J. Wu, *J. Solid State Electrochem.*, 2016, **20**, 759–766.
556 S. Yun, H. Pu, J. Chen, A. Hagfeldt and T. Ma, *ChemSusChem*, 2014, **7**, 442–450.
557 G. Yue, J. Wu, Y. Xiao, M. Huang, J. Lin and J. Lin, *J. Mater. Chem. A*, 2013, **1**, 1495–1501.
558 Z. Li, F. Gong, G. Zhou and Z. Wang, *J. Phys. Chem. C*, 2013, **117**, 6561–6566.
559 Y. Li, H. Wang, Q. Feng, G. Zhou and Z. Wang, *ACS Appl. Mater. Interfaces*, 2013, **5**, 8217–8224.
560 Y. Li, Q. Feng, H. Wang, G. Zhou and Z. Wang, *J. Mater. Chem. A*, 2013, **1**, 6342–6349.
561 X. Zhang, X. Chen, K. Zhang, S. Pang, X. Zhou, H. Xu, S. Dong, P. Han, Z. Zhang, C. Zhang and G. Cui, *J. Mater. Chem. A*, 2013, **1**, 3340–3346.
562 M. Guo, Y. Yao, F. Zhao, S. Wang, D. Wang, S. Yin, H. Zhang, H. Gao and J. Xiao, *J. Photochem. Photobiol., A*, 2017, **332**, 87–91.
563 L. Wang, Y. Wei, Y. Shi, S. Tao, Y. Wang, T. Ma, H. Zhang and H. Zhou, *Chem. Commun.*, 2014, **50**, 1701–1703.
564 H. Zhou, J. Yin, Z. Nie, Z. Yang, D. Li, J. Wang, X. Liu, C. Jin, X. Zhang and T. Ma, *J. Mater. Chem. A*, 2016, **4**, 67–73.
565 W. Hong, Y. Xu, G. Lu, C. Li and G. Shi, *Electrochem. Commun.*, 2008, **10**, 1555–1558.
566 G. Yue, J. Wu, Y. Xiao, J. Lin, M. Huang, Z. Lan and L. Fan, *Energy*, 2013, **54**, 315–321.
567 F. Gong, X. Xu, G. Zhou and Z. Wang, *Phys. Chem. Chem. Phys.*, 2013, **15**, 546–552.
568 G. Liu, H. Wang, Y. Rong, Z. Ku, M. Xu, L. Liu, M. Hu, Y. Yang and H. Han, *J. Mater. Chem. A*, 2013, **1**, 1475–1480.
569 C. Li, C. Lee, S. Li, C. Lee, I. Chiu, R. Vittal, N. Wu, S. Sun and K. Ho, *J. Power Sources*, 2016, **302**, 155–163.
570 H. Zheng, C. Neo and J. Ouyang, *ACS Appl. Mater. Interfaces*, 2013, **5**, 6657–6664.
571 Y. Jo, J. Cheon, J. Yu, H. Jeong, C. Han, Y. Jun and S. Joo, *Chem. Commun.*, 2012, **48**, 8057–8059.
572 P. Joshi, Z. Zhou, P. Poudel, A. Thapa, X. Wu and Q. Qiao, *Nanoscale*, 2012, **4**, 5659–5664.
573 A. Arbab, K. Sun, I. Sahito, M. Qadir, Y. Choi and S. Jeong, *ACS Appl. Mater. Interfaces*, 2016, **8**, 7471–7482.
574 T. Muto, M. Ikegami, K. Kobayashi and T. Miyasaka, *Chem. Lett.*, 2007, **36**, 804–805.
575 H. Xu, X. Zhang, C. Zhang, Z. Liu, X. Zhou, S. Pang, X. Chen, S. Dong, Z. Zhang, L. Zhang, P. Han, X. Wang and G. Cui, *ACS Appl. Mater. Interfaces*, 2012, **4**, 1087–1092.
576 G. Yue, J. Wu, Y. Xiao, J. Lin, M. Huang and Z. Lan, *J. Phys. Chem. C*, 2012, **116**, 18057–18063.
577 C. Tsai, W. Huang, Y. Hsu, C. Shih, I. Teng and Y. Yu, *Electrochim. Acta*, 2016, **213**, 791–801.